Experimental study on environmental improvements of alternated gravel mounts in straight channelized rivers during flood stages

（洪水期における直線河道内に交互に設置した礫層マウントによる環境改善に関する研究）

January 2024

Civil Engineering Major
Graduate School of Science and Technology
Doctoral Course
Nihon University

BERETTA PICCOLI PIETRO MARCO

Context:
This thesis was written as graduation work to obtain the title of Doctor of Philosophy (PhD) at the Graduate School of Science and Technology, Nihon University, Tokyo, Japan. Here presented are the main results gathered by the author during the 4-years period from April 2020 to January 2024.

Author:

Pietro Marco Beretta Piccoli	piberettapi@gmail.com Department of Civil Engineering, Graduate School of College of Science and Technology, Nihon University, Tokyo, Japan.

Supervisor Professor:

Prof. Dr. Youichi Yasuda	yasuda.youichi@nihon-u.ac.jp Department of Civil Engineering, College of Science and Technology, Nihon University, Tokyo, Japan.

Dissertation Committee:

Prof. Dr. Robert Boes	boes@vaw.baug.ethz.ch Laboratory of Hydraulics, Hydrology and Glaciology (VAW), ETH Zürich, Zürich, Switzerland.
Prof. Dr. Masayuki Takahashi	takahashi.masayuki@nihon-u.ac.jp Department of Civil Engineering, College of Science and Technology, Nihon University, Tokyo, Japan.
Prof. Dr. Fumio Seki	seki.fumio@nihon-u.ac.jp Department of Civil Engineering, College of Science and Technology, Nihon University, Tokyo, Japan.

Acknowledgements:
First and foremost, I would like to express my profound gratitude to Prof. Dr. Y. Yasuda, who, over the course of the past four years of our collaboration, has consistently gone above and beyond the responsibilities of a supervising professor. I am deeply indebted to him for his invaluable mentorship, which extended beyond academic matters to personal guidance. His unwavering support during my time as an expatriate in Japan and his unshakable belief in my abilities, despite my many imperfections, has been a constant source of inspiration. The great work of Prof. Dr. Yasuda has been without a doubt essential in enabling me to achieve this remarkable milestone of a Doctorate of Philosophy. The profound lessons I've learned from his boundless patience and wisdom will undoubtedly resonate with me for many years to come.
In addition to Prof. Dr. Yasuda, I would like to extend my heartfelt appreciation to each member of the Dissertation Committee: Prof. Dr. M. Takahashi, Prof. Dr. F. Seki, and Prof. Dr. R. Boes. I owe a special debt of gratitude to Prof. Dr. Boes for his unwavering interest in my research and his willingness to oversee my defences despite the substantial geographical distance separating Switzerland and Japan.
I would also like to thank to my colleagues at Laboratory of Environmental Hydraulics, in particular M. Uemura, for the great help they have given me during the experiments.
My sincere gratitude goes to the Journal of Environmental Science Studies (July Press publisher) for their gracious invitation to publish in their esteemed journal. Additionally, I am grateful to the IAHR Congress Vienna 2023 for their keen interest in my research.
Outside the field of Academia, I would like to thank my parents above all. They too have put great faith and support in the success of my academic path so far from home. The weekly conversations with my siblings have been essential in refuelling my motivation, especially during the most arduous times of this thesis.
I also wish to express my deep thanks to my friends and extended family, both in Japan and back home, who have stood by me despite my abrasive personality and perpetual complaining. While it is impossible for me to mention everyone individually, I want to acknowledge those who have been the most special to me:

- Prof. Dr. C. Feliciani, my de-facto senpai, whose invaluable advice helped me navigate life in Japan;
- R. Oka, for introducing me to the vibrant nightlife of Shinjuku Nichiome and for being the best friend one could hope for;
- Dr. X. Qiao and Dr. S. Pomes, to whom I was bound through the common experience of being PhD students in Japan but with whom I have now developed a bond strong enough to, I hope, last a lifetime;
- T. Dätwyler, C. Favre and P. Lenz, for bringing a touch of Switzerland in Japan;
- C. Morini Sumi, for reminding me that part-time jobs can be both enjoyable and enlightening;
- G. Ninivaggi, J. Focarino, T. Tateoka, T. Fontaine, M. Corbally, E. Que, E. Laghi, N. Hagspiel and the Umwelting. team of Zürich, for their understanding and support during some of my most challenging moments;
- Y.Y. Chang and her Taiwanese family, for their exceptional hospitality.

Lastly, I would like to express my appreciation to the Swiss Tokyo Club, the organizers of the monthly Pub Quiz at An Solas and the nightclub Eagle Tokyo Blue.
From all of me to all of you: thank you!

Abstract

Inside the uniform cross section of straight channelized rivers, the flow is usually fast, straight and homogeneous in all three dimensions. This causes several long-term problems, including excessive sediment transport, increased local scouring and depletion of aquatic habitat. River restoration strategies have shown to be powerful tools to invert this trend, but they often require significant research and costs to be implemented. Also, the practice of widening the river cross section is challenging inside settled areas. This thesis proposes a simpler and more cost-effective alternative that does not require alteration of the river cross section: gravel mounts with assembled boulder reinforcement along their shape are installed on alternated sides of the channel. The potential environmental improvements are examined.

The experimental set-up consists in a 15.00 m long, 0.800 m wide and 0.600 m high rectangular channel with side walls made of glass. The elevation of model and the water surface are recorded using a point gauge, while the longitudinal and lateral velocity components are measured using an electrical-magnetic current meter. Four different discharges are set: Q=0.00370, 0.00550, 0.0588, 0.155 m^3/s. A hypothetical model scale of S=15 and the hydrological data from real Japanese rivers with similar characteristics as the hypothetical prototype are used to estimate the return periods: for the smallest two discharges it is shorter than one year, while third outflow is set as a once-every-ten-year outflow. The largest discharge is also the pump capacity of the experimental channel and it might be adequate to test each model's stability under major flood stages. Two types of stones are primarily used in this research: coarse gravel (d_{50}=0.0170 m) and medium boulders (d_{50}=0.0630 m). Flow conditions are defined by the average water depth (the difference between the average water level minus the gravel bed thickness) and the Froude number expressed as the average water depth. The measured longitudinal and lateral velocity components are evaluated as the time-averaged velocity and the standard deviation of the velocity for each point. Both parameters are important for the definition of ecological improvements. This research focuses on the habitat requirements of small-sized fishes with a body length smaller than 0.200 m. The Ayu fish (*Plecoglossus altivelis*) is primarily represented, but the habits of other aquatic animals are also taken into consideration. According to the literature and the results from own experiments conducted with living fishes inside the channel, refuge able areas are defined as everywhere inside the flow field where the target species might find suitable swimming conditions. These suitable swimming conditions might be mathematically formulated by two upper thresholds: time-averaged velocity not larger than 0.100 m/s and standard deviation of the velocity smaller than 0.0700 m/s. Interstice areas are regarded as the empty spaces between assembled boulders (accounting to 30% of the total construction volume) where small fishes have been observed to escape the main flow and turbulence. Gravel grains also generate empty spaces, but these are too small for this research's target species and they are therefore neglected. The performance of each model is quantified by comparing the total suitable volume (i.e. the sum of refuge able and interstice volumes) against the mounts volume (i.e. all the space they occupy above the gravel bed).

The first phase of the experimental study focuses on the flow field around triangular gravel mounts placed on alternated sides of the channel every 0.800 m. Each mount is 0.600 m long and 0.650 m wide. Different heights 0.0240, 0.0440, 0.0640 m are tried with the purpose of finding the optimal one that could maximise the environmental improvements while minimizing the disturbance to existing flood procreation measures. Experiments without mounts, i.e. flat gravel bed, are also conducted for reference purposes. Two different channel slopes are studied (I=0.00200, 0.0100) while the discharge is fixed at Q=0.0588 m^3/s. Only one layer of gravel is used for the gravel bed (i.e. the bed thickness is 0.0170 m). The introduction of gravel mounts causes the water surface to rise while waves are formed along the centre part of the channel. Both changes get more significant when the channel steepness and/or the height of the gravel mounts increase. The flow is always subcritical and the model stability is confirmed for the tested medium-sized flood discharge. The triangular shape forces the flow to meander around the mounts, generating pockets with slow-flowing water behind each one. Here, the suitable conditions for refuge able areas are found, although the total suitable volume is never larger than 18% of the mounts volume. Further unsatisfactory results are found under the pump capacity discharge, when the model collapses and critical erosion is observed. The overall best results are found when the height of the mounts is

0.0440 m, making this the optimal value to be used from this point on.
The second phase of the experimental study aims to solve the structural problems and the low suitable volumes observed in the first phase. Experiments focus on the flow conditions around 0.600 m long, 0.200 m wide, 0.0440 m high boulders groynes built every 0.800 m apart on alternated side of the channel. The boulders are assembled in three layers like fallen dominoes facing downstream. The bed thickness is increased to 0.0400 m as it is confirmed that the gravel is more resistant to erosion when compacted together. In one experiment, three additional layers of boulders are assembled along the sides of the channel with the same method as the groynes. Channel slope and discharge are set at I=0.0100 and Q=0.0588 m^3/s, respectively. Due to the uniform height of each groyne, surface waves are formed across the channel's cross section. The flow is subcritical and the average water depth is higher than what observed above triangular grave mounts (for same discharge, channel slope and construction's height). Assembled boulders easily resist the force of the pump capacity discharge, although an increase in the gravel bed erosion is observed in the centre part of the channel. It is shown that surface waves can be reduced when boulders are installed along the sides of the channel. Large refuge able areas are found around the groynes with results confirming that, at best conditions, boulders groynes can generate a total suitable volume up to 105% of their own. The main drawback of this design is an hydraulic drag force caused by the flow impinging on the upstream face of each groyne. This causes the strong surface waves and the increased average water depth. Water appears to jump over the boulders groynes instead of meandering around it. Finally, the large space between boulders are suspected in generating a strong penetrating flow that might also affect the creation of refuge and interstice areas.
The third phase of the experimental study focuses on combining gravel mounts and assembled boulders in the final design proposal. Experiments are conducted constructing 0.0440 m high, 0.650 m wide and 0.500 m long, triangular gravel mounts every 0.800 m on alternated sides of the channel. To reinforce the stability of each mount, their shape is reinforced with two layers of assembled boulders. Further two layers of assembled boulders are placed along both sides of the channel. All boulders are placed like fallen dominoes facing downstream and their height follows the mounts' profile. Bed thickness and channel slope are 0.0400 m and I=0.0100, respectively. Four discharges are tested: Q=0.00370, 0.00550, 0.0588 and 0.155 m^3/s. Experimental results are in general highly satisfactory. The water surface profile is flat mostly due to the assembled boulders build along the sides of the channel. Thanks to the reinforcement of each gravel mount, the model is now able to endure the pump capacity discharge with only minor damages. For the same discharge and channel slope, the averaged water level is lower than that measured above both previous designs. A discharge of 0.00580 m^3/s or greater is required to completely submerge the model, while supercritical flow is expected to form for discharge Q>0.130 m^3/s. The flow meanders around triangular gravel mounts and refuge able areas are found mainly behind the mounts and in the gaps between boulders and gravel. The increase of the discharge causes to flow to straighten, in particular along the centre part of the channel. Small increases between small discharges cause the flow to straighten faster than large differences between large discharges, suggesting that the relationship might be approximated with a negative exponential. Since a combination of gravel and boulders is now used, the empty spaces inside each mount accounts for 22% of the total construction volume. Each mount is expected to generate a total suitable volume around 38% of its own, with limiting factors such as shallow water or large discharge only minimally affecting this performance.
To conclude, the effectiveness of medium boulders in protecting triangular mounts composed of coarse gravel during large-scaled floods has been demonstrated. By installing every mount alternatively along the channel, the flow is forced to meander. This has been clarified as a essential step in restoring habitat and shelter in a straight channelized river. Furthermore, the consecutively assembled boulders along the riverbank (channel side walls in the experiments) are expected to reduce the flow velocity there, flatten the water surface and increase the areas for evacuation and sheltering during flooding. Future studies could begin to investigate the feasibility of a first real prototype on the base of the proposed design. Field data will be important to evaluate how simpler and more cost-effective this method actually is compared to other river restoration strategies. Also, the investigation of habitat, spawning and refuge environments of other aquatic organisms will be essential. In further laboratory studies, systemic investigation might be significant and particular priority should be given to the discovery the still-unknown applicability range of the proposed design.

論文要旨

直線水路化された河川内の流況は，非常に速く，直線的に流れ，3次元的な不均質性はほとんどない．このような状況は，土砂の過剰な流出，局所的な洗堀の増加，河川内の棲息空間の枯渇など，いくつかの長期的な問題の原因となっている．河川環境を再生するための整備は，この傾向を改善させる手段であることが示されているが，その実施には多大な研究と費用を要することが多い．また，河川断面を広げることは，定住地域内では困難である．この研究では，河川断面を変更する必要のない，より単純で費用効率の高い代替案として，礫の積み上げと巨礫の石組みの組み合わせを交互に設置し，環境改善の可能性を検討している．

第1章では，実験概要をまとめている．実験はすべて，長さ15.00 m，幅0.800 m，高さ0.600 mの長方形の水路（側面はガラス製）内で行われた．水面を含む標高はポイントゲージを用いて記録し，縦方向と横方向の流速成分は電磁流速計を用いて測定した．4つの異なる流量を設定した： Q=0.00370，0.00550，0.0588，0.155 m^3/sである．仮想的な模型スケールをS=15とし，最初の2つの流量は年間規模の洪水確率の流量として設定され，3つ目の流量は10年に1度の洪水確率の流量として設定された．4番目の最大流量は実験水路の容量できる流量であり，この流量は大洪水時のモデルの安定性に関する検討に十分な流量と判断する．2種類の石材がマウント模型として主に使用される．すなわち，細礫（d_{50}=0.0170 m）と中礫（d_{50}=0.0630 m）である．流れの条件は，平均水深（水位と礫の天端との差を検討区間で平均したもの）と，平均水深で表されるフルード数によって定義する．測定された流速は，流線方向成分と横方向成分を含み，各ポイントの時間平均流速と流速の標準偏差として評価する．速度場は生態系改善のパラメータとして重要である．本研究では，体長0.200m以下の小型魚類の生息要件に焦点を当てている．アユが主に代表的だが，多様な水生動物の習性も避難場所の定義には重要である．参考文献や水路内の生きた魚類を使った実験の結果によると，避難場所とは，対象種が適切な遊泳条件を見つける可能性のある流れ場と定義することができる．避難可能領域の流れ場は，2つの上限閾値によって定義する： 時間平均速度は0.100 m/s以下，速度の標準偏差は0.070 m/s以下である．これらの条件を満たす流れ場内は，すべて避難可能な水域に分類される．避難可能な水域とは，小魚類が本流や乱流から逃れるために観察され，集合した岩の間の空きスペース（構造物体積の30%以下）とみなされる．細礫もまた空隙を生み出すが，この調査の対象種にとっては小さすぎるため，無視する．各マウントモデルの機能は，総避難体積（すなわち，全ての避難（可能）体積の合計）をマウント体積（すなわち，礫床上の細礫と中礫が占めるすべての空間）と比較することによって定量化することができる．

第2章では，第1段階の実験的な検討結果をまとめている．水路の両側に交互に配置された三角形状の細礫マウントの周りの流れ場に焦点を当てた．各マウントは長さ0.600 m，幅0.650 mを有し，隣のマウントまで0.800 m離れている．最適な高さ（0.0240 m，0.0440 m，0.0640 m）を見つける目的で，さまざまな高さを検討した．参考のため，マウントのない実験（平坦な砂利敷き）も行った．水路勾配は2種類（I=0.00200，0.0100），流量はQ=0.0588 m^3/sである。礫層は1層のみとした（礫層の厚さは0.0170 m）．砂利を敷き詰めると水面が上昇し，水路の中央部では波が形成される．この2つの変化は，水路の急勾配や砂利敷きの高さが増すほど強くなる．流れは常に常流であり，モデルの安定性は検討された中規模の洪水流量に対して確認した．三角形の形状により，流れはマウントの周囲を蛇行するようになり，それぞれの背後には流れの緩やかなポケットが形成される．ここで，避難場所として適切な条件が見つかったが，避難場所の総容積は山頂の容積の20%より大きくなることはなかった．さらに，不満足な結果が出たのは，水路の最大流量において，モデルが崩壊し，致命的な浸食が観察されたときである．全体として最良の結果が得られたのは，架台の高さが0.0440 mのときであり，この値をこの時点から最適な高さとしている．

第3章では，第1段階の実験的な検討の中で示された構造上の問題点と避難量の少なさを解決するために検討した第2段階目の実験的な検討結果をまとめている．第2段階目の実験では，長さ0.600 m，幅0.200 m，高さ0.0440 mの水制工，3層構造，下流側を向いた石組み構造を水路の両側に0.800 m間隔で交互に設置し，その周辺の流れに焦点を当てた．礫間隔を詰めると侵食に強くなることが確認されたため，礫床の厚を0.0400 mとした．この実験では，水路の側面に沿ってさらに3層の石組みを内向きに積み上げている．水路勾配はI=0.0100としている．石組みの設置により，水路の全断面に沿って表面波が形成された．流れは常流であり，マウントモデルは検討した流量で安定した．水路の側面に沿って石組みを設置すると，表面波は抑えられることを示した．各マウント構造の背後には大きな避難可能領域がある．その結果，石組みによるマウントでは，それ自体の体積の105%の体積，すなわち，避難空間と避難可能な体積の合計

した体積を確保できることを確認した．この場合の主な欠点は，各マウントの上流面に衝突する流れによって作用する流体力である．これが，水面に強い波が発生し，平均水深が三角形状のマウント周辺で観察される場合より大きくなる原因となる．流れは蛇行せず，石組みの上を乗り越えるようになる．さらに，礫間の隙間が大きいため，強い貫通する流れが発生する．
第4章では，第3および第4段階の実験的な検討結果をまとめている．最終的な設計方針として細礫と石組みの組み合わせのマウントを提案する．第3段階の実験では，高さ0.0440 m，幅0.650 m，長さ0.500 mの三角形状のマウントが水路の両側に沿って0.800 mごとに交互に設置され，各マウントの石組みは，下流に向かって2層で構成されマウントを補強している．石組みはマウントの形状に沿って設置され，それは，マウントの安定性を高めるためである．水路の両側には、礫のマウントと同じ高さの玉石をさらに2層，下流に向けて配置した．河床の厚さは0.04 m，河道の勾配は0.0100として検討した．ここでは，4つの流量で検討した：Q＝0.00370，0.00550，0.0588，および0.155 m^3/s．結果は非常に満足のいくものであった．第4段階の実験では，側面に沿って設置された石組みにより，水面形はほぼ平坦であることを示した．さらに，これらの石組みが各マウントの山頂を取り囲んでいるため，水路内の許容最大流量でもマウント上部で軽微な侵食が見られるが，マウントの安定性が確認される．同じ流量と水路勾配の場合，ここで測定された平均水位は，第3段階のモデルの場合よりも低い．マウントを完全に水没させるには0.00580 m^3/s以上の流量が必要であり，部分的に射流の形成が認められるのは，流量が約0.130 m^3/sより大きくなったときである．三角形状のマウントが流れを蛇行させ，避難可能な領域は，マウントの後方や中礫と細礫が接する隙間を中心に見られる．流量が増加すると，特に水路の中央部では流れが直進化する．小さな流量のわずかな増加は，大きな流量の大きな違いよりも流れが直線化しやすくなることから，この関係は負の指数関数で近似できることが示唆される．現在，細礫と中礫の組み合わせが使用されているため，各マウント内部の空間はその体積の22%を占め，各マウントはそれ自体の約38%の総避難体積を確保することができる．この機能は，浅瀬の流れや大きな流量などの影響をほとんど受けない．
第5章では，研究総括を示す．直線化された河道において棲息環境および避難環境を復元するためには，洪水時の安定性を考慮した上で細礫によって構成される三角形状のマウントを中礫の石組みで保護し，平水時には蛇行した流れが形成され，洪水時には直線化する流れが形成されるように交互に設置することの有効性を明らかにした．さらに，河岸（実験では水路側壁）に沿って石組みを行うことによって，側壁付近の流れの流速が抑えられ，増水時に避難領域および避難可能領域の増大が期待される．今後の研究では，最初の実際のプロトタイプの可能性を検討し始めることができるだろう．提案したマウントの設計法が，河川環境の復元方法と比較して，実際にどの程度単純で費用対効果が高いかを最終的に評価するためには，フィールドデータが重要である．実験室での研究では，普遍性を確立するためにもさらに検討を進めることが重要である．また，提案した設計法の適用可能範囲を見つけることも重要である．さらに，ここで得られた結果は，多様な水生生物の棲息・産卵・避難環境に対してどのように寄与するのかはフィールドで調査する必要がある．

Contents

Symbols and units

Parameter	**Symbol**	**Unit**	**Notes**
Water depth	h	[m]	
	h_{GM}	[m]	height of the construction
	h_{bed}	[m]	gravel bed thickness
	h_{ave}	[m]	average water depth
Elevation	z	[m]	
Diameter	d	[m]	
	d_{50}	[m]	characteristic diameter
Channel width	B	[m]	
Width of the construction	W	[m]	
Distance	L	[m]	distance between constructions
	L_{GM}	[m]	construction's transverse length
	L_d	[m]	construction's downstream width
	L_u	[m]	construction's upstream width
Time	t	[s]	
Total velocity	V	[m/s]	$V = \sqrt{u^2 + v^2}$
	u	[m/s]	longitudinal velocity component
	v	[m/s]	lateral velocity component
	$\overline{V}$	[m/s]	time-averaged velocity
	$std(V)$	[m/s]	standard deviation of the velocity
Discharge	Q	[m^3/s]	
Slope	I	[-]	
Gravitational acceleration	g	[m/s^2]	on Earth: g=9.807 m/s^2 ($\cong$9.810 m/s^2)
Density	ρ	[kg/m^3]	density of water: $\rho_w \cong$1000.00 kg/m^3
Froude number	Fr	[-]	subcritical flow for Fr<1.00; supercritical flow for Fr>1.00; critical conditions for Fr=1.00
Porosity	n	[-]	
Area	A	[m^2]	
	A_{GM_T}	[m^2]	total construction area
	A_{GM}	[m^2]	mounts area
	A_I	[m^2]	interstice area
	A_{RA}	[m^2]	refuge able area
Volume	V	[m^3]	
	V_{GM_T}	[m^3]	total construction volume
	V_{GM}	[m^3]	mounts volume
	V_I	[m^3]	interstice volume
	V_{RA}	[m^3]	refuge able volume

1 Introduction to the research

1.1 Introduction

River channelization is a river management strategy that allows significant land reclamation for new farmland or urban expansion. At the same time, this method causes several long-term problems such as increased local erosion, disruption of the natural flow and sediment cycles and, most relevant to this research, serious depletion of the riverine habitats (WWF (2020) [29], Boes (2017) [36], Bezzola (2017) [35]). Inside the prismatic cross sections of straight rivers, the water flows too fast and too homogeneous for aquatic animals to live in it (Weitbrecht, Detert et al. (2018) [41]). Also, barriers such as dams and weirs are an obstacle to migrating species such as trouts and salmonids (Boes (2017) [37], Lin, Chen et al. (2006) [19]). During flood stages, the flow field becomes even harsher as the flow velocity surpasses the burst swim capacity of aquatic animals, exposing them to the risk of getting flushed downstream. On top of all, the incumbent climate crisis is bringing significant and unforeseen changes in the hydrological cycles, such as more frequent extreme events (floods and/or dry periods) that may affect the performance of existing flood protection measures (www.un.org [53]). To counter these threads, modern engineering is adopting new approaches that could better balance anthropogenic and environmental needs. In hydraulic engineering, this mentality change has pushed for new research to better understand the habitat requirements of the disappearing aquatic animals. River restoration strategies have proven to be successful tools in revitalizing the lost habitats, although such projects usually require long research and high construction costs (Logar, Brouwer et al. (2019) [20]). When possible, widening of the river cross section is recommended for river reclamation, but this is infeasible inside settled areas where the little space available limits the work to focus in-stream (EEA Report 2016 [12]).
Inside the bigger picture of restoring river environments, this thesis focuses specifically on the potential for gravel mounts with assembled boulders reinforcement to become a simpler and more cost-efficient, but equally effective, river restoration alternative. A dominant aspect of this research is the definition of refuge, i.e. where the small-sized fishes might find suitable habitat conditions to escape the force of the main flood flow. The proposed strategy must also prove to be reliable against erosion and to not interfere with already installed engineering structures such as flood protection measures. The research started with the author's Master thesis written in Summer 2019 (Beretta Piccoli (2019) [34]) and whose results have been presented at the 22nd IAHR-APD Congress Conference (Beretta Piccoli and Yasuda (2020) [7]). This thesis summarizes the following 4 years of academic research from April 2020, when the author worked as contractual researcher at the Laboratory of Environmental Hydraulics of the Nihon University, College of Science and Technology, before starting his PhD course in April 2021 at the same laboratory. The writing of this thesis in January 2024 marks the end of his work.

1.2 Objectives

This thesis aims to quantify the creation of suitable areas for small-sized fishes around alternated gravel mounts for them escape the force of the main flow during flood stages inside straight rivers. The first task is:

- to mathematically define what are the suitable habitat conditions required by small-sized fishes.

Once this is complete,

- the optimal gravel mounts' design must be found that could maximise the formation of suitable areas, while minimizing the interference with existing flood protection structures.

In particular, the research focuses on:

- the shape of the gravel mounts and
- the materials used for construction.

The performance will be evaluated on the basis of the model's stability, the generated total suitable volume and the water level profile.

1.3 Experimental channel

The research is conducted inside the 15.00 m long experimental channel of the Department of Civil Engineering, College of Science and Technology, Nihon University. The rectangular cross section is build from a flat metal bed 0.800 m wide and reinforced glass side walls 0.600 m high. The upstream water tank is attached to two pumps with maximal combined discharge of 0.155 m^3/s (pump capacity discharge), while the outflow is regulated by a vertically shifting weir at the downstream end of the channel. The downstream water tank allows for flow discharge estimation by fixed point gauge station and given h-Q function. An aerial view of the infrastructure minus the downstream water tank is shown in Figure 1.

Measurements are conducted following a defined coordinates system: the longitudinal x-axis origin is placed at the upstream end of each installation area (i.e. the physical model above which the measurements are taken) with positive x-direction following the flow toward downstream; the centre of the channel is defined as lateral coordinate y=0.00 m with left and right side walls having coordinates y=0.400 m and y=−0.400 m, respectively.

Figure 1: Aerial view of the experimental channel (red arrow for flow direction).

1.4 Measurement instruments

A point gauge is used to measure elevation (usually, the heigh of the gravel bed or the water level) with resolution of 0.00100 m (Figure 2a). The flow velocity is assessed using an I-type probe electrical-magnetic current meter KENEK CO. model VM-806H/VMT2-200-04P (Figure 2b) with sampling frequency 20.00 Hz for 30.00 s (for a total 601 point-values per measurement) and ±0.00500 m/s sensitivity (information sheet [46]). The collected data sets are visually checked for anomalies such as jumps and extreme values (statistical z-score>3) that are subsequently removed. A propeller-type current meter KENEK Co. model VR-301 with sampling frequency of 8 pulses per rotation and ±0.0300 m/s sensitivity (information sheet [47], Figure 61) is used to measure the longitudinal surface velocity, wherever the electrical-magnetic current meter can not properly function. Weight is measured with a AND model SJ-20k scale with 0.0200 kg sensitivity and 20.00 kg maximal measurable weight (information sheet [42]) shown in Figure 2c.

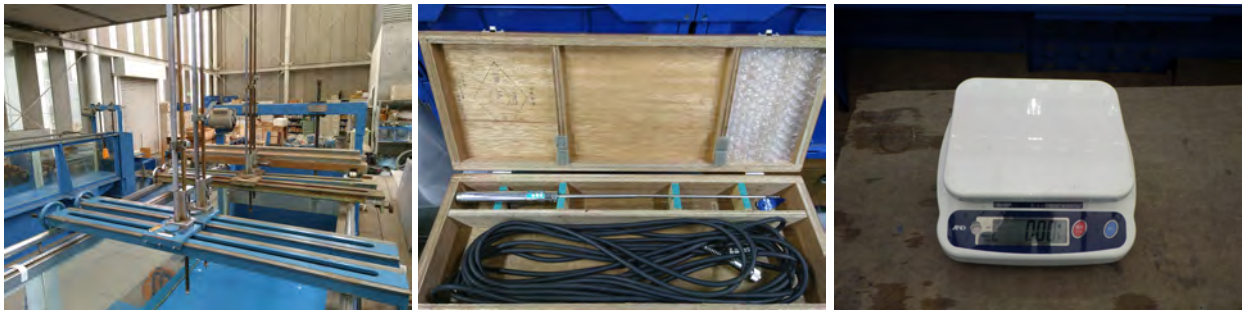

(a) Point gauge. (b) Current meter. (c) Scale.

Figure 2: The most important instruments used in this research.

1.5 Scale, prototype river and discharge

Because this is a research in the field of Engineering, the experimental channel in which the models are constructed is set to be a generic simulation of a section of an existing straight rectangular river (*generic model* means that no attempts are made to reproduce the geometrical details of the prototype river (Church, Hassan et al. (1998) [9])). The scale factor S is introduced under the principle of Froude similarity (*Froude similarity* means that the prototype and the scaled prototype share the same hydraulic characteristics (Kinzelbach (2011) [38])). Under this definition, the following equations between prototype river PR (theoretical) and experimental model EX (here researched) are defined:

- Froude number Fr [-] (Eq. 6): $Fr_{PR} = Fr_{EX}$;
- Water depth h, channel width B [m]: $h_{PR} = h_{EX} \cdot S$, $B_{PR} = B_{EX} \cdot S$;
- Flow velocity V [m/s]: $V_{PR} = V_{EX} \cdot \sqrt{S}$;
- Discharge Q [m^3/s]: $Q_{PR} = Q_{EX} \cdot S^{2.5} = h_{EX} \cdot V_{EX} \cdot B_{EX} \cdot S^{2.5}$;
- Slope I [-]: $I_{PR} = I_{EX}$.

Introducing a scaling factor S=15, the experimental channel would now simulate a 225.00 m long section of a straight, 12.00 m wide, rectangular river. Model scaling is also important in quantifying the intensity of the studied floods' discharges using their return periods (*return period* is the interval in which a flood volume is expected to be reached only once based on the historical discharge data (Bezzola (2017) [35])). Most of the experiments are conducted under discharge Q=0.0588 m^3/s, while the pump capacity discharge of the experimental channel Q=0.155 m^3/s is used to test each model's stability. In Chapter 4 two smaller discharge are also studied: Q=0.00370, 0.00550 m^3/s. Scaled 1:15, the discharges become Q_{PR}=3.22, 4.79, 51.24, 135.07 m^3/s, respectively.
Two Japanese rivers are taken as reference because their characteristics matches these of this research's theoretical prototype: the Edokami river, 江戸上川, in Ibaraki Prefecture (170 km north from Tokyo, trapezoidal cross section, width 12.00-24.00 m, slope 0.0100, rainfall-based flood statistics) and the Kawatana river, 川棚川, in Nagasaki Prefecture (Kyushu Island, trapezoidal cross section, width 7.80-10.20 m, slope 0.0100, discharge-based flood statistics). The data to build the flood curve for Edokami river come from the Ibaraki Prefectural Government, Land Development Department, River Policy Division [48], while Kawatana river's information are given by the Nagasaki Prefectural Government, River Policy Division [50]. Pictures of both the river cross sections and their respective hydrological data are exposed in the Appendices (Figure 62 and 63). The resulting return periods are here shown:

Table 1: Return period $\frac{1}{R}$ for each studied discharge and prototype river.

		Edokami	Kawatana
Q [m^3/s]	Q_{PR} [m^3/s]	$\frac{1}{R}$ [years]	
0.00370	3.22	<1	<1
0.00550	4.79	<1	<1
0.0588	51.25	11	8
0.155	135.07	30	72

1.6 Gravel

The materials used to construct each experimental model were bought at the local DIY store. Each time, a pool of at least 100, randomly selected rocks are taken and the average of each stone's three lengths is recorded. The values generate cumulative normal distributions that allow to extract the characteristic diameters of Table 2. The coarse gravel G1 is the most extensively used during this research, in particular for the construction of the gravel mounts and the gravel bed. The medium boulders B1 are used to create the assembled boulders constructions introduced in Chapter 3. The

coarse boulders B2 are utilized to construct scaled models of assembled boulders during two experiments conducted besides the main research (Chapter 5). In this thesis, each material is classified based its characteristic diameter scaled to prototype ($d_{50,S=15}$) and the table defined by Blair and McPherson (1999) [8]. The grain distribution is express with the parameter $\sigma_G=\sqrt{d_{84}/d_{16}}$. All used materials are defined as uniform distributed as $\sigma_G<1.500$ (Boes (2017) [36]).

Table 2: Characteristic diameters for the different materials used in the experiments.

ID	*Class, shape*	S [-]	d_{16} [m]	d_{30} [m]	d_{50} [m]	d_{84} [m]	d_{90} [m]	σ_G [-]	$d_{50,S=15}$ [m]
G1	*Coarse gravel*	1	0.0140	0.0150	0.0170	0.0190	0.0200	1.16	0.255
B1	*Round boulders*	1	0.0570	0.0600	0.0630	0.0690	0.0700	1.10	0.930
B2	*Coarse boulders*	2.5	0.0770	0.0840	0.0920	0.108	0.112	1.21	1.380

(a) Coarse gravel G1. (b) Medium boulders B1. (c) Coarse boulders B2.

Figure 3: The different materials used in this research.

Due to the constant sedimentation and erosion processes, natural gravel-based rivers usually have a surface armour layer build from larger stones on top of the inner layer made by significantly smaller grains. In all experiments (aside these described in Chapter 5), coarse gravel G1 is use to simulate the river armouring as a flat, uniform bed either 0.0170 m or 0.0400 m thick on top of which models are built. This simplification of the natural conditions was driven by practicality (available time and materials). Also, this research gives no focus to start of motion and transport mechanisms, as it is expected (and confirmed in Yasuda, Yasuda and Beretta Piccoli (2023) [31]) for fine sediments to deposit during normal stages and to erode during flood stages around the alternated gravel mounts.

1.7 Mathematical formulas

The electrical-magnetic current meter measures the longitudinal (x-direction) and the lateral (y-direction) velocity components. These are defined as u [m/s] and v [m/s], respectively. The total velocity V [m/s] is calculated by the vectorial sum of the two for each point measurement i [-]:

$$V_i = \sqrt{u_i^2 + v_i^2} \tag{1}$$

The time-averaged flow velocity $\overline{V}$ [m/s] and the standard deviation of the velocity $std(V)$ [m/s] are important in the definition of refuge able areas (Sub-chapter 1.9) and they are calculated as follows:

$$\overline{V} = \frac{1}{N} \cdot \sum_{i=1}^{N} V_i \quad \text{and} \quad std(V) = \sqrt{\frac{\sum_{i=1}^{N} V_i - \overline{V}}{N}} \tag{2, 3}$$

N **:** total number of point measurements [-].

The average water depth h_{ave} [m] is calculated from the difference between the averaged water level z_{ave} [m] minus the bed thickness h_{bed} [m]. The discharge Q [m^3/s] is estimated through fixed point gauge and known h-Q function inside the water tank placed downstream of the experimental channel. The average flow velocity V_{ave} [m/s] is found by dividing the discharge by the flow area A_w [m^2] (i.e. width B=0.80 m multiplied by the average water depth):

$$h_{ave} = z_{ave} - h_{bed} \quad \text{and} \quad V_{ave} = \frac{Q}{B \cdot h_{ave}} \tag{4, 5}$$

g **:** gravitation acceleration (on Earth, g=9.810 m/s^2).

The flow character is expressed by the Froude Number Fr [-]:

$$Fr = \frac{V_{ave}}{\sqrt{g \cdot h_{ave}}} = \frac{Q}{B \cdot h_{ave} \cdot \sqrt{g \cdot h_{ave}}} \tag{6}$$

Subcritical flow is defined for Fr<1.00, supercritical flow for Fr>1.00 and critical flow for Fr=1.00. The experiments presented in Chapters 3 and 4 are characterized by the combination of boulders B1 assembled over the gravel G1 bed generating a bimodal mixture (*bimodal mixtures* exhibit a clear gab in the averaged grain fractions because they contain only relative small or very large grains (Bezzola (2017) [35])). The criteria defined in Raudkivi and Ettema (1982) [24] are used to confirm the mixture stability:

- The ratio between mean diameters $\frac{d_{50,B1}}{d_{50,G1}}$=3.700;
- The friction velocity of the flow $u_* = \sqrt{g \cdot h_{ave} \cdot I}$=0.100..0.110 m/s. As the experimental channel's side walls are made of glass, their friction can be neglected and therefore assumed that $B>>h_{ave}$ and the hydraulic radius is R_{hy}=h_{ave}. The range of u_* takes into account the average water depths found at the different experiments (h_{ave}=0.111...0.128 m);
- The friction velocity of the boulders B1 $u_{*,B1} = \sqrt{\theta_{cr} \cdot g \cdot (s-1) \cdot d_{50,B1}}$=0.230 m/s. The critical friction coefficient and the relative density of the stones over water are assumed θ=0.0500 and s=2.650, respectively;
- the ratio between the friction velocities $\frac{u_*}{u_{*,B1}}$=0.430..0.480.

According to the Raudkivi and Ettema's diagrams, the boulders might face the risk of overpassing (i.e. rolling or sliding) over the gravel bed, although this eventuality is considered improbable in reality as the results are close to the "no erosion" field as well and the applied construction method of partially burying the assembled boulders (instead of just placing them over the gravel) has proven to increase their stability, as further confirmed by the experimental results shown in Chapters 3 and 4.
All the space that gravel and/or boulders take above the bed thickness h_{bed} [m] is defined as the total construction area A_{GM_T} [m^2]. In case of single-layer bed cover, the bed thickness is assumed to be equal to the average diameter (h_{bed}=d_{50}). For each measurement's lateral coordinate y, the formula is given as:

$$A_{GM_T,y} = \sum \frac{(z_{bed,x} - h_{bed}) + (z_{bed,x+\Delta x} - h_{bed})}{2} \cdot \Delta x \tag{7}$$

$z_{bed,x}$, $z_{bed,x+\Delta x}$ **:** bed elevation at coordinates (x, y) and $(x + \Delta x, y)$, respectively [m];
Δx **:** distance between two measurements along the longitudinal x-axis [m].

The total construction volume V_{GM_T} [m^3], is calculated by the sum of all the areas multiplied by the distance between them Δy [m]:

$$V_{GM_T} = \sum \frac{A_{GM_T,y} + A_{GM_T,y+\Delta y}}{2} \cdot \Delta y \tag{8}$$

For constructions made of gravel (e.g. gravel mounts), the mounts area A_{GM} [m^2] and volume V_{GM} [m^3] are equal to the total construction area A_{GM_T} and volume V_{GM_T}, respectively. This is possible because in this case, the interstice volume is neglected. For constructions made from boulders (e.g. boulders groynes), the mounts area A_{GM} [m^2] and volume V_{GM} [m^3] are 70% percent of the total construction area A_{GM_T} and volume V_{GM_T}, respectively. In this case, the porosity n=0.300 must be taken into account (see following Sub-chapter 1.9).

1.8 Target species

Figure 4: Two Ayu fish. Source: `https://www.honda.co.jp/fishing/picture-book/ayu/`.

This research does not have a specific target species, but rather focuses on the environmental requirements of small-sized fishes, here defined as all the individual having a body length not larger 0.200 m. In theory, small-sized fishes should be small enough to fit and swim inside the empty spaces between assembled boulders, but at the same time be too big to infiltrate the gravel forming the river's substratum. For practicality, the Ayu fish (*Plecoglossus altivelis*, order of the Osmeriformes, アユ魚 in Japanese) is taken as reference due to its prominence inside Japanese rivers. An amphidromus species, its members spawn in the salty water of river deltas and coastlines before returning to the sweet water of rivers once they have become adults (body length larger than 7.00 cm). Primarily plankton-feeder, Ayu prefer environments with clean water and are known to be extremely territorial. A single adult (usual body length around 0.200 m, but rarely up to 0.300 m) can claim up to 10.00-20.00 m^2 of territory for himself. The information about this species has been gathered from: Wildlife Division (2015) [28]; Onitsuka, Nagaya et al. (2009) [22] and (2005) [23]; Yamamoto and Honda (2005) [30] and Nakamura, Ishikawa et al. (1995) [21].
Other species taken into consideration are: the common carp *Cyprinus carpio* (Edwards and Twomey (1982) [11]); the Atlantic cod *Gadus morhua* (Gerstner (1998) [14]); the Formosan landlocked salmon *Oncorhynchus masou formosanus* (Lin, Chen et al.(2006) [19]); the longfin eels *Anguilla dieffenbachii* (Graynoth and Booker (2009) [15]); the rainbow trout *Oncorhynchus mykiss* (Stewart, Tian et al. (2016) [26]); common reef flat species *Halichoeres margaritaceus*, *Pomacentrus chrysurus* and *Chrysiptera brownriggi* (Johnasen, Fulton and Bellwood (2008) [17] and (2007) [18]), as well as benthic New Zealand fish species Canterbury galaxias *Galaxias vulgaris* and upland bullies *Gobiomorphus breviceps* (Davey, Kelly and Biggs (2006) [10]). Pictures of all these species are attached in Figure 65.

1.9 Refuge able area and interstice area

Johnasen, Fulton and Bellwood (2008) [17] have given the following definition: *flow refuge is a behavioural mechanism that may facilitate the occupation of turbulent, high-flow habitats by reducing the extreme environmental demands on their swimming capacities.* Although their research focused on fishes living inside coral reefs, they highlighted how the formation of areas of refuge allows fishes to better conserve energy and therefore swim longer in regions that would have been otherwise inaccessible (also Johansen, Fulton and Bellwood (2007) [18]). Other research also highlighted the potential of refuge for preys against predators (Felten, Dolédec and Statzner (2008) [13], as well as Hart and Merz (1998) [16]), although this dynamic was not considered in this research. Other scientists focused on refuge habitats for micro-organisms or shell-fishes inside freshwater flows (Strayer (1999) [27]). As far as the author could gather, there was no research conducted specifically aiming at small-sized fished inside straight freshwater channelized rivers.
For model simplicity, differences in body shape, size, sex, age and swimming ability within each fish individual and species are not taken into account. Also, the definition of "suitable swimming conditions for small-sized fishes" refers to the "sustained swim capacity", as this research focuses on generate pockets in the flow field that can be used for the entire duration of the flood stage. Fishes can also maintain a "burst swim capacity" against stronger flow velocities than that, but only for a limited period of time.
Two kind of refuge are defined: a) the *refuge able areas*, i.e. everywhere inside the flow field where suitable conditions are found, and b) the *interstice areas*, i.e. the empty spaces inside the assembled boulders. Mathematically, the definition is based on the literature research, as well as the experiments

conducted in the author's Laboratory with living fishes and prototype-scaled boulders (the full list of the sources is presented in Table 3). Two thresholds are set as the general upper limit for the definition of suitable conditions:

$$\overline{V} \leq 0.100 \text{ m/s} \quad \text{and} \quad std(V) \leq 0.070 \text{ m/s} \tag{9, 10}$$

The refuge able area A_{RA} [m^2] is defined as all the flow area where the given hydraulics thresholds are met. The highest elevation where this is true is called z_{RA} [m]. At each point, the height of the refuge able area is found from the difference between z_{RA} and the elevation of the model's surface z_{bed} [m]. For each lateral measurement coordinate y, the formula is:

$$A_{RA,y} = \sum \frac{(z_{RA,x} - z_{bed,x}) + (z_{RA,x} - z_{bed,x+\Delta x})}{2} \cdot \Delta x \tag{11}$$

The refuge able volume V_{RA} [m^3] is calculated by the sum of all the areas multiplied by the distance between them Δy [m]:

$$V_{RA} = \sum \frac{A_{RA,y} + A_{RA,y+\Delta y}}{2} \cdot \Delta y \tag{12}$$

In this research, interstice area A_I [m^2] and interstice volume V_I [m^3] are considered to occur only inside assembled boulders constructions (B1 and B2 in Table 2). The empty spaces between the grains of gravel G1 are expected to meet the habitat requirements for micro-organisms or to be suitable for aquatic plants to root (Stocker and Fernandez (2018) [40] and Strayer (1999) [27]), but not for the targeted small-sized fishes as they are too large. In this research it is V_I=0.00 m^3 inside the gravel. When assembled boulders are constructed, the interstice area is calculated as 30% of the mounts area (i.e. porosity of 0.300). The process to obtain this value is explained in details in Sub-chapter 3.2.1. Therefore, in case of model using assembled boulders:

$$A_{I,y} = 0.300 \cdot A_{GM_T,y} = 0.300 \cdot \sum \frac{(z_{bed,x} - h_{bed}) + (z_{bed,x+\Delta x} - h_{bed})}{2} \cdot \Delta x \tag{13}$$

$$V_I = 0.300 \cdot V_{GM_T} = 0.300 \cdot \sum \frac{A_{GM,y} + A_{GM,y+\Delta y}}{2} \cdot \Delta y \tag{14}$$

Table 3: Literature research for the definition of refuge able and interstice areas.

Literature	Stocker and Fernandez (2018, unpublished) [40]; W. J. Stewart, F.-B. Tian et al. (2016) [26]; Wildlife Division (2015) [28]; Graynoth and Booker (2009) [15]; Onitsuka, Nagaya et al. (2009) [22] and (2005) [23]; Johnasen, Fulton and Bellwood (2008) [17] and (2007) [18]; Davey, Kelly and Biggs (2006) [10]; Lin, Chen et al. (2006) [19]; Yamamoto and Honda [30]; Gerstner (1998) [14]; Nakamura, Ishikawa et al. (1995) [21]; Edwards and Twomey (1982) [11]; online databases on aquatic animals are used to a smaller extent [43], [44], [45], [51].
Experiments	The first experiment with living fishes and prototype-scale boulders was conducted in July 2019 and it has been presented in Beretta Piccoli and Yasuda (2020) [7] (and Beretta Piccoli (2019, unpublished) [34]). In July of 2020, similar experimental conditions were recreated to study the behaviour of Japanese eels around the prototype-scaled boulders (Sub-chapter 5.2) and the results were published in Yasuda (2021) [32]. In August 2022, 100 small-sized fishes of different species were released in the experimental channel filled with assembled coarse boulders B2. The observed behaviours are described in Sub-chapter 5.4.

2 Optimal height of the gravel mounts

2.1 Introduction

The author's PhD research starts where his Master thesis ended (Beretta Piccoli, Yasuda and Boes (2020) [7] (and (2019, unpublished) [34])). There, the flow conditions around triangular alternated gravel mounts were investigated for channel slope I=0.0100 (i.e. 1%) and discharge ranging from small- to medium-sized flood stage. The observed water surface was wavy in the centre part of the channel and generally flat along the sides. The average water depth appeared to significantly rise from the reference scenario with flat gravel bed. The creation of regions with significantly slower flowing water was observed behind each gravel mounts. The size of these areas appeared to reduce with the increase of discharge and/or elevation form the gravel bed.
Based these results, the first chapter of this PhD research focuses on finding the optimal height of the gravel mounts that could maximise the creation of refuge able areas, while at the same time minimize the water level rise. Experiments were conducted between May 2020 and March 2021 and the main results have been published in Beretta Piccoli and Yasuda (2021) [6].

2.2 Methods

Since the research focuses on the gravel mounts height, most of the characteristics inside the installation area are kept constant between experiments (experiment GM2.5 being the only exception to this rule). Following the morphology proposed in the author's Master thesis, seven arrowhead-shaped gravel mounts are constructed on alternated sides on top a 5.400 m long, flat gravel bed. For both bed and mounts, coarse gravel G1 is used. Because the bed is composed by one single layer of grains, the bed thickness is considered equal to the average diameter (i.e. h_{bed}=d_{50}=0.0170 m). The distance between gravel mounts L is kept uniform at 0.800 m (1.600 m when considering two mounts on the same side of the channel). The mounts' transverse length L_{GM} and downstream width L_d are always 0.600 m and 0.350 m, respectively. The upstream width L_u is 0.300 m for all experiments except GM1.3bis, where it is reduced to 0.200 m. The mount's height h_{GM} linearly decreases from the side wall to the mount's toe. In this chapter several different heights are tested: h_{GM}=0.00 m (flat gravel bed morphology), 0.0240, 0.0440, 0.0640 m, the latter having been firstly used in the author's Master thesis. Experiments conducted when the channel slope is I=0.00200 (i.e. 0.20%) are marked with *GM1.* prefix, while these in case of I=0.0100 (i.e. 1%) use the identification *GM2.* (prefix *GM* stands for *gravel mounts*). In the case of experiment GM2.5, the distance between each gravel mounts is doubled to L=1.600 m. For this reason, only 5 gravel mounts are constructed inside the now 7 m long model. The rest of the characteristics are kept in conformity with the other experiments: h_{bed} =0.0170 m, h_{GM}=0.0440 m, L_{GM}=0.600 m, L_u=0.300 m, L_d=0.350 m, I=0.0100. The discharge Q=0.0588 m^3/s (medium-sized flood stage, Table 1) is fixed in all experiments. Also, a metal bar is consistently placed at the downstream end of each model to increase its stability. Pictures of the installed models are visible in Figures 5 and 6, while each experiment's characteristics are summarized in Table 4. A definition sketch of the installation area is shown in Figure 7.
Measurements are collected uniformly between experiments with gravel mounts: the bed elevation is measured every 0.100 m in x-direction for 0.00≤ x (m)≤5.40 (1.60≤x (m)≤7.00 for experiment GM2.5) and y-coordinate: y=−0.380, −0.300, −0.200, −0.100, 0.00, 0.100, 0.200, 0.300, 0.380 m; the water level is assessed every 0.100 m in x-direction for 0.00≤x (m)≤5.400 and y=−0.380, 0.00, 0.380 m (y=−0.300, 0.00, 0.300 m for experiment GM2.4). Velocity measurements are collected every 0.0100 m in vertical z-direction between the gravel bed and the water surface and every 0.100 m inside the interval 1.90≤x (m)≤5.10 (3.50≤x (m)≤6.70 for GM2.5) for y=−0.380, −0.300, −0.200, 0.00 m. In the cases of GM1.1 and GM2.1 (i.e. flat gravel bed), bed surface and water elevation are measured in 7 points at the centre of the channel (x=1.10, 1.90, 2.70, 3.50, 4.30, 5.10, 5.40 and y=0.00 m), while the velocity is collected every 0.0100 m in z-direction between gravel bed and water surface at x=3.80,

4.00, 4.20 m and y=−0.380, −0.300, −0.200, 0.00 m.

(a) GM1.4 (and GM2.4). (b) GM2.5. (c) Metal bar.

Figure 5: The installation areas for experiments GM1.4 (left) and GM2.5 (centre) viewd from downstream. On the right, the metal bar installed at the downstream end of each model.

(a) h_{GM}=0.00 m (GM1.1, GM2.1). (b) h_{GM}=0.0240 m (GM1.2). (c) h_{GM}=0.0440 m (GM1.3, GM2.3, GM2.5).

(d) h_{GM}=0.0440 m (GM1.3bis). (e) h_{GM}=0.0640 m (GM1.4 and GM2.4).

Figure 6: Side view of the different gravel mounts' height. The modified upstream width of model GM1.3bis is presented in (d). The flow direction would be from left to right.

Table 4: Main characteristics of this chapter's experiments.

ID	h_{GM} [m]	L_{GM} [m]	L_u [m]	L_d [m]	L [m]	h_{bed}, d_{50} [m]	I [-]	Q [m^3/s]
GM1.1	0.00	0.00	0.00	0.00	0.00	0.0170	0.00200	0.0588
GM1.2	0.0240	0.600	0.300	0.350	0.800	0.0170	0.00200	0.0588
GM1.3	0.0440	0.600	0.300	0.350	0.800	0.0170	0.00200	0.0588
GM1.3bis[1]	0.0440	0.600	0.200	0.350	0.800	0.0170	0.00200	0.0588
GM1.4	0.0640	0.600	0.300	0.350	0.800	0.0170	0.00200	0.0588
GM2.1[2]	0.00	0.00	0.00	0.00	0.00	0.0170	0.0100	0.0588
GM2.3	0.0440	0.600	0.300	0.350	0.800	0.0170	0.0100	0.0588
GM2.4[2]	0.0640	0.600	0.300	0.350	0.800	0.0170	0.0100	0.0588
GM2.5[1]	0.0440	0.600	0.300	0.350	1.60	0.0170	0.0100	0.0588

[1] The results of these experiments has never been published.

[2] These experiments have been imported from the author's Mater thesis (Beretta Piccoli, Yasuda and Boes (2020) [7] and (2019) [34]).

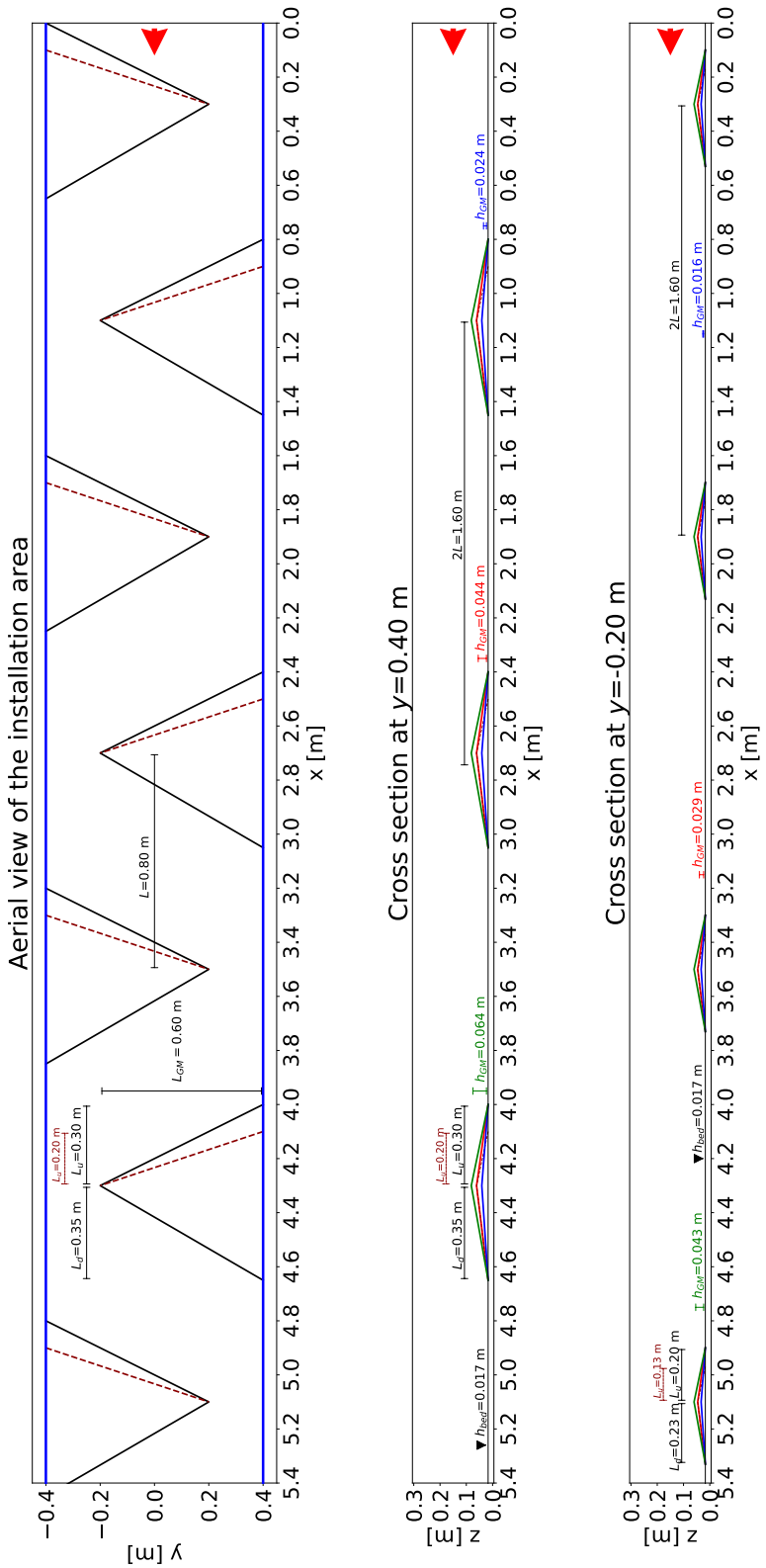

Figure 7: Definition sketch of the installation area for all experiments except GM2.5. The different heighst of the gravel mounts are marked in different colours: blue for h_{GM}=0.0240 m (GM1.2); red for h_{GM}=0.0440 m (GM1.3, GM1.3bis and GM2.3) and green for h_{GM}=0.0640 m (GM1.4 and GM2.4). The reduction of the upstream width tested in experiment GM1.3bis is shown in dark red. The flow direction is given by the red arrow.

2.3 Results and Discussion

2.3.1 Average water depth and Froude number

None of the studied morphologies is shown to reach total erosion conditions in case of a medium-sized flood. Local transport is generally observed in the channel's centre part, between the gravel mounts. Experiment GM2.5 is the only one where the erosion is large enough to expose the metal surface of the experimental channel. During the other experiments, only a few stones, if any at all, are collected outside the installation area, while grain shaking is much more widespread than erosion. For both studied channel slopes, the activity in the gravel bed appears to increase around higher gravel mounts. The average water surface is also shown to increase with the gravel mounts' height while the Froude number decreases, as shown in Table 5. All conducted experiments can be classified as subcritical flow, with only GM2.1 approaching critical conditions. Changes in the flow conditions are more significant between the experiments conducted above I=0.0100 (GM2.x) than above I=0.00200 (GM1.x). The reduction of the upstream width (GM1.3bis) does not affect the average flow characteristics since the results in Table 5 are identical between experiments GM1.3 and GM1.3bis. Doubling the distance between gravel mounts in model GM2.5 appear to reduce the effect of the gravel mounts, since the average water depth is smaller and Froude number is larger than what measured in experiment GM2.3 (same gravel mounts' height).

Table 5: Flow characteristics of the different experiments (Q=0.0588 m^3/s).

	GM1.1	GM1.2	GM1.3	GM1.3bis	GM1.4	GM2.1	GM2.3	GM2.4	GM2.5
h_{ave} [m]	0.148	0.150	0.151	0.151	0.166	0.102	0.117	0.137	0.110
Fr [-]	0.410	0.400	0.400	0.400	0.350	0.720	0.590	0.470	0.640

The water surface above flat gravel bed is also flat, as shown in Figures 8a and 9a. With increasing gravel mounts' height, waves are forming in the centre part of the channel. The amplitude of these waves is more prominent in case of steeper slope I=0.0100 (Figure 9) than I=0.00200 (Figure 8). In both cases, the water surface along the sides of the channel remains generally flat. In case of GM2.5 (Figure 9d), the water surface plummets right after each gravel mounts. This behaviour might explain the significant erosion in the gravel bed described in the previous paragraph.
Figure 10 shows the rise of the average water surface from the reference scenario of flat gravel bed (i.e. experiments GM1.1 and GM2.1). The data are plotted in relationship to the gravel mounts' height over the distance between them ($\frac{h_{GM}}{L}$). As shown, the water level appear to increase exponentially with increasing gravel mounts' height and the growth steepness appears related to the channel slope. Experiments GM1.3 and GM1.3bis produce almost the same results, while the increased distance between gravel mounts in GM2.5 significantly reduces both the water surface rise and the $\frac{h_{GM}}{L}$ ratio. The marker position appear to take the place where an hypothetical experiment GM2.2 (h_{GM}=0.0240 m and I=0.0100) would have been expected.

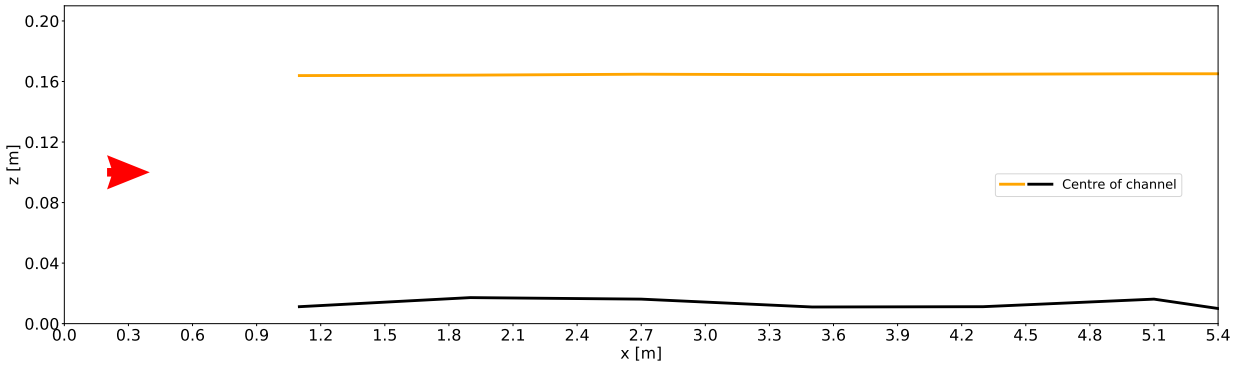

(a) h_{GM}=0.00 m (GM1.1). Measurements were taken only for 1.10≤x (m)≤5.40.

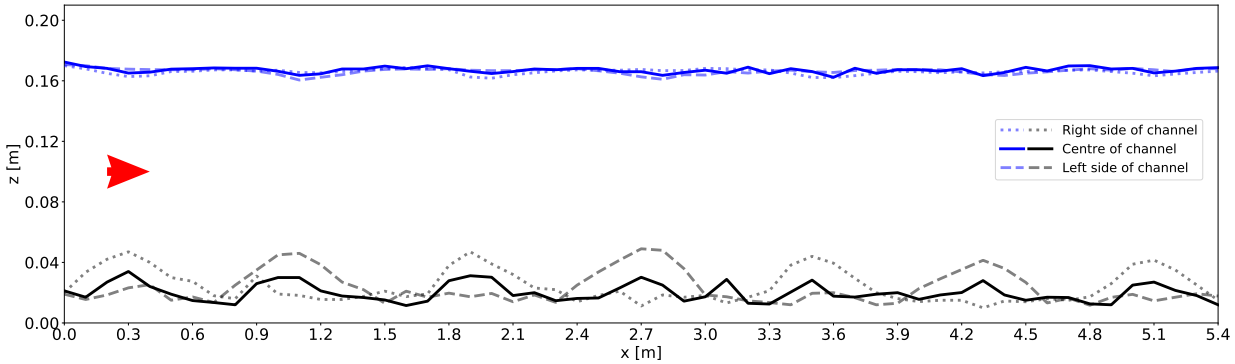

(b) h_{GM}=0.0240 m (GM1.2).

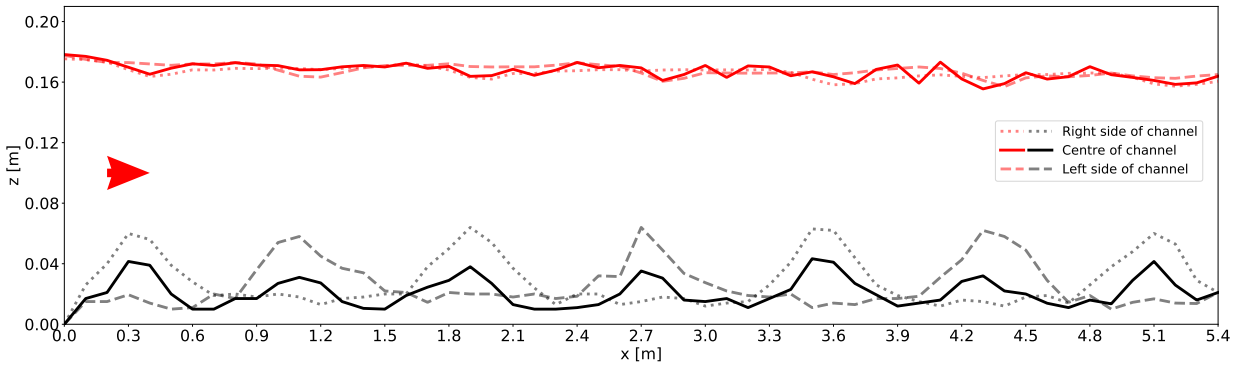

(c) h_{GM}=0.0440 m (GM1.3).

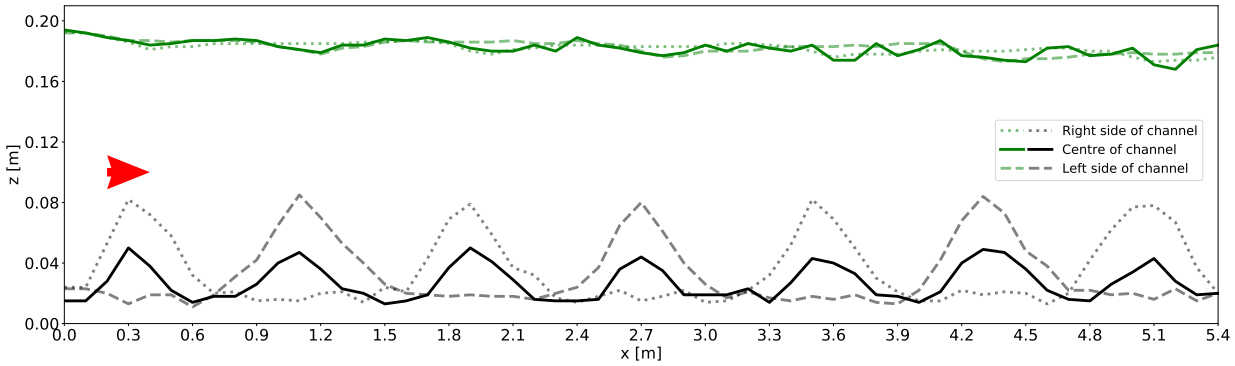

(d) h_{GM}=0.0640 m (GM1.4).

Figure 8: Bed and water surface profiles at the centre and the sides of the channel are here presented in case of channel slope I=0.00200. The flow direction is given by the red arrow.

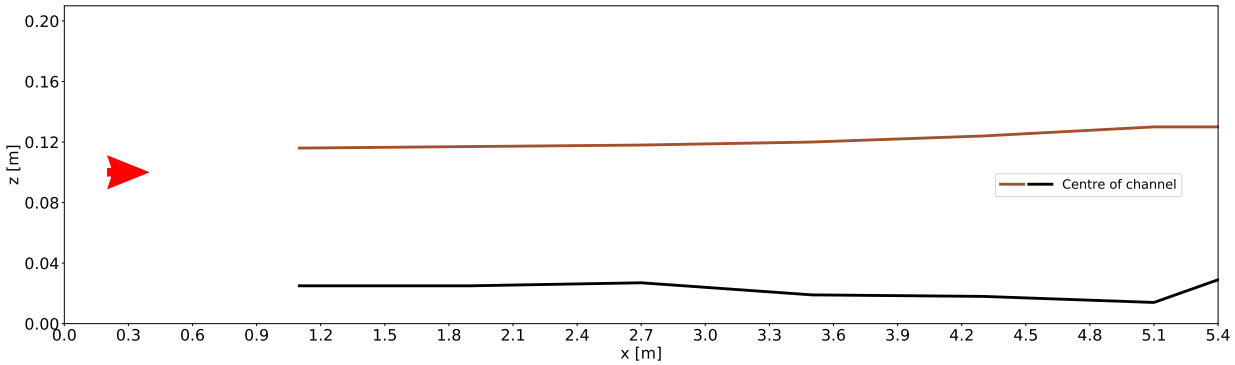

(a) h_{GM}=0.00 m (GM2.1). Measurements were taken only for 1.10≤x (m)≤5.40.

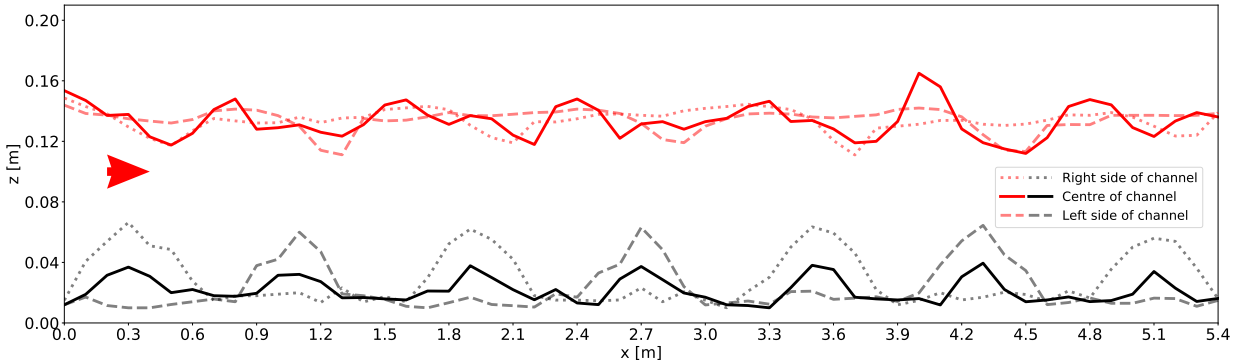

(b) h_{GM}=0.0440 m (GM2.3).

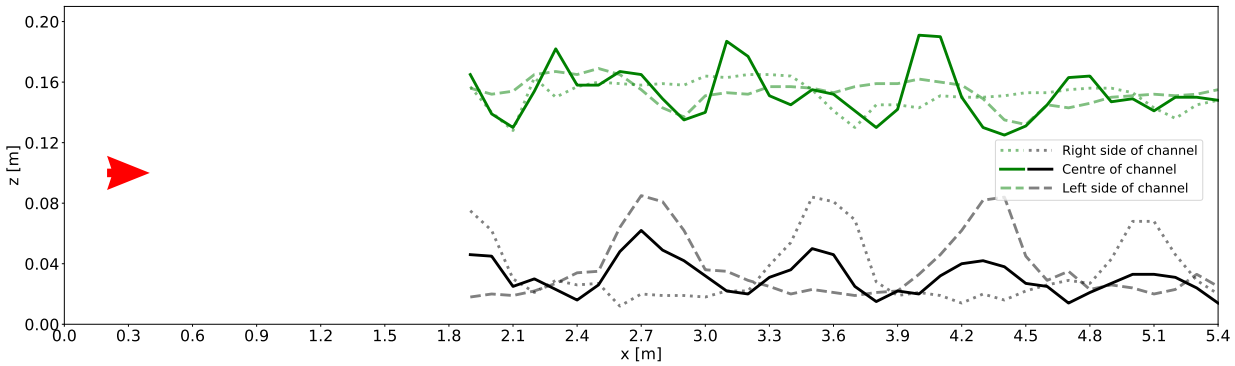

(c) h_{GM}=0.0640 m (GM2.4). Measurements were taken only for 1.90≤x (m)≤5.40.

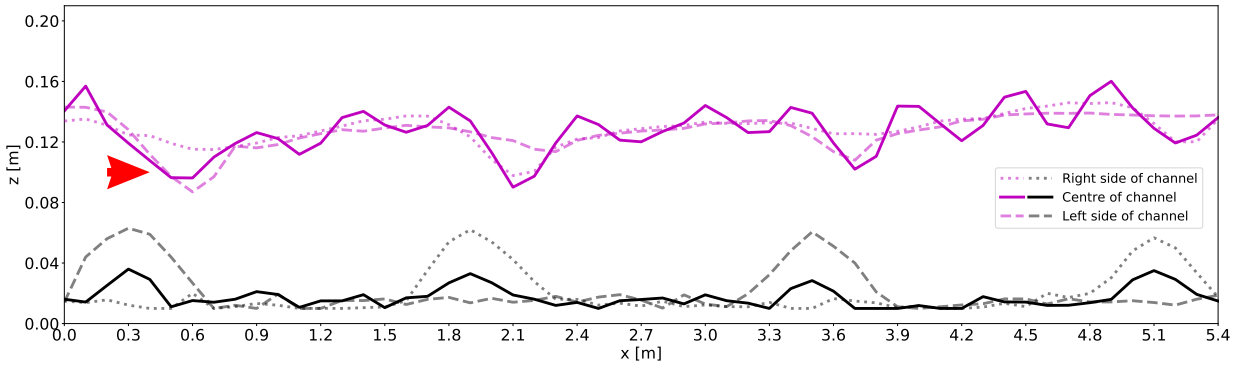

(d) h_{GM}=0.0440 m (GM2.5).

Figure 9: Bed and water surface profiles at the centre and the sides of the channel are here presented in case of channel slope I=0.0100. The flow direction is given by the red arrow.

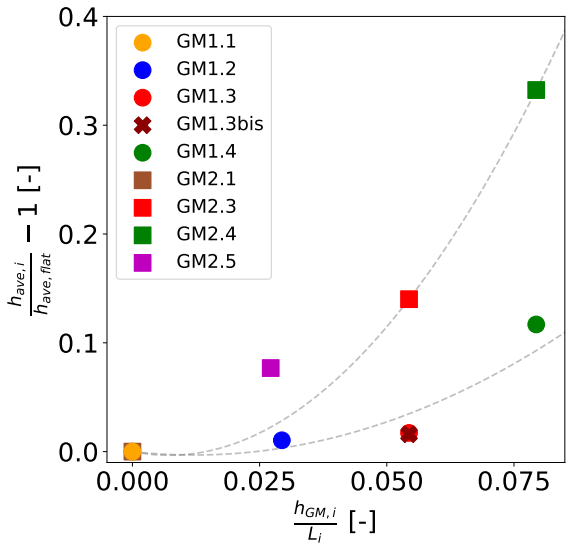

Figure 10: The water surface rise is expressed by the ratio between each experiment's average water depth h_{ave} divided by the average water depth above flat gravel bed conditions $h_{ave,flat}$ (i.e. reference experiments GM1.1 and GM2.1). These ratios are plotted in relationship with gravel mounts' height h_{GM} over the distance between them L. The trends for each channel slope are given by the gray dotted lines.

2.3.2 Vertical velocity profiles

Figures 11 through 19 show the vertical profiles of the time-averaged velocity and the standard deviation of the velocity for each conducted experiment. Near the gravel surface, the values are estimated by fitting the discrete measurement points to the 1st, 2nd or 4th polynomial approximation, depending on the number of available measurements and the performance of the fitting. As described in the Methods 2.2, data are collected for 1.90≤x (m)≤5.10 (3.50≤x (m)≤7.0 for GM2.5) and y=0.00, −0.200, −0.300, −0.380 m. For the experiments with flat gravel bed (i.e. GM1.1 and GM2.1), the gravel bed and water surface measurements are taken only at the centre of the channel (i.e. y=0.00 m) and their profiles are then translated to the other plots. Some plots above the gravel mounts morphology are missing the water surface profile, as these data were not collected there. Refuge able area is defined by the thresholds $\overline{V}$ ≤0.100 m/s and $std(V)$≤ 0.070 m/s, as first introduced in Sub-chapter 1.9. All the gravel surface above the bed thickness h_{bed}=0.0170 m is considered mounts area (Sub-Chapter 1.7). Above flat gravel bed, water flows very homogeneously in both longitudinal an lateral directions, as shown in Figures 11 (GM1.1) and 16 (GM2.1). A refuge able area is found in Figure 11d, although its size so small that it could be considered negligible. Very small changes are observed after the introduction of 0.0240 m high gravel mounts (Figure 12, GM1.2). Only for h_{GM} ≥0.0440 m remarkable flow heterogeneity is shown near the gravel surface. The largest refuge able areas are observed primarily around the sides of the channel (y=−0.300, −0.380 m), where the mounts area is the largest. Also, refuge able areas appear to increase in size with increasing gravel mounts' height, underlying a direct relationship between the two (Figure 13 (GM1.3) and 17 (GM2.3) compared to Figure 15 (GM1.4) and 18 (GM2.4)). Little differences in the results are observed between experiments 1.3 (Figure 13) and 1.3bis (Figure 14), where the upstream width was reduced to 0.200 m. Between the two, the original gravel mount's shape appear to generate slightly bigger refuge able areas. Finally, unsatisfactory results are observed in Figure 19 (GM2.5) where the doubled distance between gravel mounts pushes the water to jump over the mounts instead of meander around them. This cause local flow acceleration on the downstream side of the gravel mounts where the refuge able areas would have been otherwise expected to form.

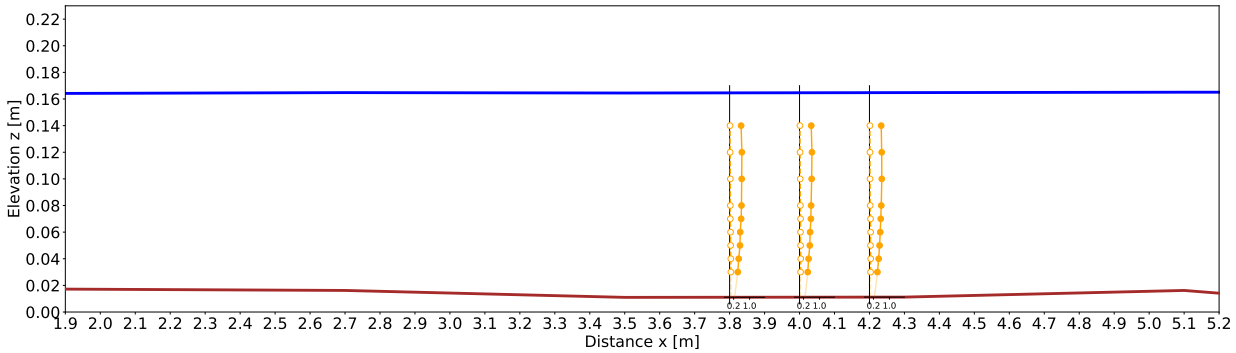

(a) h_{GM}=0.00 m (GM1.1), y=0.00 m.

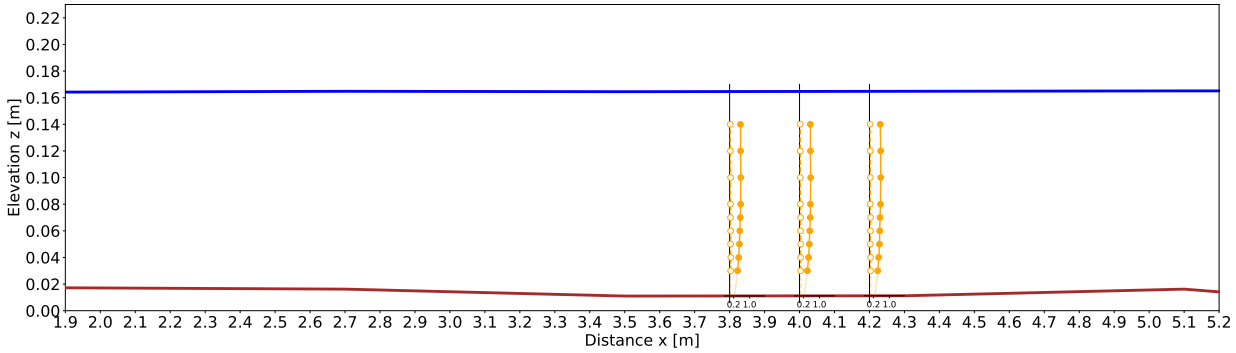

(b) h_{GM}=0.00 m (GM1.1), y=−0.200 m.

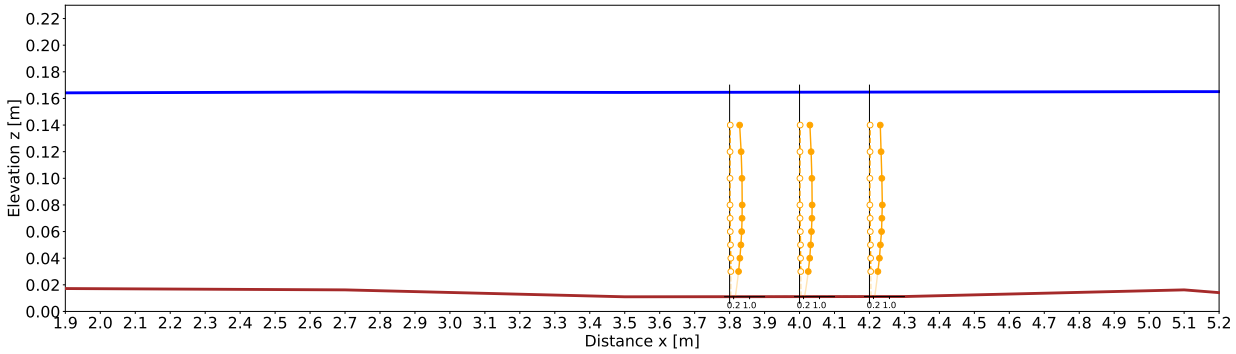

(c) h_{GM}=0.00 m (GM1.1), y=−0.300 m.

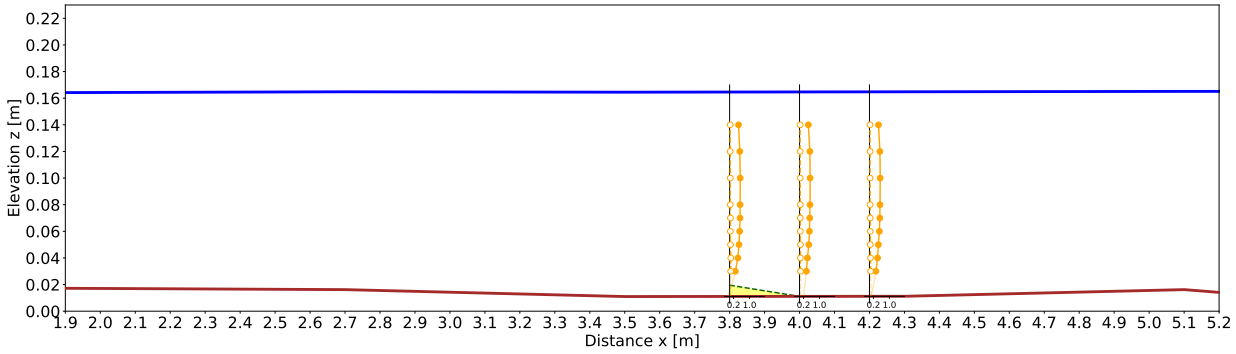

(d) h_{GM}=0.00 m (GM1.1), y=−0.380 m.

Figure 11: Vertical profiles of time-averaged velocity (filled markers) and standard deviation of the velocity (empty markers) for experiment GM1.1. The units of the smaller plots are velocity [m/s] on the x-axis and elevation [m] on the y-axis. The water surface profile is marked in blue and the refuge able areas are highlighted in yellow.

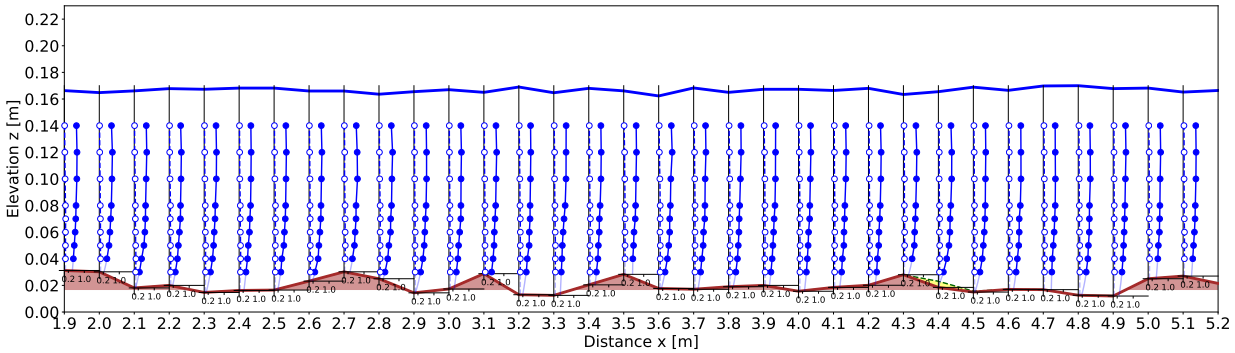

(a) h_{GM}=0.0240 m (GM1.2), y=0.00 m.

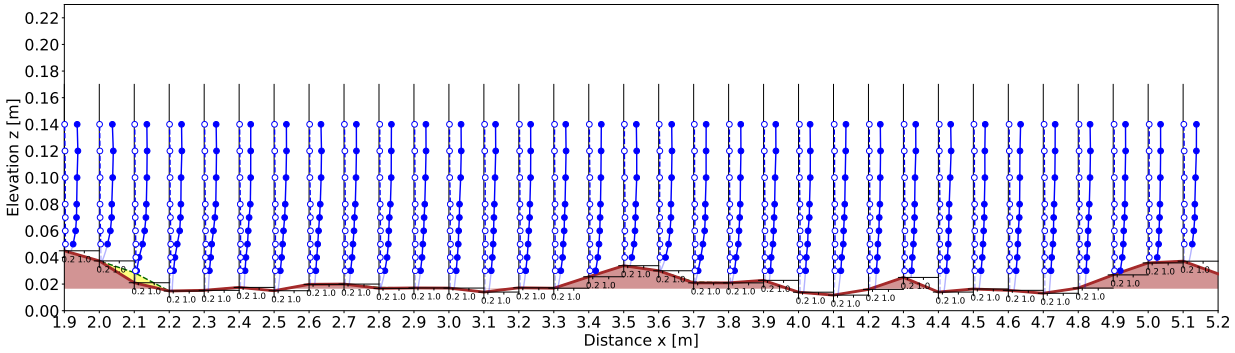

(b) h_{GM}=0.0240 m (GM1.2), y=−0.200 m. The water surface is not measured at this coordinate.

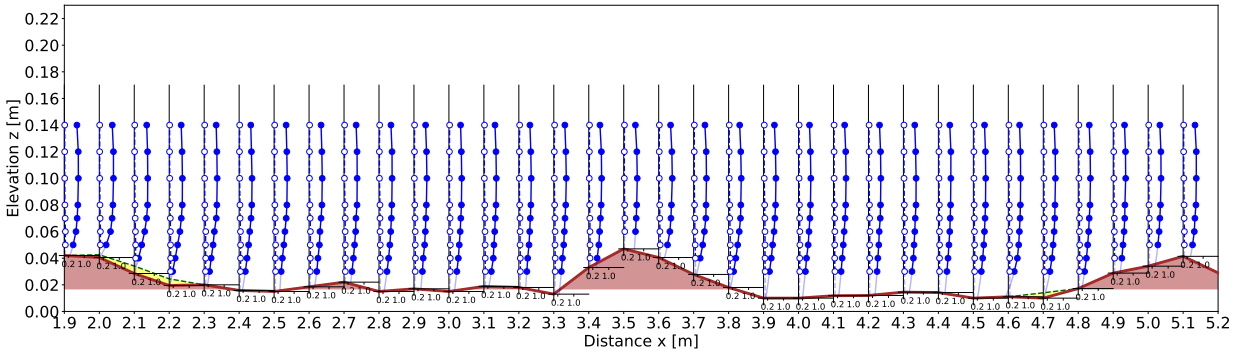

(c) h_{GM}=0.0240 m (GM1.2), y=−0.300 m. The water surface is not measured at this coordinate.

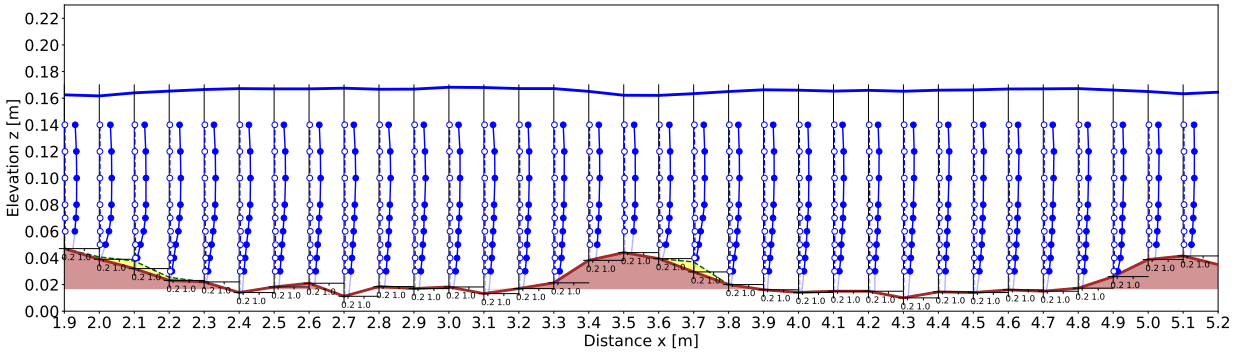

(d) h_{GM}=0.0240 m (GM1.2), y=−0.380 m.

Figure 12: Vertical profiles of time-averaged velocity (filled markers) and standard deviation of the velocity (empty markers) for experiment GM1.2. The units of the smaller plots are velocity [m/s] on the x-axis and elevation [m] on the y-axis. The mounts area is coloured brown, the water surface profile is marked in blue and the refuge able areas are highlighted in yellow.

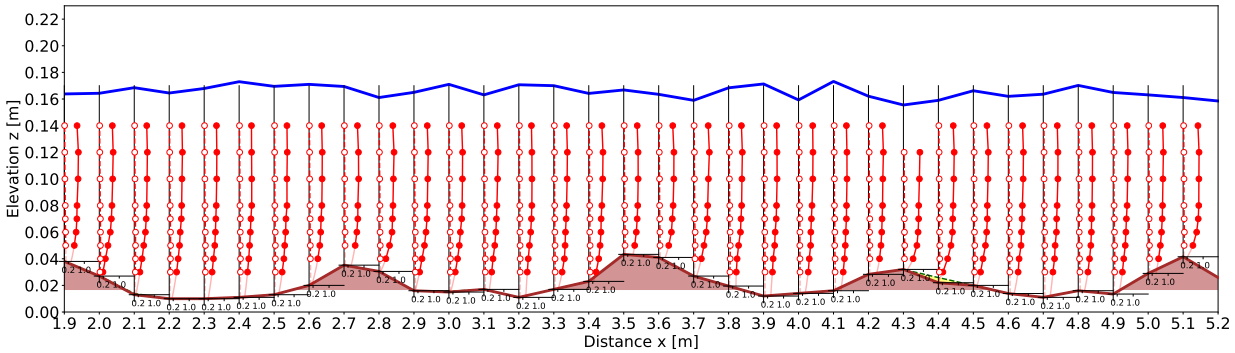

(a) h_{GM}=0.0440 m (GM1.3), y=0.00 m.

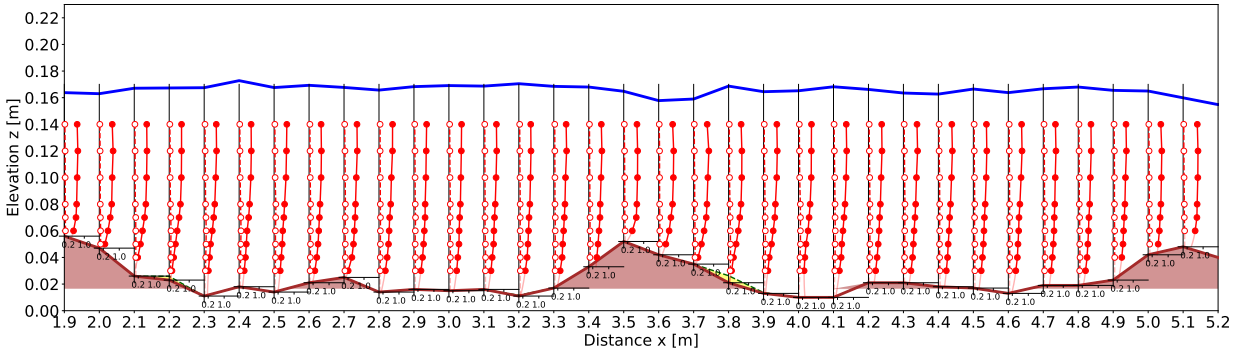

(b) h_{GM}=0.0440 m (GM1.3), y=−0.200 m.

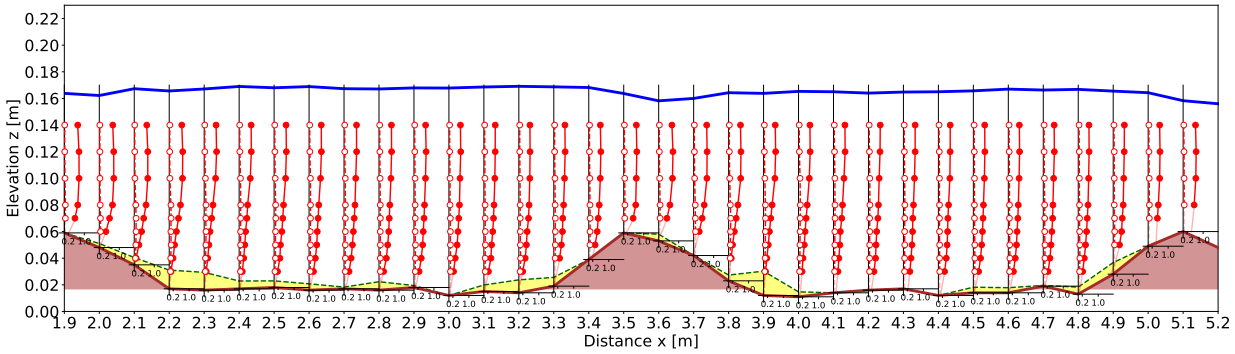

(c) h_{GM}=0.0440 m (GM1.3), y=−0.300 m.

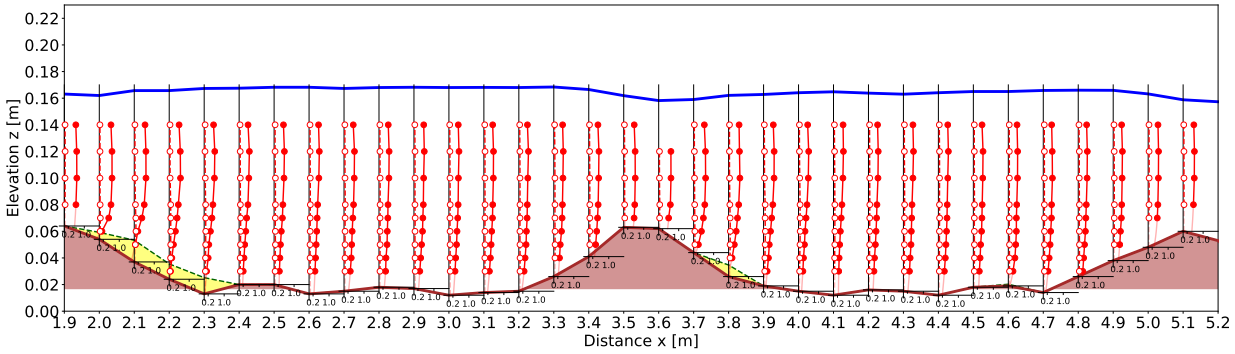

(d) h_{GM}=0.0440 m (GM1.3), y=−0.380 m.

Figure 13: Vertical profiles of time-averaged velocity (filled markers) and standard deviation of the velocity (empty markers) for experiment GM1.3. The units of the smaller plots are velocity [m/s] on the x-axis and elevation [m] on the y-axis. The mounts area is coloured brown, the water surface profile is marked in blue and the refuge able areas are highlighted in yellow.

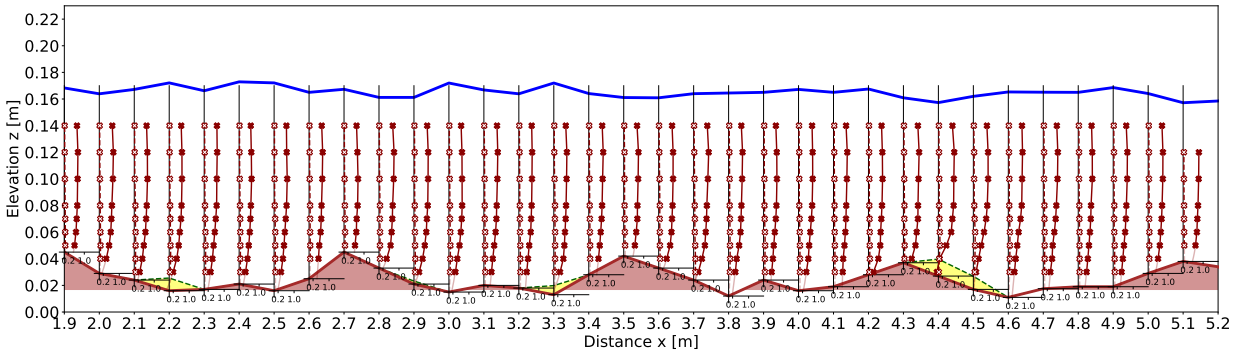

(a) h_{GM}=0.0440 m (GM1.3bis), y=0.00 m.

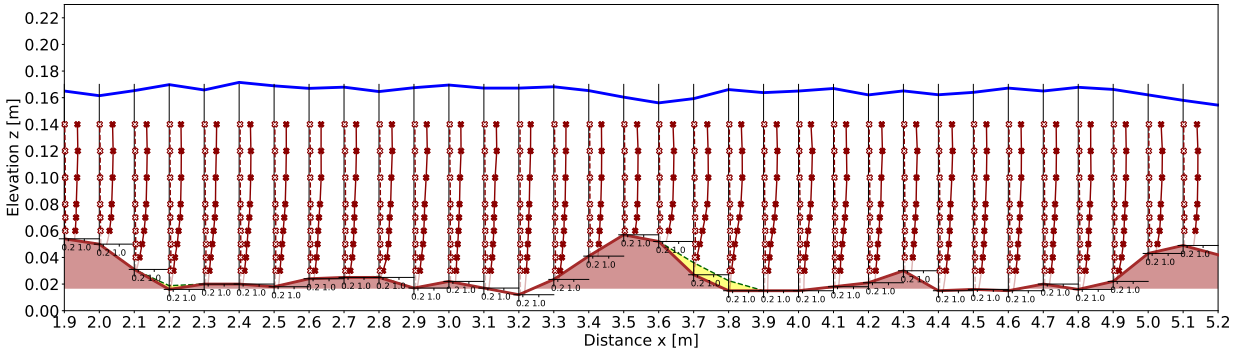

(b) h_{GM}=0.0440 m (GM1.3bis), y=−0.200 m.

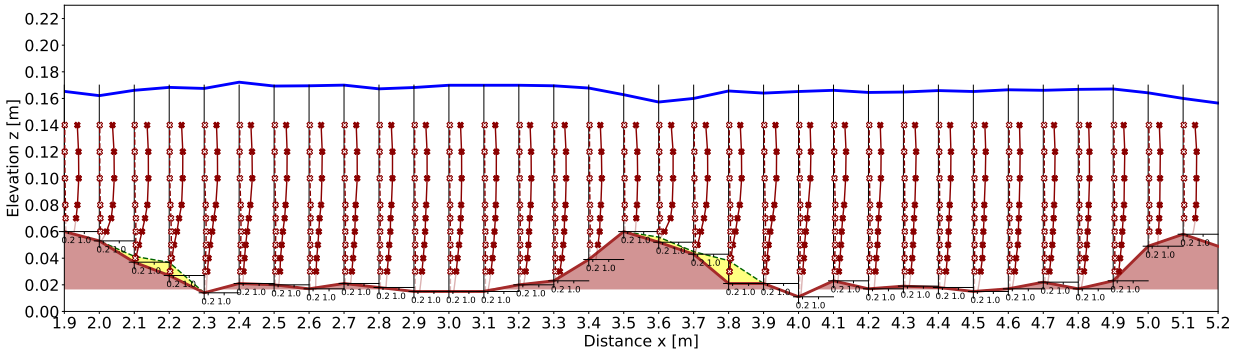

(c) h_{GM}=0.0440 m (GM1.3bis), y=−0.300 m.

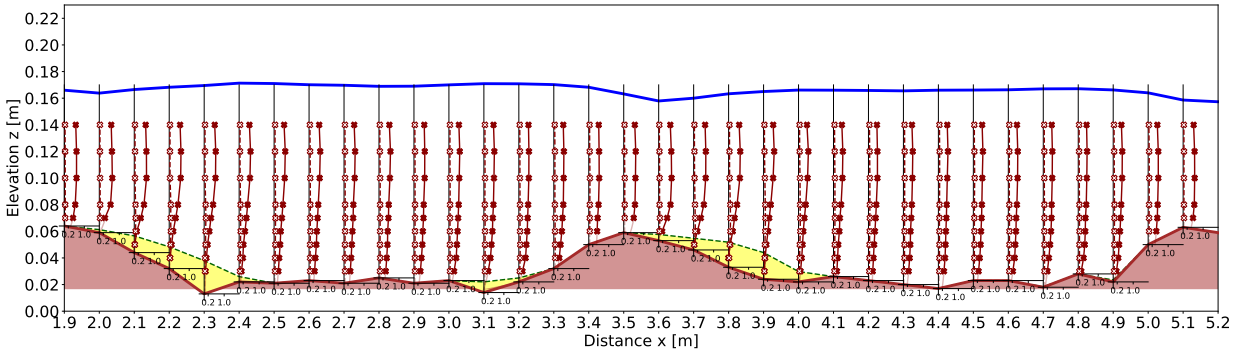

(d) h_{GM}=0.0440 m (GM1.3bis), y=−0.380 m.

Figure 14: Vertical profiles of time-averaged velocity (filled markers) and standard deviation of the velocity (empty markers) for experiment GM1.3bis. The units of the smaller plots are velocity [m/s] on the x-axis and elevation [m] on the y-axis. The mounts area is coloured brown, the water surface profile is marked in blue and the refuge able areas are highlighted in yellow.

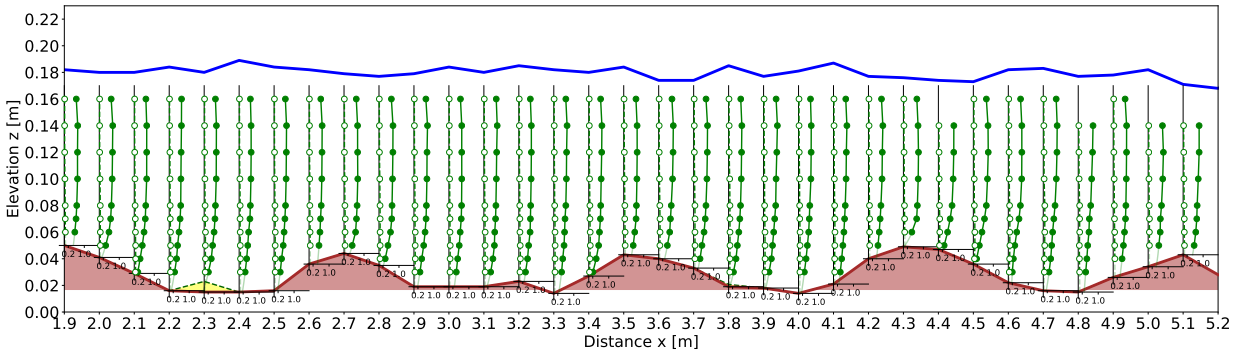

(a) h_{GM}=0.0640 m (GM1.4), y=0.00 m.

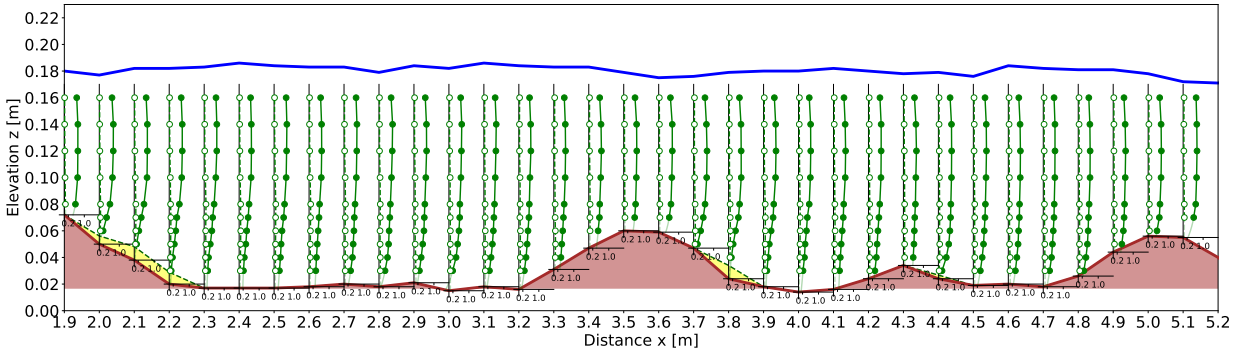

(b) h_{GM}=0.0640 m (GM1.4), y=−0.200 m.

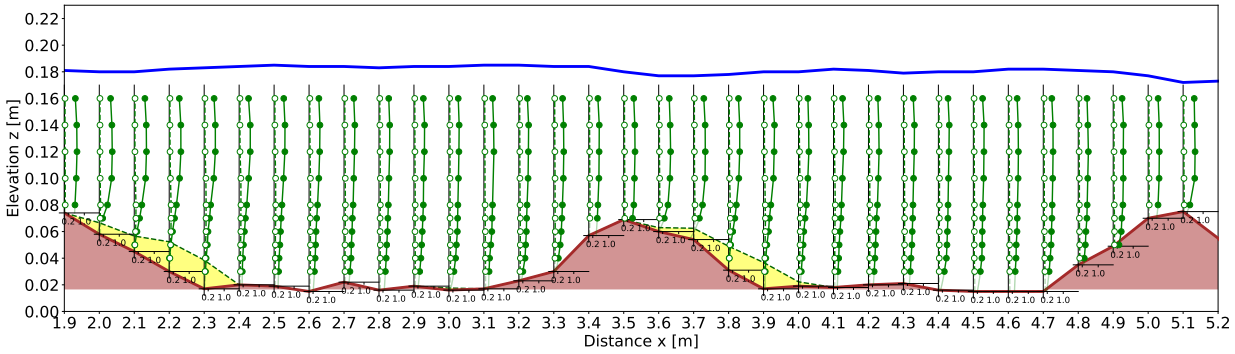

(c) h_{GM}=0.0640 m (GM1.4), y=−0.300 m.

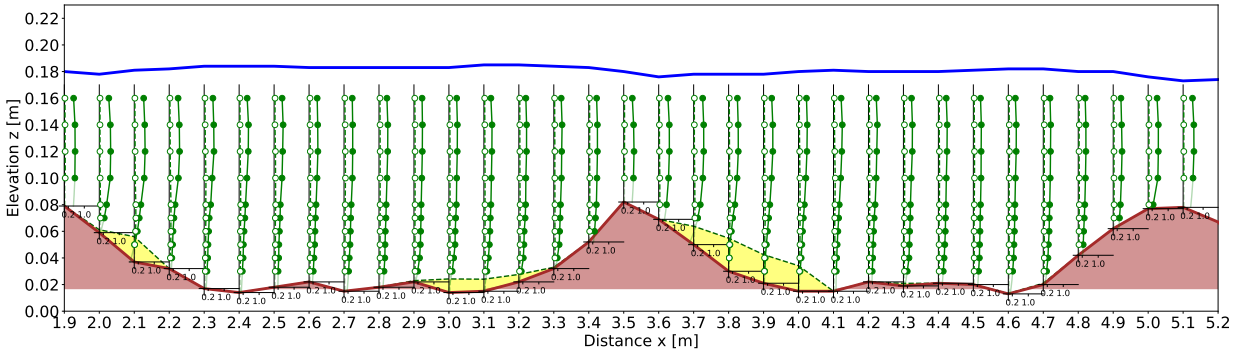

(d) h_{GM}=0.0640 m (GM1.4), y=−0.380 m.

Figure 15: Vertical profiles of time-averaged velocity (filled markers) and standard deviation of the velocity (empty markers) for experiment GM1.4. The units of the smaller plots are velocity [m/s] on the x-axis and elevation [m] on the y-axis. The mounts area is coloured brown, the water surface profile is marked in blue and the refuge able areas are highlighted in yellow.

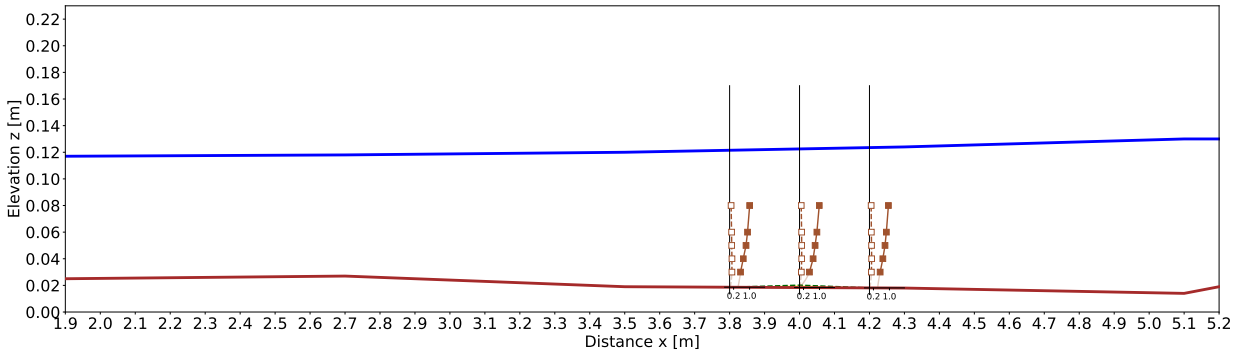

(a) h_{GM}=0.00 m (GM2.1), y=0.00 m.

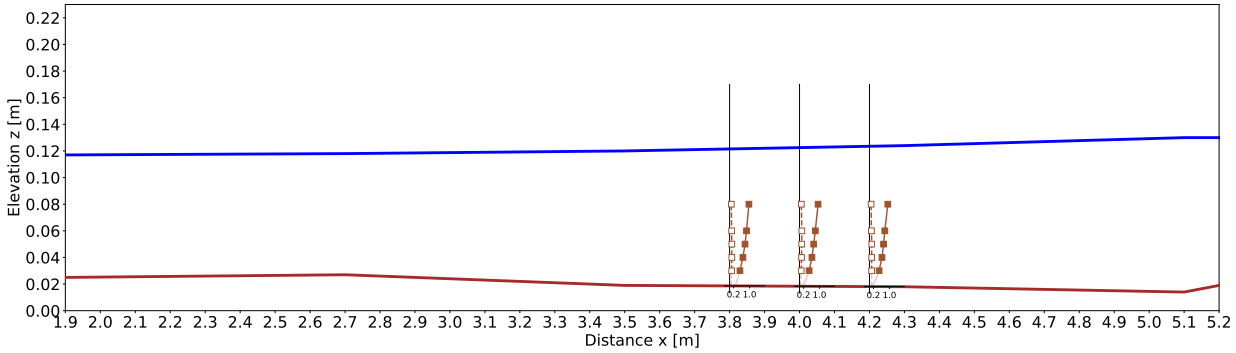

(b) h_{GM}=0.00 m (GM2.1), y=−0.200 m.

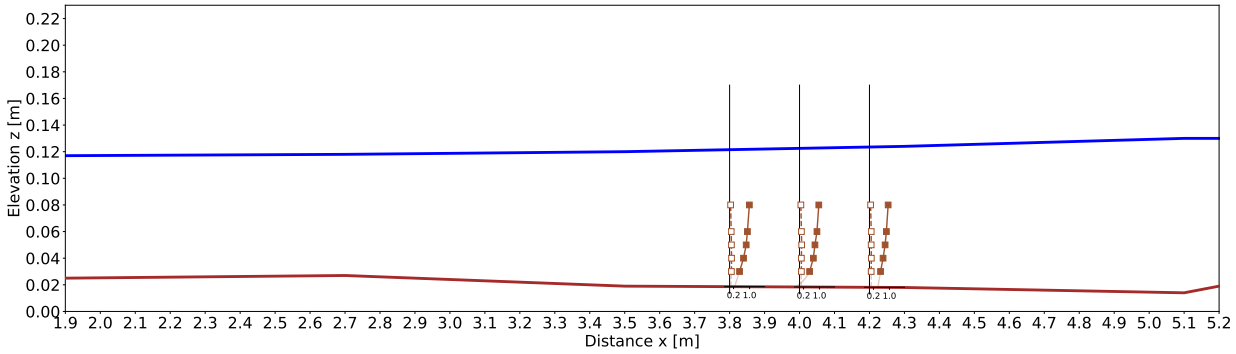

(c) h_{GM}=0.00 m (GM2.1), y=−0.300 m.

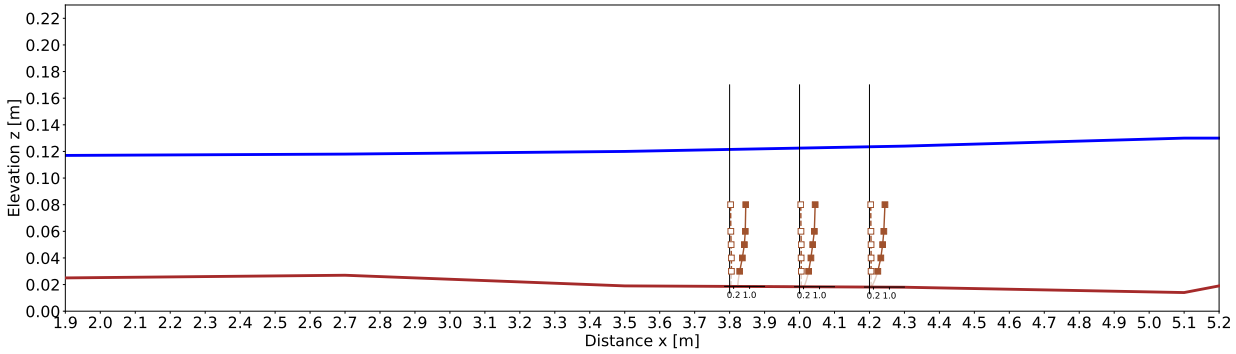

(d) h_{GM}=0.00 m (GM2.1), y=−0.380 m.

Figure 16: Vertical profiles of time-averaged velocity (filled markers) and standard deviation of the velocity (empty markers) for experiment GM2.1. The units of the smaller plots are velocity [m/s] on the x-axis and elevation [m] on the y-axis. The water surface profile is marked in blue and the refuge able areas are highlighted in yellow.

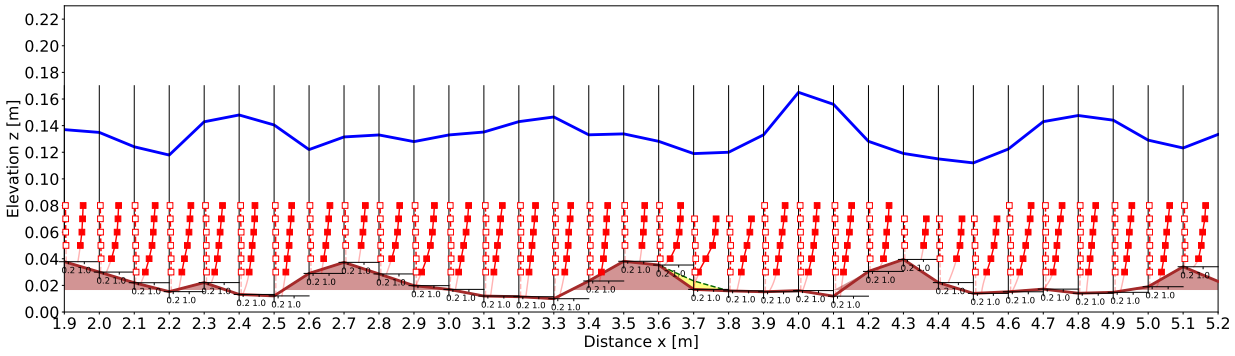

(a) h_{GM}=0.0440 m (GM2.3), y=0.00 m.

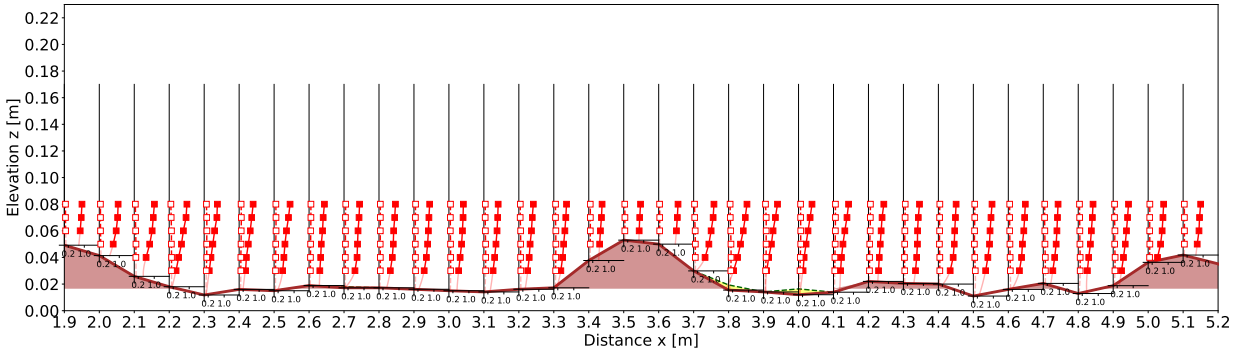

(b) h_{GM}=0.0440 m (GM2.3), y=−0.200 m. The water surface is not measured at this coordinate.

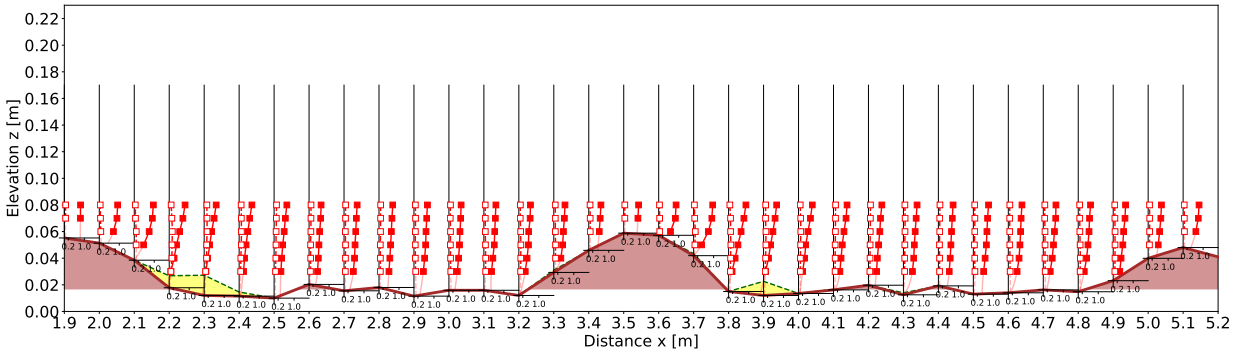

(c) h_{GM}=0.0440 m (GM2.3), y=−0.300 m. The water surface is not measured at this coordinate.

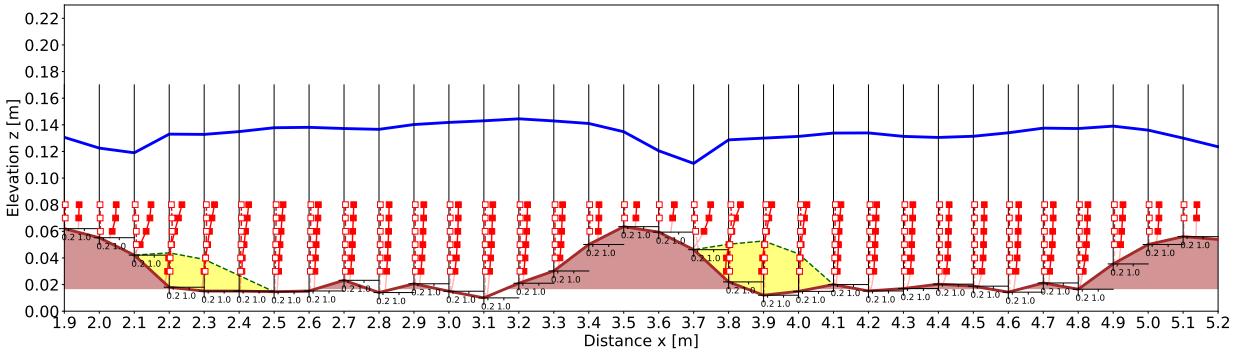

(d) h_{GM}=0.0440 m (GM2.3), y=−0.380 m.

Figure 17: Vertical profiles of time-averaged velocity (filled markers) and standard deviation of the velocity (empty markers) for experiment GM2.3. The units of the smaller plots are velocity [m/s] on the x-axis and elevation [m] on the y-axis. The mounts area is coloured brown, the water surface profile is marked in blue and the refuge able areas are highlighted in yellow.

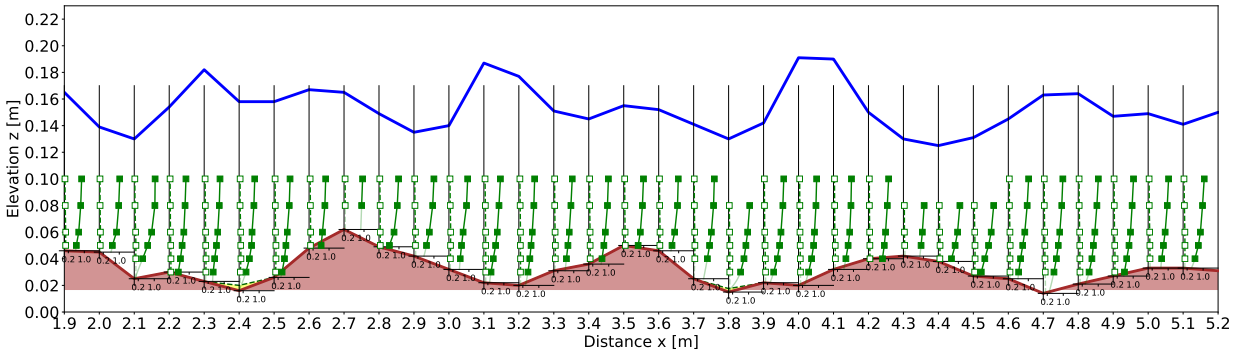

(a) h_{GM}=0.0640 m (GM2.4), y=0.00 m.

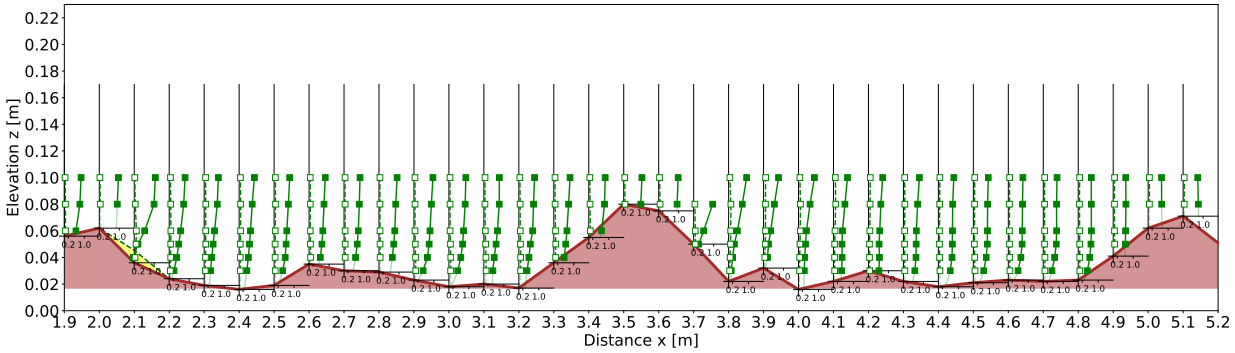

(b) h_{GM}=0.0640 m (GM2.4), y=−0.200 m. The water surface is not measured at this coordinate.

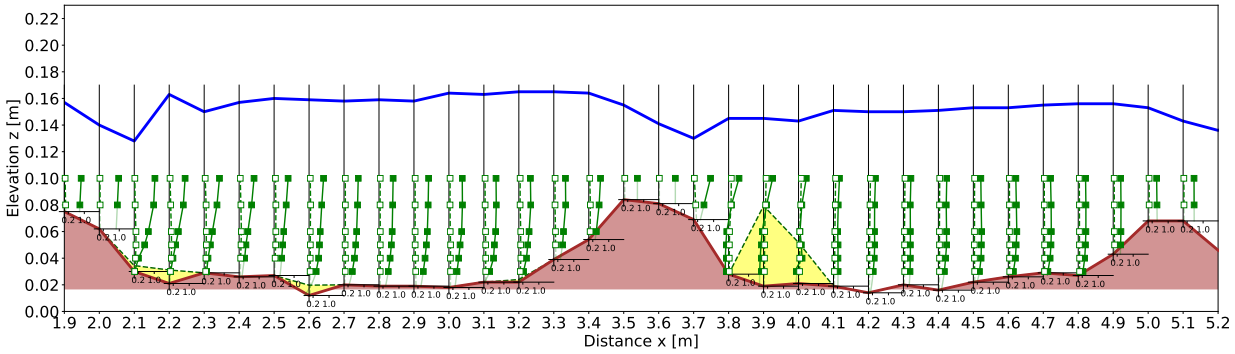

(c) h_{GM}=0.0640 m (GM2.4), y=−0.300 m.

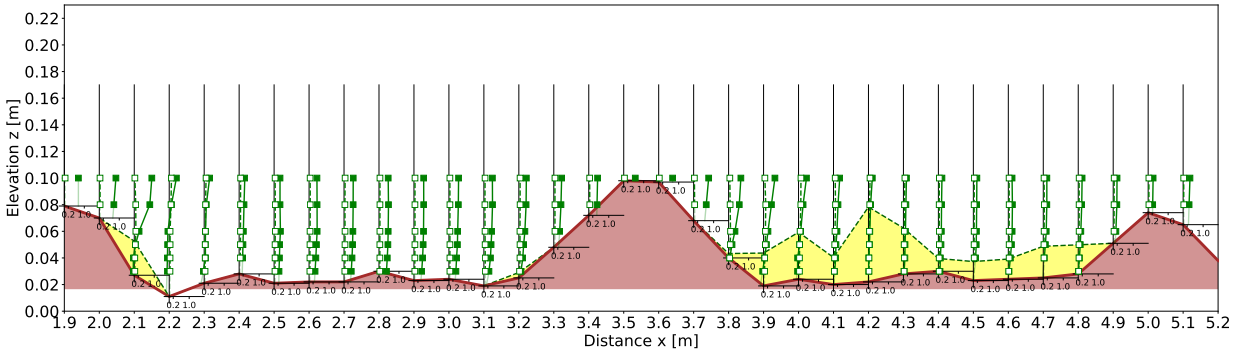

(d) h_{GM}=0.0640 m (GM2.4), y=−0.380 m. The water surface is not measured at this coordinate.

Figure 18: Vertical profiles of time-averaged velocity (filled markers) and standard deviation of the velocity (empty markers) for experiment GM2.4. The units of the smaller plots are velocity [m/s] on the x-axis and elevation [m] on the y-axis. The mounts area is coloured brown, the water surface profile is marked in blue and the refuge able areas are highlighted in yellow.

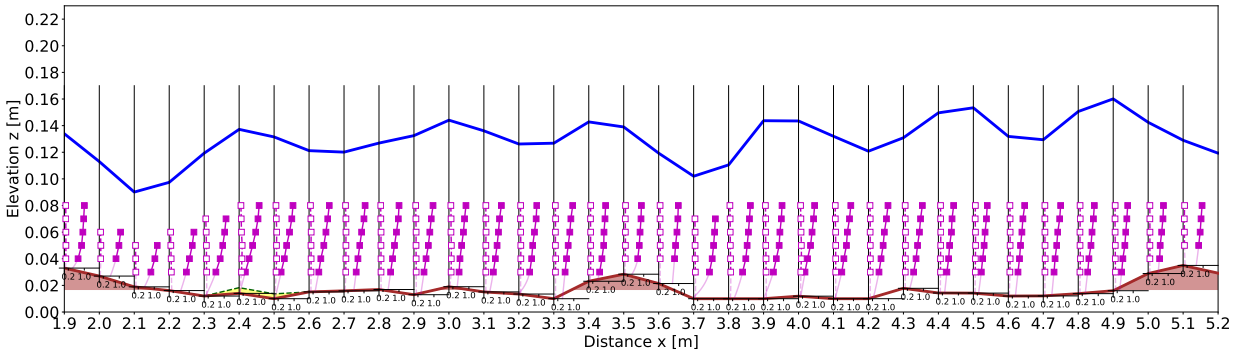

(a) h_{GM}=0.0440 m (GM2.5), y=0.00 m.

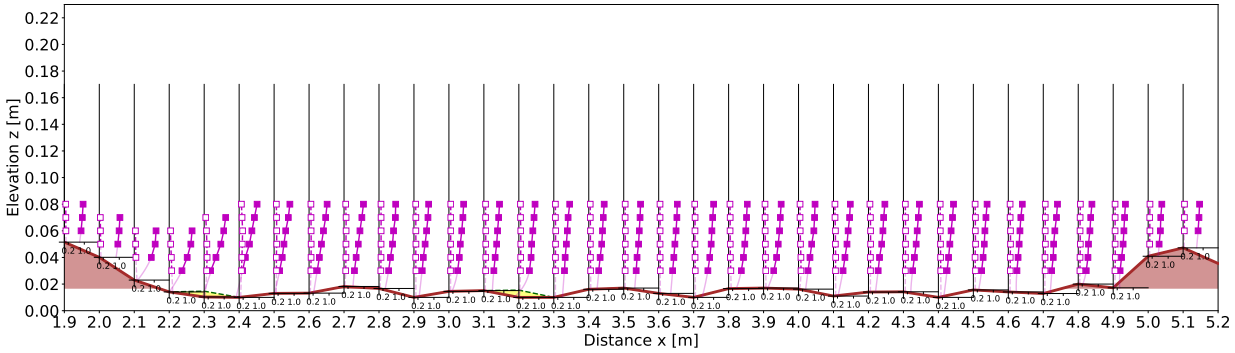

(b) h_{GM}=0.0440 m (GM2.5), y=−0.200 m. The water surface is not measured at this coordinate.

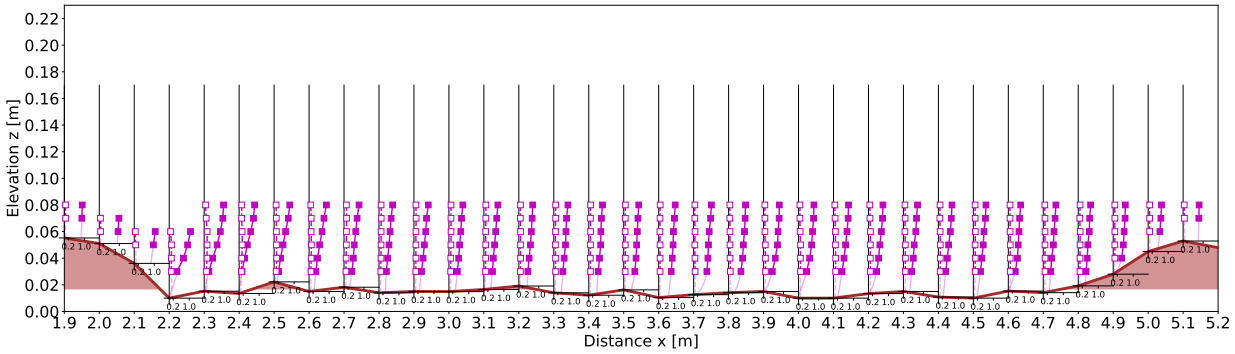

(c) h_{GM}=0.0440 m (GM2.5), y=−0.300 m. The water surface is not measured at this coordinate.

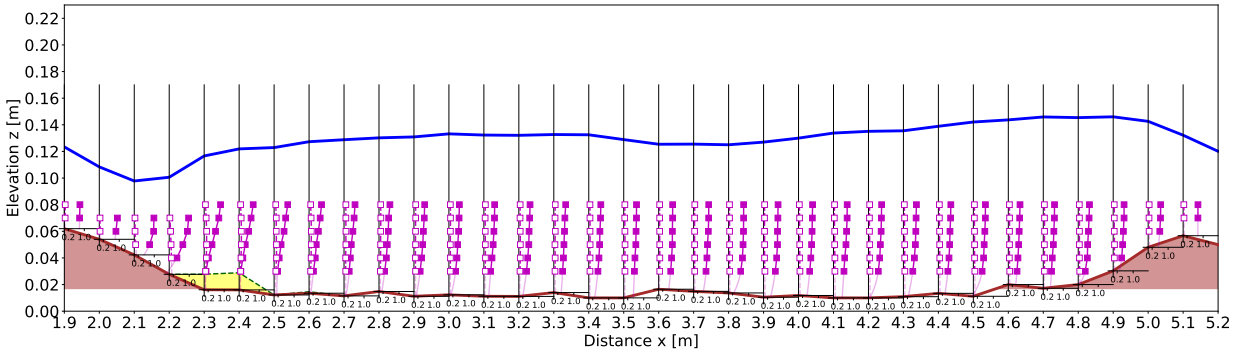

(d) h_{GM}=0.0440 m (GM2.5), y=−0.380 m.

Figure 19: Vertical profiles of time-averaged velocity (filled markers) and standard deviation of the velocity (empty markers) for experiment GM2.5. The units of the smaller plots are velocity [m/s] on the x-axis and elevation [m] on the y-axis. The mounts area is coloured brown, the water surface profile is marked in blue and the refuge able areas are highlighted in yellow.

2.3.3 Refuge able volume and mounts volume

The mounts volume and the refuge able volume are calculated inside the measurement area $1.90 \leq x$ (m)≤ 5.10 and $-0.380 \leq y$ (m)≤ 0.00 and the results are shown in Table 6. As explained in Sub-chapter 1.9, interstice volume is not considered for gravel mounts.

Table 6: Mounts volume V_{GM} [10^{-4} m^3], refuge able volume V_{RA} [10^{-4} m^3] and the relative suitable volume $100 \cdot \frac{V_{RA}}{V_{GM}}$ [%] are shown for each experiment.

	GM1.1	GM1.2	GM1.3	GM1.3bis	GM1.4	GM2.1	GM2.3	GM2.4	GM2.5
V_{GM} [m^3]	0.00	60.00	90.00	110.00	160.00	0.00	90.00	200.00	40.00
V_{RA} [m^3]	0.300	4.00	16.00	16.00	23.00	0.400	12.00	24.00	3.00
$100 \cdot \frac{V_{RA}}{V_{GM}}$ [%]	-	7	18	14	14	-	14	12	8

Table 6 confirms the remarks written observing the vertical velocity profiles: above flat gravel bed morphology there are very small refuge able volume; slightly less negligible but still small is the refuge able volume formed around the 0.0240 m high gravel mounts of experiment GM1.2. From that point on, the extent of the refuge able volume grows with the mounts volume and height h_{GM}, as the overall largest volumes is observed for h_{GM}=0.0640 m in experiments GM1.4 and GM2.4. The relationship does not appear to be linear, because the best relative suitable volumes per unit gravel mount is found for h_{GM}=0.0440 m of experiments GM1.3 and GM2.3. The modified upstream width of experiment GM1.3bis is inferior to this result. Finally, experiment GM2.5 confirms the previous negative observations and the results show significantly smaller refuge able volume than experiment GM2.3. In Table 6, no significant difference is observed between experiments conducted above channel slope I=0.00200 or I=0.0100. When studying the formation of refuge able areas, the gravel mounts' height appear to be a much more important parameter than the channel slope.

2.3.4 Discharge Q=0.155 m^3/s

Under medium-sized flood Q=0.0588 m^3/s, the gravel stability is confirmed for all experiments except GM2.5. To toughen the hydraulic conditions, three experiments are tested again under the pump capacity discharge. Model GM2.4 was constructed before the improvement works on the channel's pumps and because of it the maximal allowed discharge is Q=0.123 m^3/s, while experiments GM1.3 and GM2.3 are tested under discharge Q=0.155 m^3/s. All three times, only qualitative measurements of the water depth at the sides of the channel and photographic material are taken. A selection is shown in Figure 20.

(a) Water surface above model GM1.3 for Q=0.155 m^3/s.

(b) Side view of the water surface above a gravel mount (model GM2.4) for Q=0.123 m^3/s.

(c) Gravel eroded downstream for Q=0.155 m^3/s (model GM1.3).

Figure 20: Hydraulic conditions under large-sized flood stages. Flow direction is always from right to left.

Despise the short duration of the tests with large-sized flood stages (about half an hour), the changes in the flow field are immediate to see. The water depth increases due to the bigger discharge, with large waves now forming along both the centre part and the sides of the channel (Figures 20a and 20b). Inside the gravel bed, grain shaking becomes more common, as does widespread short- and long-distance transport. The grains flushed downstream of the installation area (Figure 20c) primarily come from the gravel bed around the centre of the channel between gravel mounts. The grains on the gravel mounts are generally seen rolling on the downstream side, thus flattening the model's surface. Again, the effects appear to become more significant in case of steeper channel slope I=0.0100 than I=0.00200. Based of these observations, the gravel mounts' stability can not be guaranteed for any of the three experiments where the large-sized flood stage is tested.

2.4 Conclusions

The introduction of alternated gravel mounts inside channelized rivers causes waves to forms in the centre part of the channel, the average water surface to rise, the Froude number to sink and the water heterogeneity to increase. Behind each gravel mounts and close to the gravel surface, pockets are created where the assumed conditions for refuge are met. The size of the refuge able areas appear to be directly proportional to the gravel mounts' size, therefore the maximal extent is usually observed at the channel's sides. Results suggest that the gravel mounts' height is the primary parameter that affects the average surface rise and the size of the refuge able volume. For the former, their relationship is exponential, with the growth rate related to the channel slope steepness. For the latter, the relation is less straightforward, as the best relative suitable volumes per unit gravel mount $V_{RA}/V_{GM} \cdot 100$ =14% and 18% are found in the case of h_{GM}=0.0440 m (experiments GM1.3 and GM2.3, respectively). Considering also the limited water elevation rise observed above these same experiments, h_{GM}=0.0440 m is considered, for the purposes of this research chapter, as the optimal height of the gravel mounts. In general, harsher flow conditions appear to be created when the steepness of the channel slope is larger.

Further results suggest that modifications of the gravel mounts' morphology might not be necessary, nor useful. The reduction of the upstream width in experiment GM1.3bis almost always produces the same, when not inferior, results observed around the unmodified gravel mounts of experiment GM1.3. Doubling the distance between gravel mounts reduces their effect on the flow field, returning the hydraulic characteristics closer to what has been observed above flat gravel bed. Finally, the stability of the model can be confirmed for medium-sized flood stages, but not when the discharge is increased above that point.

A quick summaries of the main discoveries of this chapter are shown here:

- The introduction of gravel mounts causes the Froude number to sink, the average water depth to increase and the flow to become more heterogeneous;
- The water surface above alternated gravel mounts is wavy in the centre part and generally flat along the sides;
- The amplitude of the waves, as well as the increase of the average water depth appear to be directly related to the gravel mounts' height;
- The relationship between water surface rise and gravel mounts' height is considered to be exponential, which growth rate is related to the channel slope steepness;
- Behind each gravel mount and near the gravel bed, suitable hydraulic conditions for refuge are expected to be met;
- The size of the generated refuge able volume appear to be related to the mounts volume, which in turn is directly related to the gravel mounts' height;
- The channel slope steepness seems to be less important in the formation of refuge able areas than the height of the gravel mounts;

- It is not recommended to change any parameter of the model's morphology besides the height, as their impact on the formation of refuge able area is expected to be minimal when not counter-productive;
- The best relative suitable volume per unit gravel mount is observed for height h_{GM}=0.0440 m, although the suitable volume is, at best conditions, smaller than a fifth of the mounts volume;
- Based on this, h_{GM}=0.0440 m is considered to be the optimal height for gravel mounts inside straight rivers, whatever the slope steepness might be.
- The proposed gravel mounts' design remains stable in case of medium-sized floods, but collapses when tested under the stress of large-sized floods.

2.5 From this point onward

Although the creation of refuge able areas is confirmed by the experimental results, their size has never been found larger than a fifth of the mounts volume. The exponentially rising water surface causes concern to the discharge capacity of the straight channel and the subsequent higher risk of overflowing. Furthermore, the proposed model morphology has shown clear deficiencies when faced with the hydraulic forces of large-sized flood stages. Future research should focus on improving the gravel mounts performance while reducing the hydraulic friction between them and water flow. The improved gravel mount should be smaller and more stable, while at the same time being able to generate the same or even larger refuge able areas per unit mount observed so far.

3 Assembled boulders groynes

3.1 Introduction

Based on the results presented in the previous chapter, the main drawbacks of triangular gravel mounts appear to be: the structural instability under large-scaled flood stages, the small total suitable volume generated, the wavy water surface and the rise of the water level. Aiming to improve all these aspects, the research proposes to replace the tested morphology with rectangular boulders groynes assembled on on top of each others in three layers.
This chapter analyses the flow conditions around the new design and compares its performance with what has been learned studying the triangular gravel mounts. Experiments were conducted between July and November 2021 and the main results have been presented at the 39$^{\text{th}}$ IAHR World Congress (Beretta Piccoli and Yasuda (2022) [5]).

3.2 Methods

In continuation with the previous experiments, the installation area remains 5.40 m long and still uses coarse gravel G1 gravel for the gravel bed. The bed thickness is h_{bed}=d_{50}=0.0170 m (one single layer) in experiment AB2 or h_{bed}=0.0400 m (multi-layered) for all other experiments. The increase of the bed thickness (Figures 22c and 22e) brings significant stability improvements, as better explained in Sub-chapter 5.1. Experiment AB1 is characterized by a simple 0.040 m thick flat gravel bed. For the other experiments, seven boulders groynes are built over the gravel bed on alternated sides of the channel every L=0.800 m apart (i.e. at the same coordinates where the gravel mounts were placed). Each boulders groyne is rectangular-shaped with transversal length L_{GM}=0.600 m, width W=0.200 m and height h_{GM}=0.0440 m (in conformity to the previous chapter's results). Differently to the triangular gravel mounts, the height is kept constant along each groyne's transverse length. Each time, three layers of medium boulders B1 (d_{50}=0.0630 m) are placed on top of each others like fallen dominoes facing downstream. The first layer is partially buried inside the gravel bed with an general inclination of 20°-30° from the horizontal. The second and third layers are added on top of it (upstream side) with bigger steepness angles and also partial buried in the gravel. Figures 22b and 22c show the cross section of an installed boulders groyne. For model AB4, all features of AB3 are kept with the exception of the reduction of the transverse length to L_{GM}=0.350 m and the installation of further assembled boulders structures along both sides of the channel. To construct these, the same method is applied, although the boulders are now placed like fallen dominoes facing inward in the channel. The height h_{sides}=0.0400 m and the width W_{sides}=0.180 m are kept along the entire length of the model. Figures 21c and 22d show the modified design. The flat gravel bed of experiment AB1 is used as reference to assess the changes in the hydraulic conditions after the installation of assembled boulders constructions in models AB3 and AB4, while in the case of AB2, the previously presented experiment GM2.1 is used since they share the same bed thickness. In continuation with the previous chapter, a metal bar is consistently placed at the downstream end of each model. The channel slope and discharge are I=0.0100 and Q=0.0588 m^3/s (medium-sized flood stage according to Table 1), respectively. Pictures of the models are shown in Figures 21 and 22, while each experiment's characteristics are summarized in Table 7. Definition sketches of the installation areas are shown in Figures 24 (AB2 and AB3) and 25 (AB4).
In experiment AB1, bed elevation and water level are measured in seven points along the centre of the channel (x=1.10, 1.90, 2.70, 3.50, 4.30, 5.10, 5.40 m and y=0.00 m), while velocity measurements are conducted at coordinates x=2.20, 2.40, 2.60 m and y=−0.380, −0.300, −0.200, −0.100, 0.00 m every 0.0100 m in z-direction between the gravel bed and the water surface. For all other experiments, the bed elevation is measured every 0.100 m (0.0500 m when above a gravel mount) in x-direction for 0.00≤x (m)≤5.40 and y-coordinate y=−0.380, −0.300, −0.200, −0.100, 0.00, 0.100, 0.200, 0.300, 0.380 m, while the water level is assessed every 0.100 m in x-direction for 0.00≤x (m)≤5.40 and y=−0.380,

0.00, 0.380 m. The flow velocity is measured every 0.0100 m in z-direction within the water depth and the measurement grid depends on the experiment: for AB2, data are collected for $1.90 \leq x$ (m)≤ 5.10 and y=−0.380, −0.300, −0.200, 0.00 m; for AB3 two separate flow areas are researched for $1.10 \leq x$ (m)≤ 3.10 and y=0.200, 0.300, 0.038 m and for $1.90 \leq x$ (m)≤ 3.90 and y=−0.380, −0.300, −0.200 m. The two areas are joint at y=0.00 m where the data are collected between $1.10 \leq x$ (m)≤ 3.90. The same grid is used during experiment AB4, with the only difference being that this time the measurements are collected at y=±0.100 m instead of y=±0.300 m due to the installation of the assembled boulders along the sides of the channel.

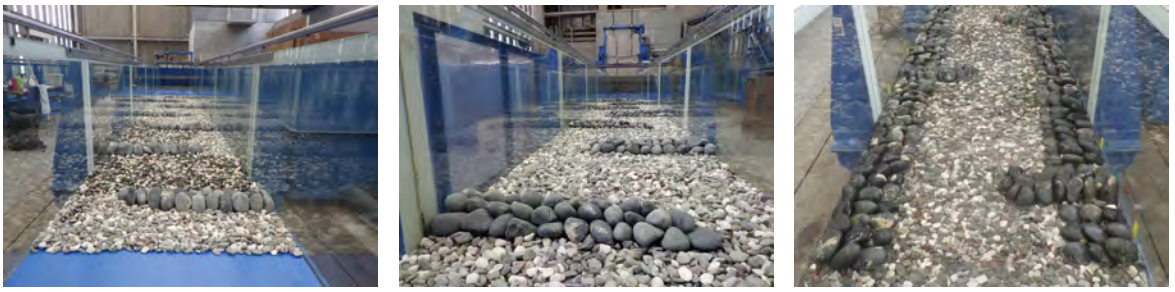

(a) AB2 (from upstream). (b) AB3 (from downstream). (c) AB4 (from upstream).

Figure 21: View of the installation areas of models AB2 (left), AB3 (centre) and AB4 (right).

(a) h_{bed}=0.0400 m (AB1). (b) h_{bed}=0.0170 m (AB2). (c) h_{bed}=0.0400 m (AB3).

(d) h_{bed}=0.0400 m and side assembled boulders construction (AB4). (e) Aerial view of a assembled boulders construction (AB3).

Figure 22: Side view (upstream always on the right) of the different assembled boulders' models (a-d). A boulders groyne viewed from above (flow dicterion from bottom to top) is presented in (e).

Table 7: Main characteristics of this chapter's experiments.

ID	h_{GM} [m]	L_{GM} [m]	W [m]	L [m]	h_{bed} [m]	d_{50} [m]	I [-]	Q [m^3/s]
AB1	0.00	0.00	0.00	0.00	0.0400	0.0170	0.0100	0.0588
AB2	0.0440	0.600	0.200	0.800	0.0170	0.0630	0.0100	0.0588
AB3	0.0440	0.600	0.200	0.800	0.0400	0.0630	0.0100	0.0588
AB4	0.0440	0.350	0.200	0.800	0.0400	0.0630	0.0100	0.0588
AB4 (sides)[1]	0.0400	5.40	0.180	-	0.0400	0.0630	0.0100	0.0588

[1] In this experiment, three further layers of assembled boulders are constructed on both sides of the channel.

3.2.1 Estimation of empty spaces inside assembled boulders constructions

As mentioned in Sub-chapter 1.9, assembled boulders constructions have a porosity n=0.300 and the empty spaces could act as area of refuge for the target small-sized fishes (Table 8). Here is described how this value has been found.
Three 0.400 m long, 0.200 m wide and 0.0440 m high, rectangular, three-layered boulders groynes are constructed on top of a 0.0400 m thick flat gravel bed (i.e. similar conditions to experiments AB3 and AB4), as shown in Figure 23a. Elevation is measured every 0.0400 m across both each construction's width and transverse length, firstly with the installed boulders (Figure 23b) and then after their removal (Figure 23c). From the height difference between the two measurements, the total construction volume V_{GM_T} is found. The volume of the assembled boulders V_{GM} is found using the equivalent water volume method: the boulders of each construction are places in separate buckets (Figure 23d) that are then filled with water (Figure 23e); the boulders are then removed and the buckets, now containing just water, are weighted; finally, the buckets are filled once more with water and weighted again. The difference between the two masses multiplied by the density of water (ρ_w=1000.00 kg/m^3) gives the water volume equivalent of the removed assembled boulders. In the final step, the volume of the empty spaces (i.e. the interstice volume V_I) is found by the difference between the total construction volume minus the volume of the assembled boulders. Each step of the process is repeated three times to improve the results' accuracy.

(a) Aerial view of one of the three boulders groynes.

(b) The same construction, seen from aside.

(c) The same construction, seen from aside after removing boulders.

(d) A bucket full of boulders is weighted.

(e) A bucket filled with boulders and water is weighted.

(f) The working environment during the measurements.

Figure 23: Pictures collected during the estimation of the empty spaces inside boulders groynes.

Table 8: Experimental results for the estimation of empty spaces in boulders groynes. The porosity n [-] is found by the division of interstice volume V_I [^{3}] over total construction volume V_{GM_T} [^{3}].

ID	V_{GM_T} [m^3]	V_{GM} [m^3]	V_I [m^3]	n [-]
A	$3.470{\cdot}10^{-3}$	$2.473{\cdot}10^{-3}$	$0.996{\cdot}10^{-3}$	0.290
B	$3.614{\cdot}10^{-3}$	$2.473{\cdot}10^{-3}$	$1.141{\cdot}10^{-3}$	0.320
C	$3.386{\cdot}10^{-3}$	$2.287{\cdot}10^{-3}$	$1.099{\cdot}10^{-3}$	0.320

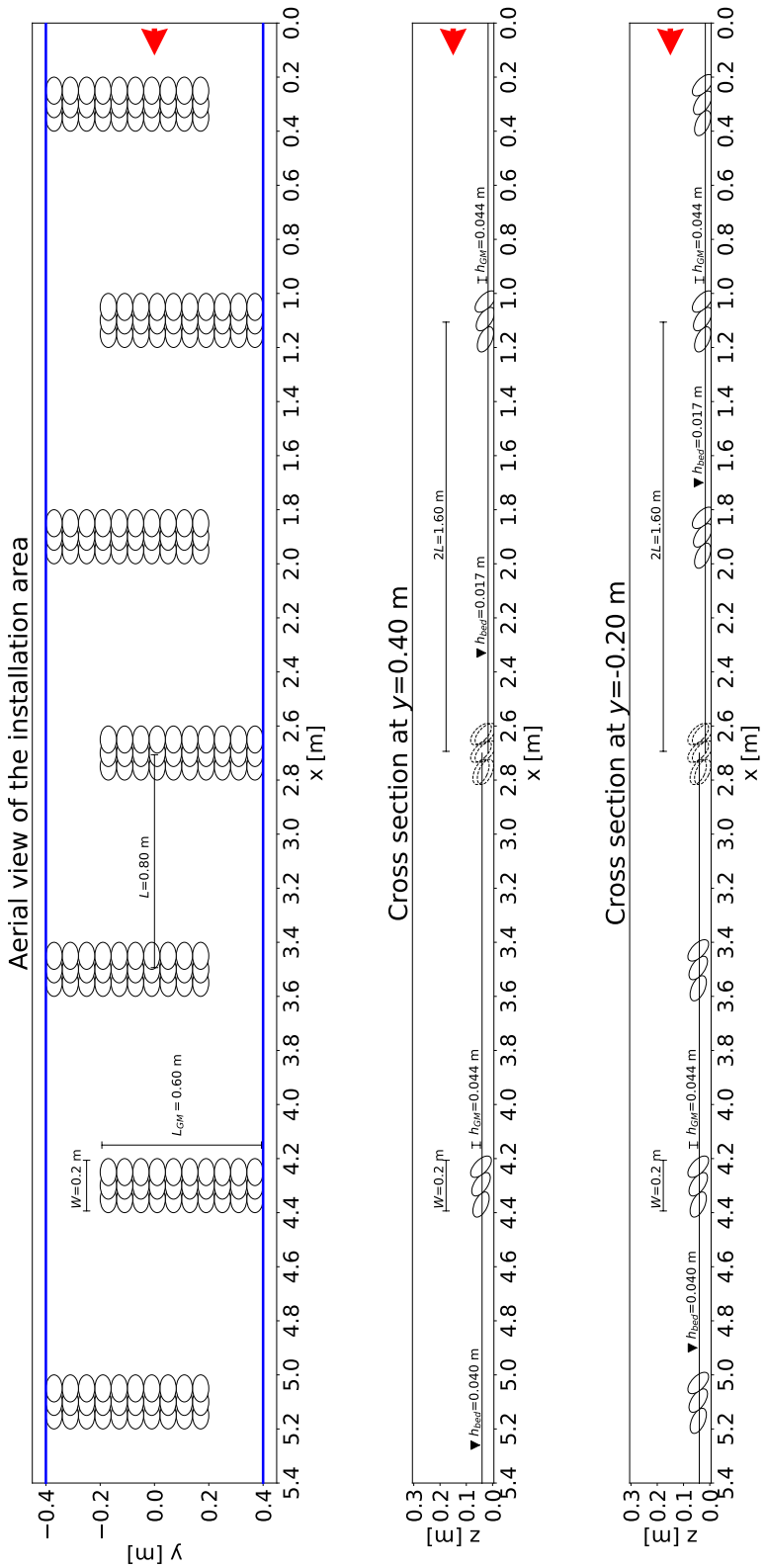

Figure 24: Definition sketch of the installation area for experiments AB2 and AB3. The difference in the experimental bed thickness is taken into account in the cross-sectional views (y=−0.200, 0.400 m): right side in the case of h_{bed}=0.0170 m (AB2), left in case of h_{bed}=0.0400 m (AB3). In the center, both cases are presented. The flow direction is given by the red arrow.

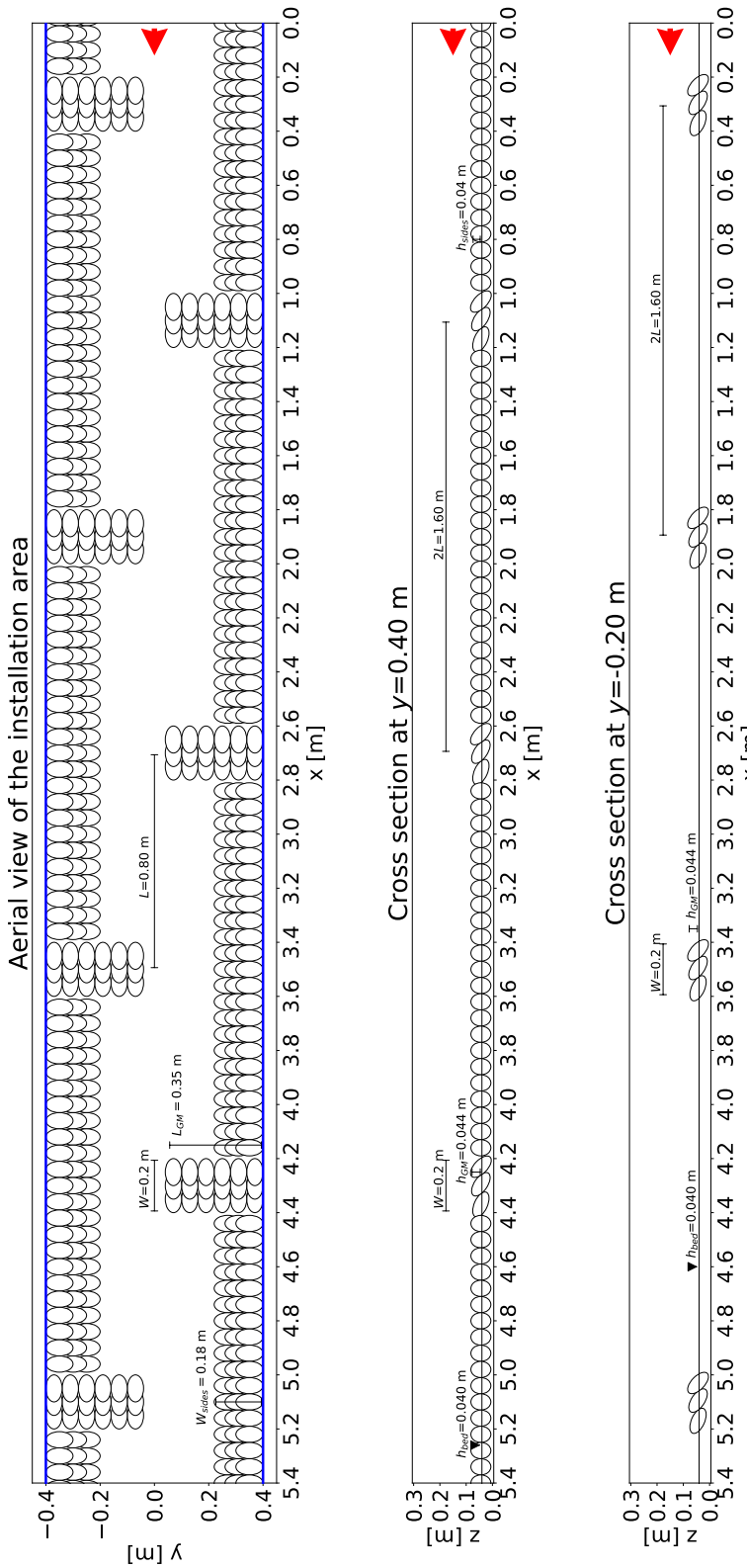

Figure 25: Definition sketch of the installation area for experiment AB4. The flow direction is given by the red arrow.

3.3 Results and Discussion

3.3.1 Average water depth and Froude number

The smallest average water depth in Table 9 is observed above the flat gravel bed of experiment AB1. The measured h_{ave}=0.0910 m is around 0.0100 m lower than what observed in experiment GM2.1 (Table 5), where the same slope, but different bed thickness h_{bed}=0.0170 m was studied. In case of experiment AB2, the gravel bed and the water surface have been measured twice. The resulting identical average water surfaces h_{ave}=0.127 m confirm the results' accuracy. The average water depth above boulders groynes remains similar between experiments AB2, AB3 and AB4, although all three measure higher values than h_{ave}=0.117 m (Table 5), the average water depth above the triangular gravel mounts of experiment GM2.3, with whom they share the same discharge, channel slope and h_{GM}. The introduction of further assembled boulders along the sides of the channel, causes an increase in the average water surface between AB3 and AB4. All four experiment with boulders groynes can be classified as subcritical flow, with critical conditions approached above the flat gravel bed of experiment AB1. These remarks reflect what has been observed in the previous chapter.

Table 9: Flow characteristics of the different experiments (Q=0.0588 m^3/s).

	AB1	AB2	AB2 (2)	AB3	AB4
h_{ave} [m]	0.0910	0.127	0.127	0.124	0.128
Fr [-]	0.860	0.520	0.520	0.540	0.510
h_{bed}	0.0400	0.0170	0.0170	0.0400	0.0400

The stability of the assembled boulders constructions has been confirmed visually, as the experimental conditions were insufficient to dislodge or even shake the boulders. The gravel bed has shown to be less stable, in particular in the case of experiment AB2, when significant erosion areas along the centre part of the channel are observed (Figure 26a). Thanks to the increase in the bed thickness to h_{bed}=0.0400 m, the situation significantly improves in experiment AB3, where widespread grain shaking is still present but only sparse local transport is observed (Figure 26b). Results recommend that following experiments may keep the increased bed thickness, as also highlighted in Sub-chapter 5.1.

(a) Gravel erosion visible in model AB2.

(b) More stable gravel bed of model AB3.

Figure 26: Effect of the bed thickness on gravel erosion. Left for model AB2 (h_{bed}=0.0170 m); right for model AB3 (h_{bed}=0.0400 m)

Above flat gravel bed, the water surface is flat as shown in Figure 27a. Above boulders groynes, the water surface is very wavy in both centre part of the channel and along the sides (Figures 27b and 27c). Differently to triangular gravel mounts with linearly decreasing height, boulders groynes have uniform height along the entire transverse length. This causes the constructions to act as a dam to the flow, increasing the flow friction and spreading the waves to the sides of the channel. The water surface is flat upstream of each groyne, before sinking steeply once reached the construction's downstream side. The installation of further assembled boulders along both sides of the channel (experiment AB4) significantly reduces the wave amplitude there, as shown in Figure 27d. This results is very satisfactory and their construction is recommended in future experiments as well.

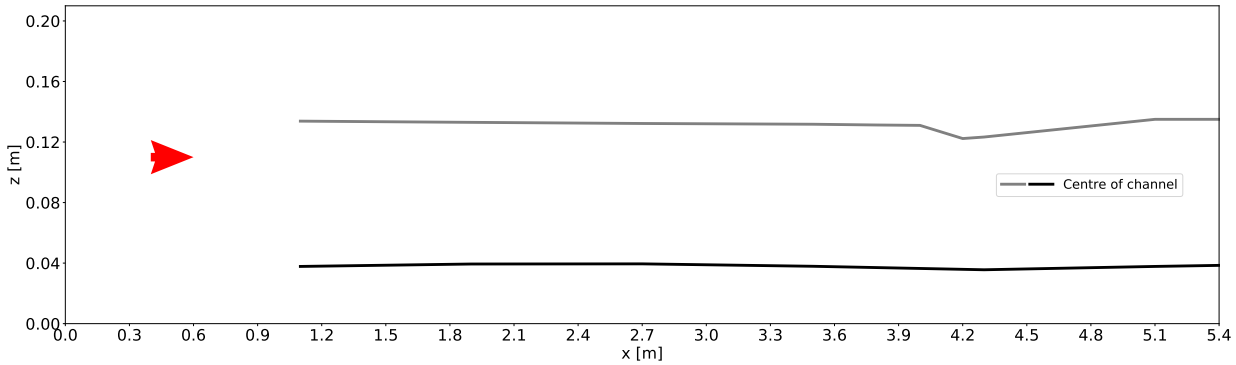

(a) h_{GM}=0.00 m (AB1), h_{bed}=0.0400 m. Measurements were taken only for 1.10≤x (m)≤5.40.

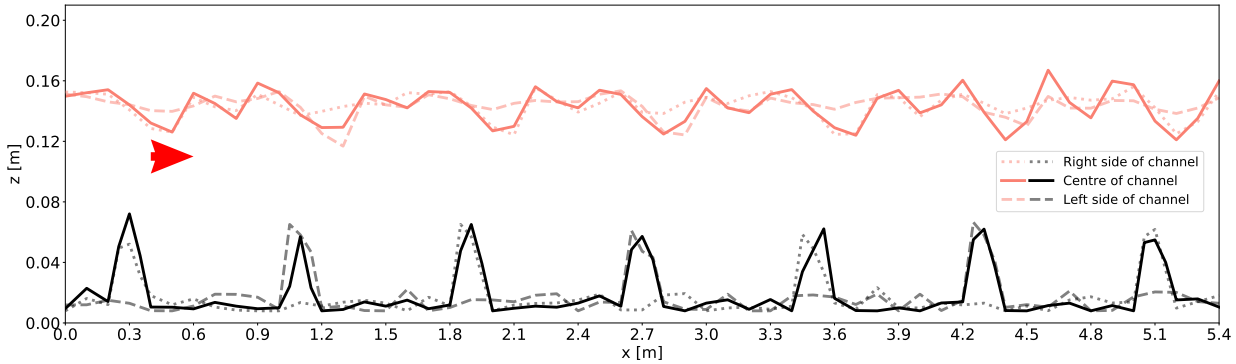

(b) h_{GM}=0.0440 m, h_{bed}=0.0170 m (AB2).

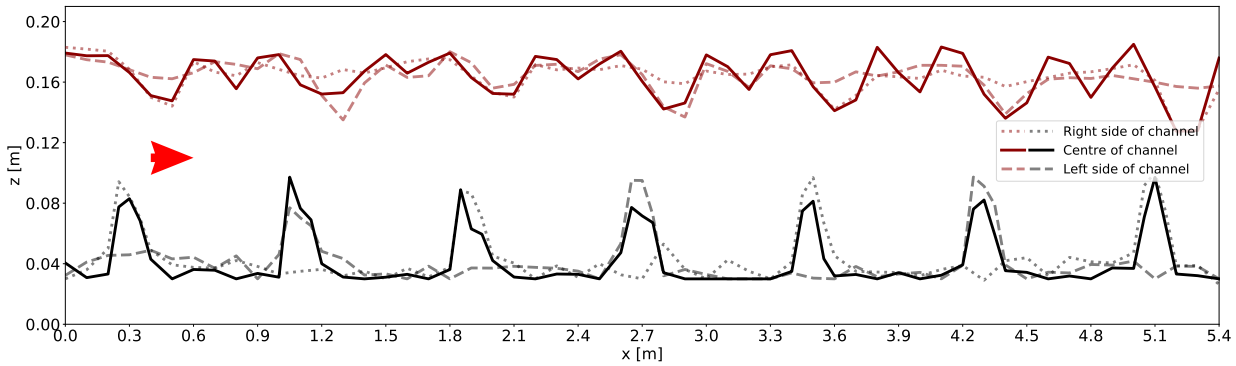

(c) h_{GM}=0.0440 m, h_{bed}=0.0400 m (AB3).

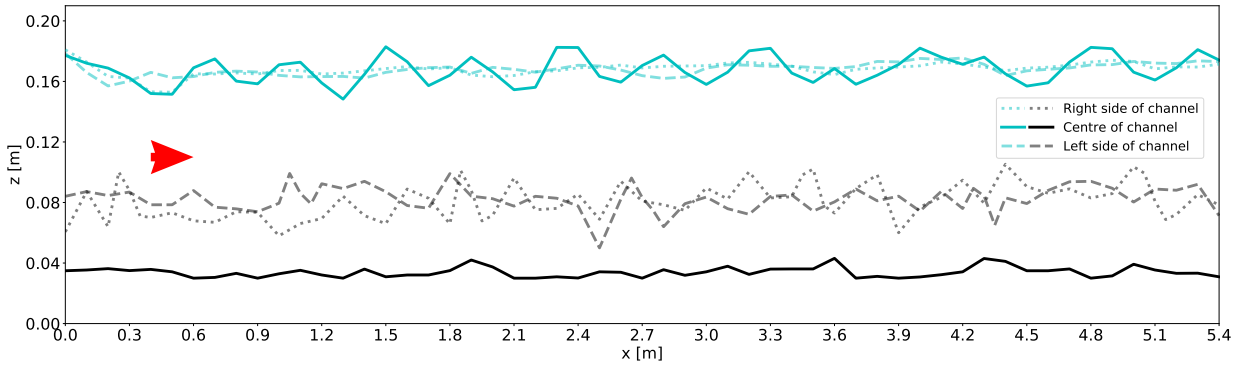

(d) h_{GM}=0.0440 m, h_{bed}=0.0400 m, side assembled boulders (AB4).

Figure 27: Bed and water level profiles at the centre and the sides of the channel are here presented for this chapter's experiments. The flow direction is given by the red arrow.

3.3.2 Vertical velocity profiles

Figures 28 through 31 show the vertical profiles of the time-averaged velocity and the standard deviation of the velocity for each conducted experiment. The plots are built using the same method described in Sub-chapter 2.3.2: polynomial approximations of 1st, 2nd or 4th order are used to simulate the vertical velocity profiles close to the model's surface; refuge able areas are defined by the thresholds $\overline{V}$ $\leq$0.100 m/s and *std(V)*$\leq$0.070 m/s (Sub-chapter 1.9), while the water surface profile is shown for coordinates y=0.00, $\pm$0.380 m since data are collected only there. In experiment AB1, gravel bed and water surfaces are measured only in the centre of the channel (y=0.00 m) and the same profiles are translated to all the plots of Figure 28. Experiments AB3 and AB4 display two separate Sub-figures for data taken at $|y|\geq$0.100 m because measurements are taken on both sides of the channel (Figures 30b, 30c, 30d and 31b, 31c, 31d, respectively).
Experiment AB1 confirms what has been already seen above experiments GM1.1 and GM2.1: above flat gravel bed, the water surface is also flat and the flow field is extremely homogeneous. The size of the refuge able areas is negligible, if detected at all (Figure 28). The installation of boulders groynes causes significant distortion in the flow field, with similar results observed in experiments AB2 (Figure 29) and AB3 (Figure 30). The boulders groynes visually occupy significant less volume than the triangular gravel mounts, without taking into account that 30% of the total construction volume of each assembled boulders construction is empty and should be considered interstice volume. The velocity measurements right downstream of each groyne are missing close to the water surface because of the sink in the water level profile discussed in the previous Sub-chapter 3.3.1. The local flow acceleration is visible in the collected data. These hydraulic conditions are expected to reduce the refuge suitability in the same regions where the largest refuge able areas are observed in models with triangular gravel mounts (Chapter 2). The flow passing through the empty spaces between the assembled boulders might also increase the local flow velocity in the close downstream proximity of each groyne. In general, the creation of refuge able areas around boulders groynes appears to be less place-specific, as suitable conditions are found between two groynes (e.g. Figure 30d, experiment AB3 and y=$\pm$0.380 m), in the right downstream (e.g Figure 31b, experiment AB4 and y=$\pm$0.100 m) or upstream proximity of a groyne (e.g. Figure 29c, experiment AB2 and y=$-$0.300 m). There are also sections where no refuge able areas are measured (e.g. Figure 30c, experiment AB3 and y=$-$0.300 m). No clear relationship between the formation of refuge able area and the measurement's coordinates could be found, suggesting that the specific disposition of the boulders might be more relevant than their place in the model. In other words, how the stones are placed might be more important than where they are placed. The increase of the gravel bed thickness from h_{bed} =0.0170 m (AB2) to h_{bed} =0.0400 m (AB3) appear to generate visually bigger refuge able areas. To this comparison, Experiment AB4 show different results: due to the reduction of the groynes' transverse length to 0.350 m, the flow conditions at the centre of the channel are very uniform (Figure 31a) and the wavy water surface is the only visible difference from what is observed above flat gravel bed conditions in experiment AB1. Along the sides of the channel, the assembled boulders creates a roughness layer with their irregular surface (Figure 31d) and suitable conditions can be found, in particular where the boulder surface creates small sinks. For the coordinates in-between (y=$\pm$0.100, $\pm$0.200 m), the flow field is similar to what observed in experiments AB2 and AB3.

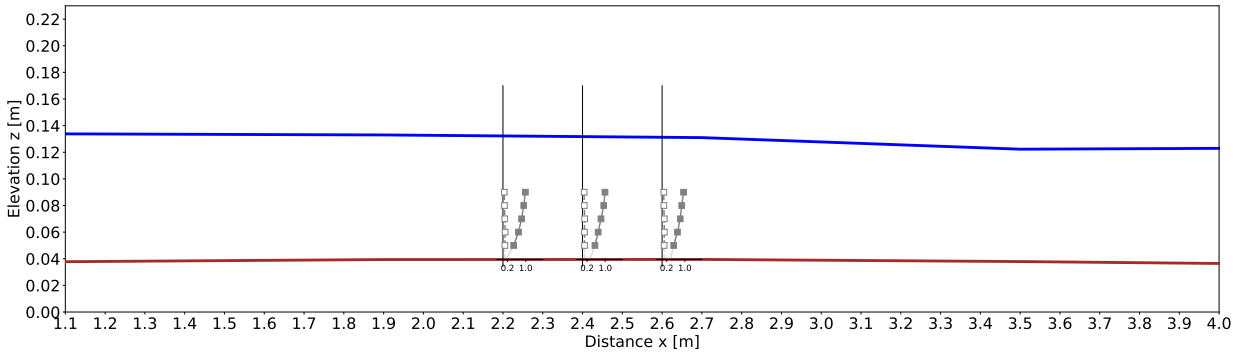

(a) h_{GM}=0.00 m (AB1), h_{bed}=0.0400 m, y=0.00 m.

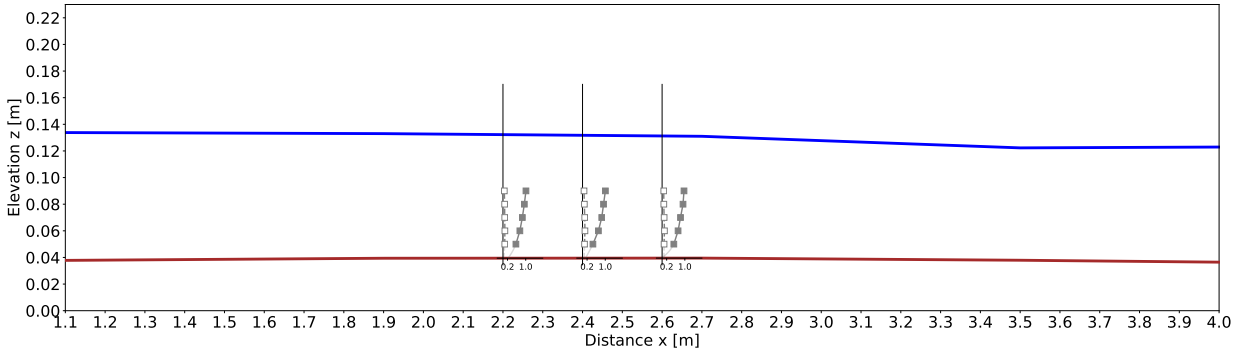

(b) h_{GM}=0.00 m (AB1), h_{bed}=0.0400 m, y=−0.200 m.

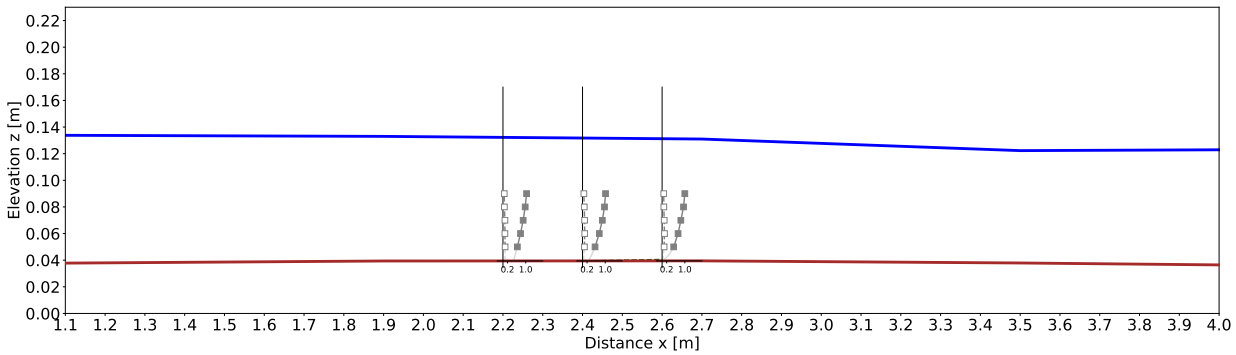

(c) h_{GM}=0.00 m (AB1), h_{bed}=0.0400 m, y=−0.300 m.

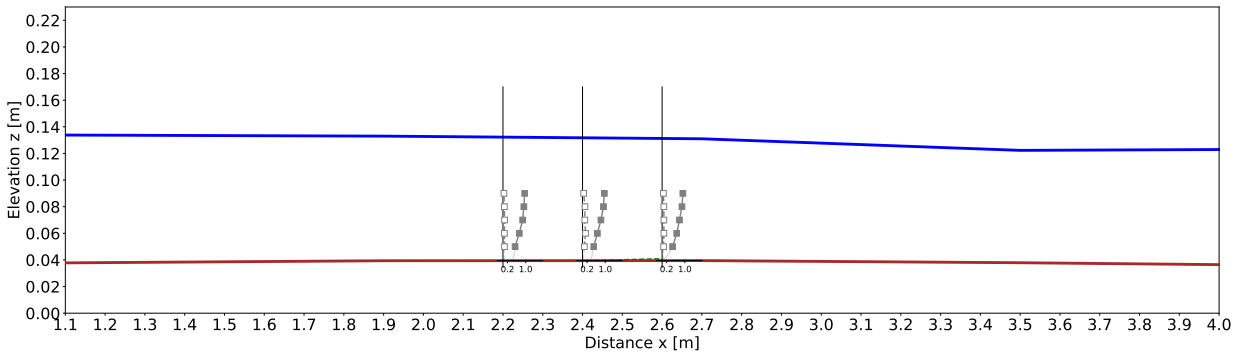

(d) h_{GM}=0.00 m (AB1), h_{bed}=0.0400 m, y=−0.380 m.

Figure 28: Vertical profiles of time-averaged velocity (filled markers) and standard deviation of the velocity (empty markers) for experiment AB1. The units of the smaller plots are velocity [m/s] on the x-axis and elevation [m] on the y-axis. The water surface profile is marked in blue and the refuge able areas are highlighted in yellow.

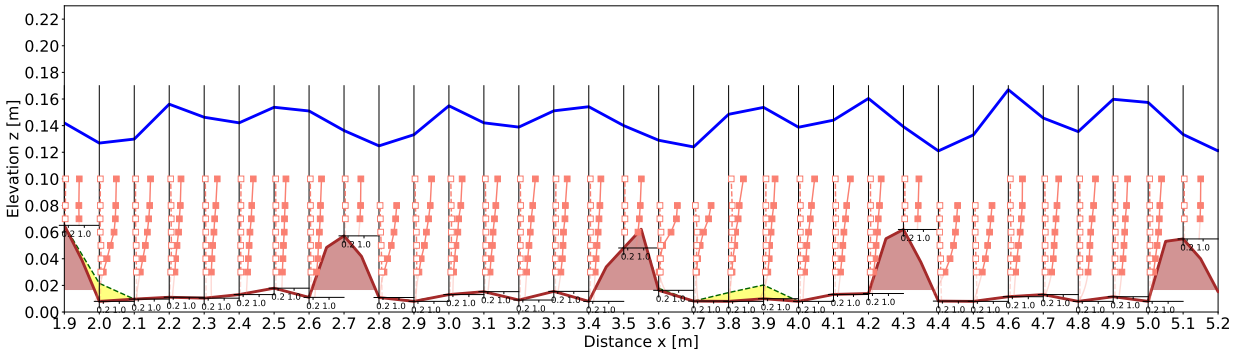

(a) h_{GM}=0.0440 m (AB2), h_{bed}=0.0170 m, y=0.00 m.

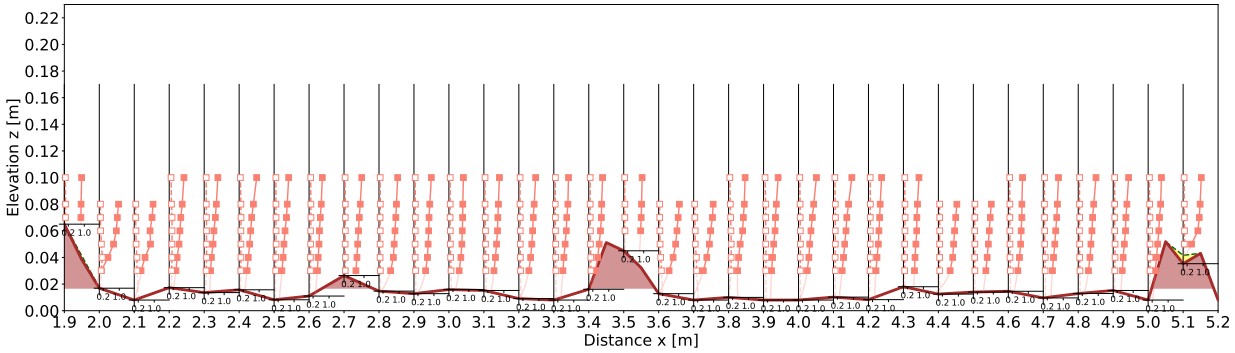

(b) h_{GM}=0.0440 m (AB2), h_{bed}=0.0170 m, y=−0.200 m. The water surface is not measured here.

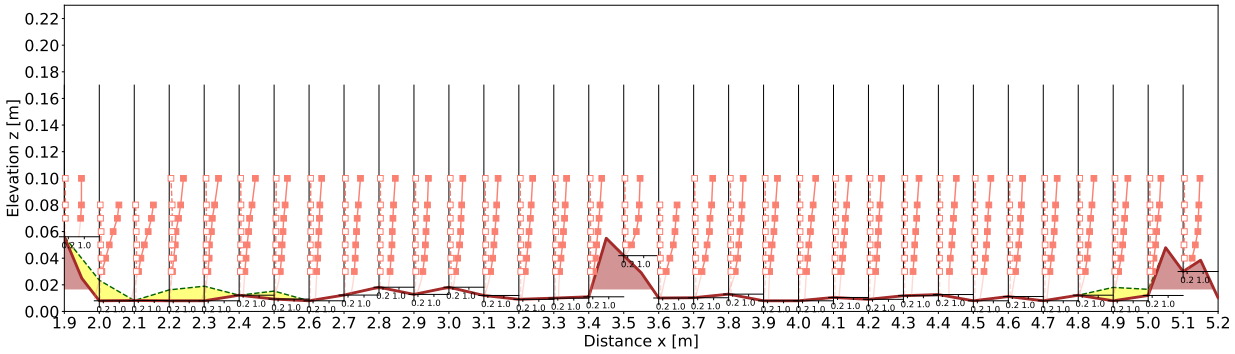

(c) h_{GM}=0.0440 m (AB2), h_{bed}=0.0170 m, y=−0.300 m. The water surface is not measured here.

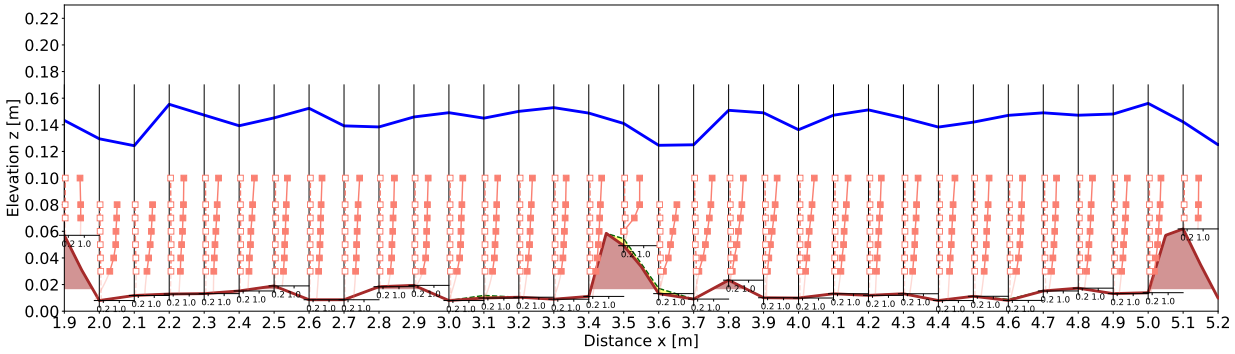

(d) h_{GM}=0.0440 m (AB2), h_{bed}=0.0170 m, y=−0.380 m.

Figure 29: Vertical profiles of time-averaged velocity (filled markers) and standard deviation of the velocity (empty markers) for experiment AB2. The units of the smaller plots are velocity [m/s] on the x-axis and elevation [m] on the y-axis. The total construction area is coloured brown, the water surface profile is marked in blue and the refuge able areas are highlighted in yellow.

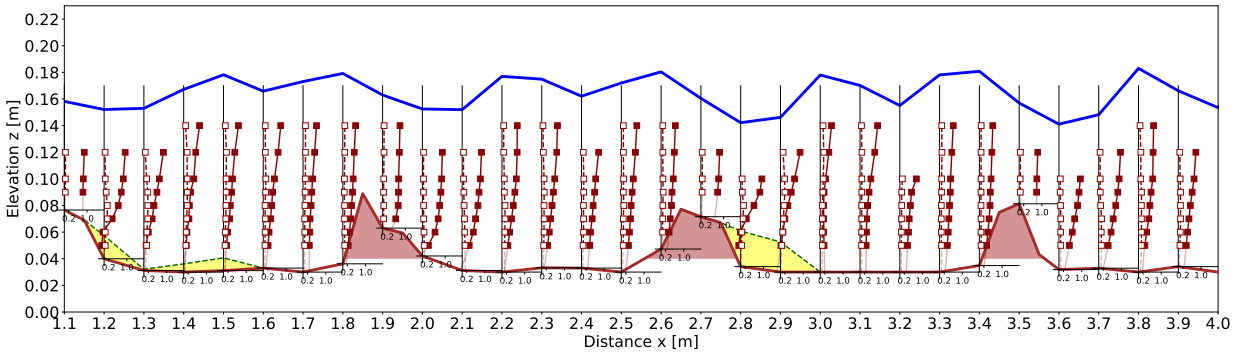

(a) h_{GM}=0.0440 m (AB3), h_{bed}=0.0400 m, y=0.00 m.

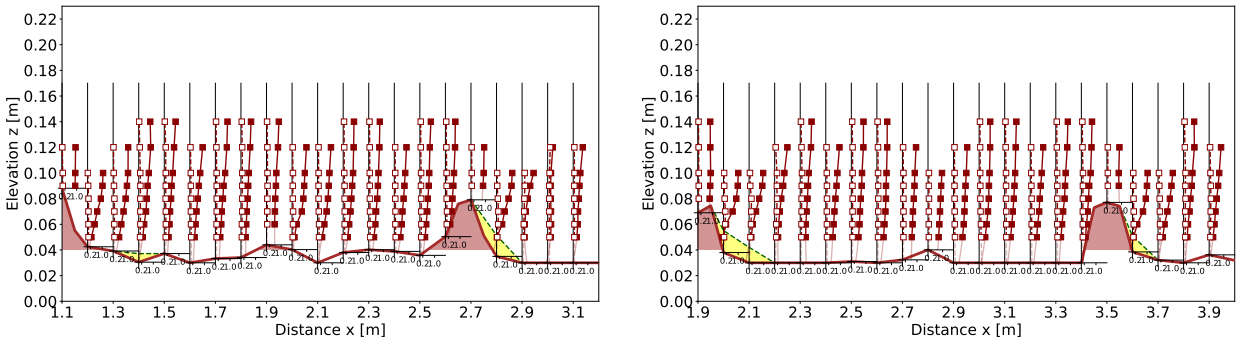

(b) h_{GM}=0.0440 m (AB3), h_{bed}=0.0400 m, y=0.200 m (left) or y=−0.200 m (right). The water surface is not measured here.

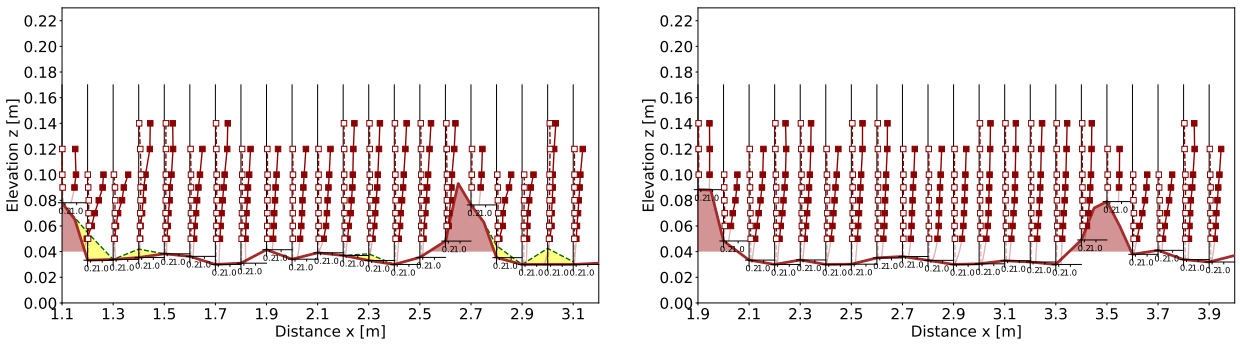

(c) h_{GM}=0.0440 m (AB3), h_{bed}=0.0400 m, y=0.300 m (left) or y=−0.300 m (right). The water surface is not measured here.

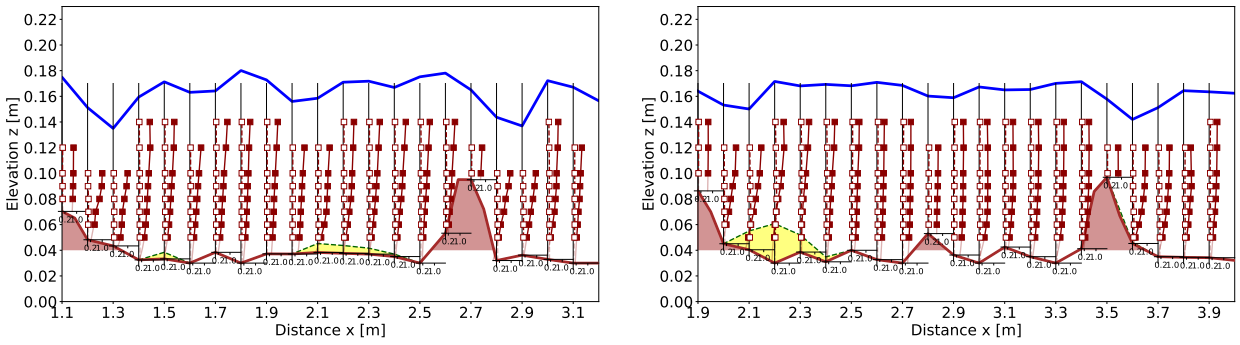

(d) h_{GM}=0.0440 m (AB3), h_{bed}=0.0400 m, y=0.380 m (left) or y=−0.380 m (right).

Figure 30: Vertical profiles of time-averaged velocity (filled markers) and standard deviation of the velocity (empty markers) for experiment AB3. The units of the smaller plots are velocity [m/s] on the x-axis and elevation [m] on the y-axis. The total construction area is coloured brown, the water surface profile is marked in blue and the refuge able areas are highlighted in yellow.

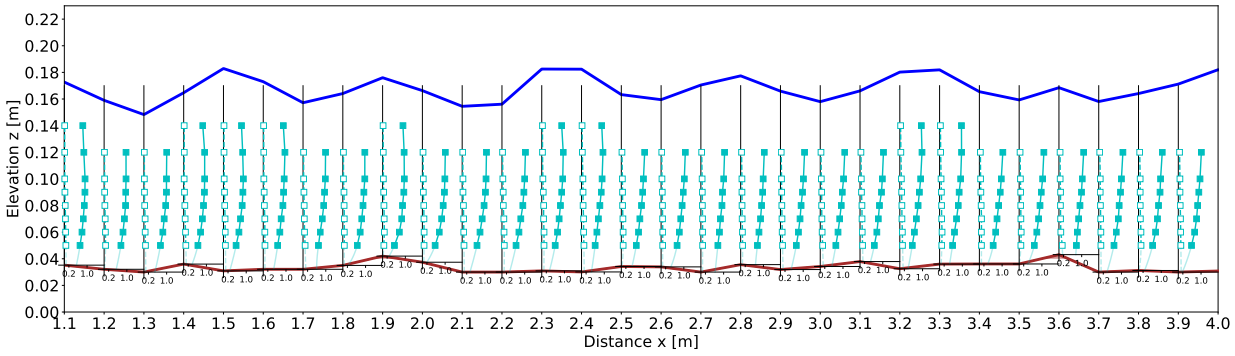

(a) h_{GM}=0.0440 m (AB4), h_{bed}=0.0400 m, y=0.00 m.

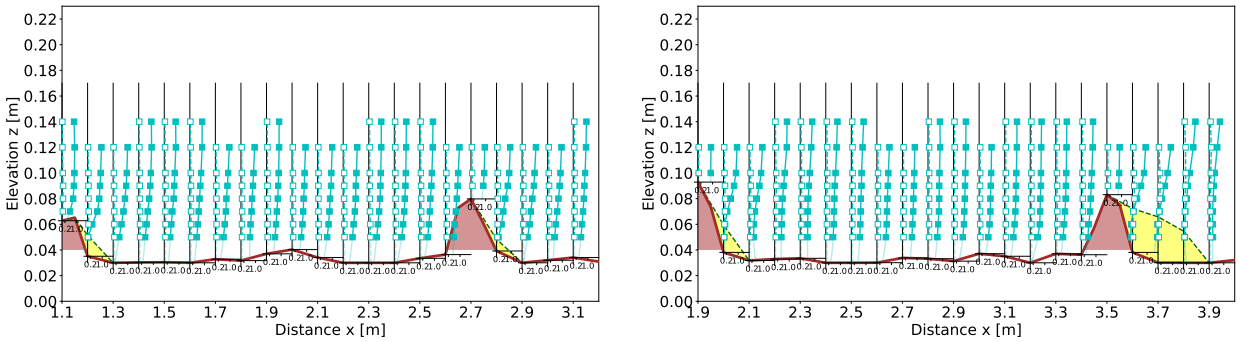

(b) h_{GM}=0.0440 m (AB4), h_{bed}=0.0400 m, y=0.100 m (left) or y=−0.100 m (right). The water surface is not measured here.

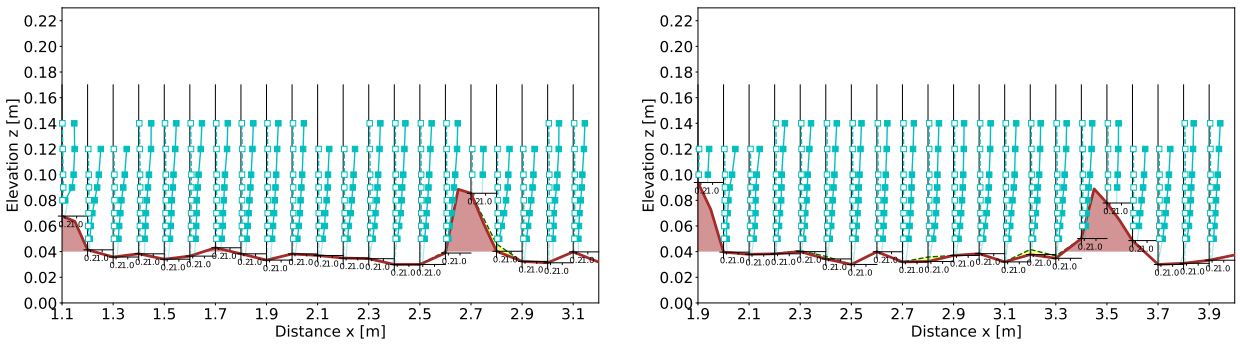

(c) h_{GM}=0.0440 m (AB4), h_{bed}=0.0400 m, y=0.200 m (left) or y=−0.200 m (right). The water surface is not measured here.

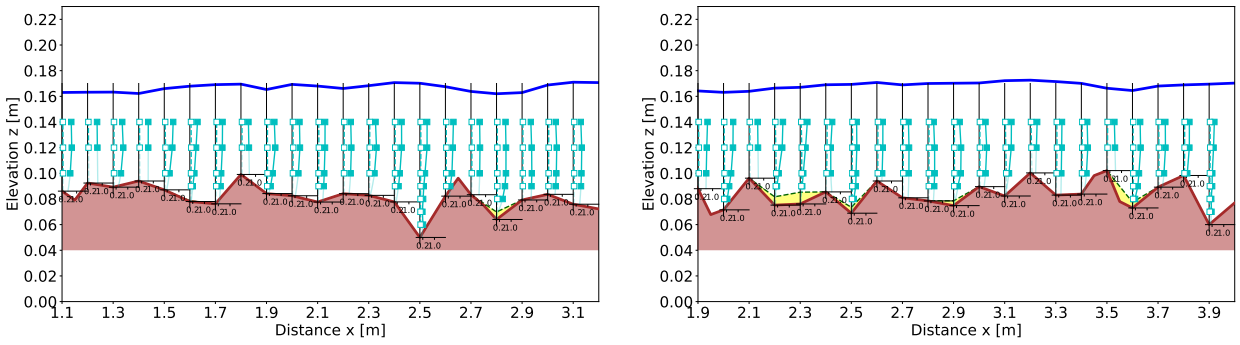

(d) h_{GM}=0.0440 m (AB4), h_{bed}=0.0400 m, y=0.380 m (left) or y=−0.380 m (right).

Figure 31: Vertical profiles of time-averaged velocity (filled markers) and standard deviation of the velocity (empty markers) for experiment AB4. The units of the smaller plots are velocity [m/s] on the x-axis and elevation [m] on the y-axis. The total construction area is coloured brown, the water surface profile is marked in blue and the refuge able areas are highlighted in yellow.

3.3.3 Assembled boulders volume, refuge able volume and interstice volume

For each experiment, Table 10 presents the assembled boulders volume V_{GM}, the refuge able volume V_{RA} and the interstice volume V_I. The relative suitable volume is calculated as $100 \cdot \frac{V_I+V_{RA}}{V_{GM}}$. As measured in Sub-chapter 3.2.1, the total construction volume V_{GM_T} is build from the assembled boulders volume and the interstice volume, in a ratio of 70% and 30% respectively.

Table 10: Assembled boulders volume V_{GM} [10^{-4} m^3], refuge able volume V_{RA} [10^{-4} m^3], interstice volume V_I [10^{-4} m^3] and the relative suitable volume $100 \cdot \frac{V_I+V_{RA}}{V_{GM}}$ [%] are shown for each experiment.

	AB1	AB2	AB3	AB4
V_{GM} [10^{-4} m^3]	0.00	30.00	50.00	130.00
V_{RA} [10^{-4} m^3]	0.100	9.00	34.00	20.00
V_I [10^{-4} m^3]	0.00	14.00	23.00	57.00
$100 \cdot \frac{V_I+V_{RA}}{V_{GM}}$ [%]	-	71	105	58

Table 10 confirms again that the flow above flat gravel bed (experiment AB1) is not suitable for small-sized fishes. The introduction of assembled boulders significantly improves the situation: in the case of experiments AB2 and AB3, the assembled boulders volume is 30.00-50.00·10^{-4} m^3, i.e. around half of the space required to construct triangular gravel mounts with the same height and transverse length (experiment GM2.3, Table 6). The generated refuge able volume is significant, with the best result of 34.00·10^{-4} m^3 calculated in experiment AB3. The result difference between experiments AB2 and AB3 is not believed to have been caused by the change in the bed thickness, but rather by the specific dispositions of the assembled boulders on top of each others (as discussed previously in Sub-chapter 3.3.2). Small assembled boulders volume with large total suitable volume, results in extremely high relative suitable volume: in the case of experiment AB3, the refuge able and the interstice volumes combined are larger than the volume of the assembled boulders, specifically 1.05 times bigger. These results are a significant improvement from what is observed around triangular gravel mounts, where, at same channel slope, the largest relative suitable volume is 14% of the mounts volume. The assembled boulders volume in experiment AB4 is significantly larger than the other experiments because of the extra assembled boulders built along the sides of the channel. This change causes the interstice volume to significantly increase as well, while the refuge able volume shrinks because of shorter groynes' traverse length and less space available. The total suitable volume is nonetheless more than half (specifically 58%) of the assembled boulders volume.

3.3.4 Discharge Q=0.155 m^3/s

As discussed previously, the assembled boulders constructions remain motionless under medium-sized flooding discharge Q=0.0588 m^3/s, while the gravel bed is significantly less stable, particularly when built with a single layer of grains (model AB2). The erosion conditions become worse when the discharge is increased to Q=0.155 m^3/s, the pump capacity of the channel (Figure 32). Similarly to what described in Sub-chapter 2.3.4, here as well only photographic material is collected during the test. Under large-size flood stages, the assembled boulders are never seen moving nor shaking, while steady waves are formed along the water surface. Each wave peak corresponds to the coordinates of a boulders groyne (Figure 32a) and the amplitude is uniform along the channel's width (Figure 32b). The strength of assembled boulders constructions is here confirmed, as are the advantages of multi-layered gravel bed are highlighted.

(a) Water surface above the model (flow direction right to left). Local erosion is visible in several areas.

(b) Side view of the water surface (flow direction right to left).

(c) The model after being exposed to Q=0.155 m^3/s. Significant erosion is visible.

Figure 32: Hydraulic condition of model AB2 under large-sized flood stage Q=0.155 m^3/s.

3.4 Conclusions

Rectangular boulders groynes have improved several of the problem faced when experimenting with triangular gravel mounts. At same height h_{GM}=0.0440 m, assembled boulders constructions are significantly more stable under both medium- and large-scale flood stages. They also occupy significantly less space and have a porosity of n=0.300, as proven by experimental results. Further improvements on the stability of the gravel bed are achieved by increasing the bed thickness from one layer (h_{bed}=0.0170 m) to multiple (h_{bed}=0.0400 m). The introduction of further assembled boulders along the sides of the channel can remarkably flatten the water surface profile there, as shown in experiment AB4. In centre part of the channel, the water surface remains wavy as it was observed around triangular gravel mounts. The average water depth remains generally similar between experiments, but for same discharge, channel slope and h_{GM}, it is larger than what measured above triangular gravel mounts. The steep faces of each groyne cause the water to plunge once reached the top. The local flow acceleration reduce the hydraulic suitability in the close downstream proximity of each construction. The flow trough the empty spaces between boulders might also increase the local velocity there, but no quantitative measurements are conducted to prove this speculation. Refuge able areas are found at least once for every lateral y-coordinate measured. Also, experimental results suggest that they might not necessarily form downstream of each assembled boulders construction, but also along the upstream face or between two groynes or do not form at all in some flow sections. These observations suggest that processes behind the formation of refuge able areas around assembled boulders constructions is more complex than what observed around triangular gravel mounts (Chapter 2). Here, the specific disposition of the assembled boulders is believed to be the main factor in the formation of refuge able areas, although no quantitative data on this speculation has been collected. The combination of small assembled boulders volume and large total suitable volume (as the sum of refuge able volume plus interstice volume) results in very high relative suitable volumes for all conducted experiments. The best result is found in case of model AB3 (h_{bed}=0.0400 m and h_{GM}=0.0440 m), where the total suitable volume is larger than the assembled boulders volume by 1.05 times. The other two experiments score 71% (AB2, h_{bed}=0.0170 m and h_{GM}=0.0440 m) and 58% (AB4, h_{bed}=0.0400 m and h_{GM}=0.0440 m with assembled boulders along both sides of the channel), respectively. These results are significantly higher than what observed around triangular gravel mounts where, at same experimental conditions, the largest total suitable volume is 14% of each mounts volume.
A quick summaries of the main discoveries of this chapter are shown here:

- Under same experimental conditions, rectangular boulders groynes are significantly more stable and occupy less space than triangular gravel mounts;
- The stability of the gravel bed can be improved by increasing the bed thickness from one layer of grains to multiples;

- Experimental results suggest that assembled boulders constructions have a porosity of n=0.300. The empty spaces are classified as interstice area, as it is assumed that the suitable conditions for refuge are met there;
- Above boulders groynes, the water surface is wavy in both the centre part and the sides of the channel.
- For same experimental conditions, the average water surface is larger than what observed around triangular gravel mounts.
- The flow is subcritical;
- The introduction of further assembled boulders along the sides of the channel successfully flatten the water surface there;
- The formation of refuge able areas around assembled boulders is confirmed, although the process is not completely clear. Suitable conditions for refuge can be found at any lateral y-coordinate downstream of, upstream of and between groynes, but their existence is not guaranteed;
- The steep walls of each groyne cause the water to plunge once reached the top. The local flow acceleration reduced the refuge suitability at the close downstream proximity of each construction. The flow passing through the large empty spaces between assembled boulders might also have an effect in reducing the suitability of these areas, but no data have been collected in this regard;
- The specific disposition of the assembled boulders on top of each others is considered to be the main factor deciding the formation and size of the refuge able areas around boulders groynes;
- Because of small assembled boulders volume and large total suitable volume (the sum of refuge able volume plus interstice volume), the relative suitable volume is very large;
- The overall best result is calculated in experiment AB3 (h_{bed}=0.0400 m and h_{GM}=0.0440), where the total suitable volume is larger than the volume of the assembled boulders. All experiments of this chapter have scored relative suitable volumes above 58%;
- This is a significant improvement from what observed in case of triangular gravel mounts.

3.5 From this point onward

The experiments conducted in this chapter has shown several promising results: significant improvements in the gravel bed stability are obtained by increasing bed thickness to a multi-layered grain substratum and the installation of assembled boulders structures along the sides of the channel stabilizes the water surface there. Both innovations are recommended to be kept for the following experiments. The stability of assembled boulders under medium- and large-scale flood stages is confirmed, although the tested rectangular design creates strong hydraulic friction inside the flow field. The transverse walls of each boulders groyne are very steep and cause the water to plunge over the top, reducing the refuge suitability in the close downstream proximity of each construction. As results shown, the total suitable volume is exceptionally large considering the assembled boulders volume. However, suitable conditions do not form as large, compact regions, but rather as small pockets distant from each others. The relationship between the specific assembled boulders' placement and the formation of refuge able areas appear to be complex and to require significant additional experimental time to be understood. Lastly, the flow generated by the large gaps between assembled boulders might play an important role in the formation of refuge able areas behind each construction, but further data are necessary to prove this assessment. Following these observations, the improvements that assembled boulders constructions can bring to the research are undeniable, but significant changes in the design are still required.

4 Combination of boulders and gravel

4.1 Introduction

The main drawbacks of boulders groynes presented in the previous Chapter 3 are: the impinging flow on the upstream face of each construction, the large average water depth and the penetrating flow though the interstices. Despise these points, the overall resilience of the assembled boulders and the significant ecological improvements are both very promising results. Also, assembled boulders structures built along the sides of the channel are effective in stabilizing the water surface there. In this chapter, the research proposes to combine gravel and boulders to extract the most positive traits of both previously tested designs. The triangular gravel mounts are brought back into consideration, this time with the addition of two layers of assembled boulders as reinforcement along their shape. Further two layers of assembled boulders are built along both sides of the channel, while the multi-layered gravel bed is now considered the default. Experiments were conducted between February 2022 and February 2023 and the main results have been presented at the 77$^{\text{th}}$ Annual Conference of the Japanese Society of Civil Engineers (Beretta Piccoli and Yasuda (2022b) [4]), the 11$^{\text{th}}$ International Conference on Fluvial Hydraulics - River Flow 2022 (Beretta Piccoli and Yasuda (2022c) [3]), the 40$^{\text{th}}$ IAHR World Congress (Beretta Piccoli and Yasuda (2023b) [1]) and published on the June 2023 edition of the Journal of Environmental Science Studies (Beretta Piccoli and Yasuda (2023a) [2]).

4.2 Methods

The 5.400 m long installation area is built with a h_{bed}=0.0400 m thick flat gravel bed (type G1, d_{50}=0.0170 m). On top of it, seven triangular gravel mounts are built every 0.800 m on alternated sides of the channel (same positions as the experiments presented in Chapter 2). Each one is an almost exact copy of these previous experiments: the transverse length L_{GM}=0.500 m is reduced from the original 0.600 m, while upstream and downstream widths remain the same L_u=0.300 and L_d=0.350 m, respectively. The height is h_{GM}=0.0440 m above the bed thickness and it linearly decreases from the side wall to the mount's toe. Around the profile of each gravel mount, two layers of assembled boulders (type B1, d_{50}=0.0630 m) are constructed using the same method described in the previous Chapter 3: the first layer is partially buried in the gravel bed with an angle of around 20°-30° from the horizontal; the second is placed over this (upstream side) with a steeper angle like a fallen domino facing downstream. Further two layers of assembled boulders are build on both sides of the channel along the entire installation area's length. They also looks like fallen dominoes facing downstream (change from experiment AB4 presented in the previous chapter) and have a general angle of 60°-70° from the horizontal. The height of all assembled boulders match the mount's profile as much as possible, meaning that the boulders along the side walls are around 0.0440 m high above the gravel bed, while these at the mount's toe are completely buried in it (i.e. local height is 0.00 m). A metal bar is placed at the downstream side of each model, as it was in all previous experiments. The channel slope is set at I=0.0100 and four different discharges are studied: Q=0.00370 m^3/s (GM+AB1), 0.00550 m^3/s (GM+AB2), 0.0588 m^3/s (GM+AB3), 0.155 m^3/s (GM+AB4). The first two are supposed to represent small-sized floods without full submersion of the installation area; The third represent a medium-sized flooding event, while the last is the the pump capacity of the experimental channel (Table 1). Pictures of the new gravel mount design are shown in Figure 33, while the characteristics of each experiment are summarized in Table 11. A definition sketch of the installation areas is shown in Figure 35. Experiment GM+AB4 (Q=0.155 m^3/s) has been conducted twice, since the results of first try have been classified as unsatisfactory and they are relegated to the Appendices D).
Data is collected generally uniformly throughout the experiments. The gravel bed elevation is measured every 0.100 m (0.0500 m when above a gravel mount) in x-direction and y-coordinates y=−0.380, −0.300, −0.200, −0.100, 0.00, 0.100, 0.200, 0.300, 0.380 m along the entire installation area. The water surface profile is measured similarly every 0.100 m along the entire installation area with y-

coordinates depending on the experiment: for GM+AB1 and GM+AB2, y=−0.300, 0.00, 0.300 m since the emerging boulders along the sides of the channel makes measurements there impossible; for GM+AB3 and GM+AB4, y=−0.380, 0.00, 0.380 m. The velocity field is measured is two regions: for 1.10≤x (m)≤3.20 and y=0.00, 0.100, 0.200, 0.300 (GM+AB1 and GM+AB2) or 0.380 (GM+AB3 and GM+AB4) m; for 1.90≤x (m)≤4.00 and y=−0.380 (GM+AB3 and GM+AB4) or −0.300 (GM+AB1 and GM+AB2), −0.200, −0.100, 0.00 m.

(a) The model. (b) Boulders reinforcement. (c) The toe of a mount.

Figure 33: The experimental model is always shown from a downstream point of view.

Table 11: Main characteristics of this chapter's experiments.

ID	h_{GM} [m]	L_{GM} [m]	L_u [m]	L_d [m]	h_{bed} [m]	I [-]	Q [m^3/s]
GM+AB1	0.0440	0.500	0.300	0.350	0.0400	0.0100	0.00370
GM+AB2	0.0440	0.500	0.300	0.350	0.0400	0.0100	0.00550
GM+AB3	0.0440	0.500	0.300	0.350	0.0400	0.0100	0.0588
GM+AB4	0.0440	0.500	0.300	0.350	0.0400	0.0100	0.155

4.2.1 Estimation of empty spaces inside the improved gravel mounts

In the previous Chapter 3, it was found that assembled boulders constructions have a porosity of 0.300 and the empty spaces build the interstice volume V_I [m^3], as suitable conditions for refuge are believed to be found there. In contrast, gravel is considered to have V_I=0.00 m^3 because the spaces between grains are too small for the target small-sized fishes. Since a combination of gravel and boulders is presented in this chapter, the calculation of the refuge volume is less straightforward.

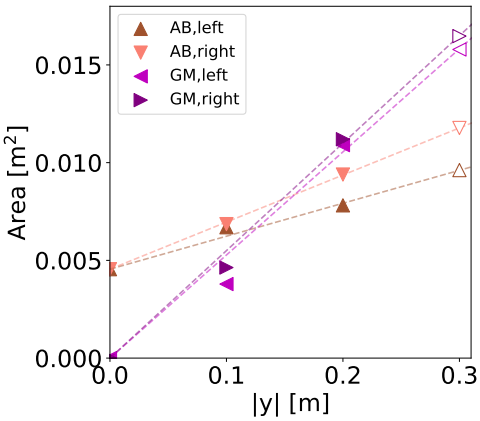

Figure 34: Gravel and boulders areas at y=±0.300 m are estimated using the other coordinates to extract a trend.

For each measured y-coordinate, the space occupied by gravel (A_{gr} [m^2]) or boulders (A_{ab} [m^2]) above the bed thickness is considered. At the sides of the channel ($|y|$>0.300 m) and the centre (y=0.00 m), only assembled boulders are used, therefore the gravel area is 0.00 m^2 and interstices account 30% of the local area. For the coordinates in between, A_{gr} and A_{ab} are treated separately using the sinks at both sides of each mount's profile to separate the first from the second. At coordinate y=±0.300 m, the single components' areas are found with first polynomial approximation on the known coordinates' values as shown in Figure 34 (at y=0.00 m, the boulders area is divided by two since each channel side is calculated separately). The gravel volume V_{gr} [m^3] and the boulders volume V_{ab} [m^3] are found by the sum of the areas per the distance between them. Finally, the interstice volume of each mount V_I is found as 30% of the boulders volume, while the mounts volume V_{GM} [m^3] is the sum of gravel volume plus the remaining 70% of the boulders volume, i.e. $V_{GM} = V_{gr} + 0.7 \cdot V_{ab}$.

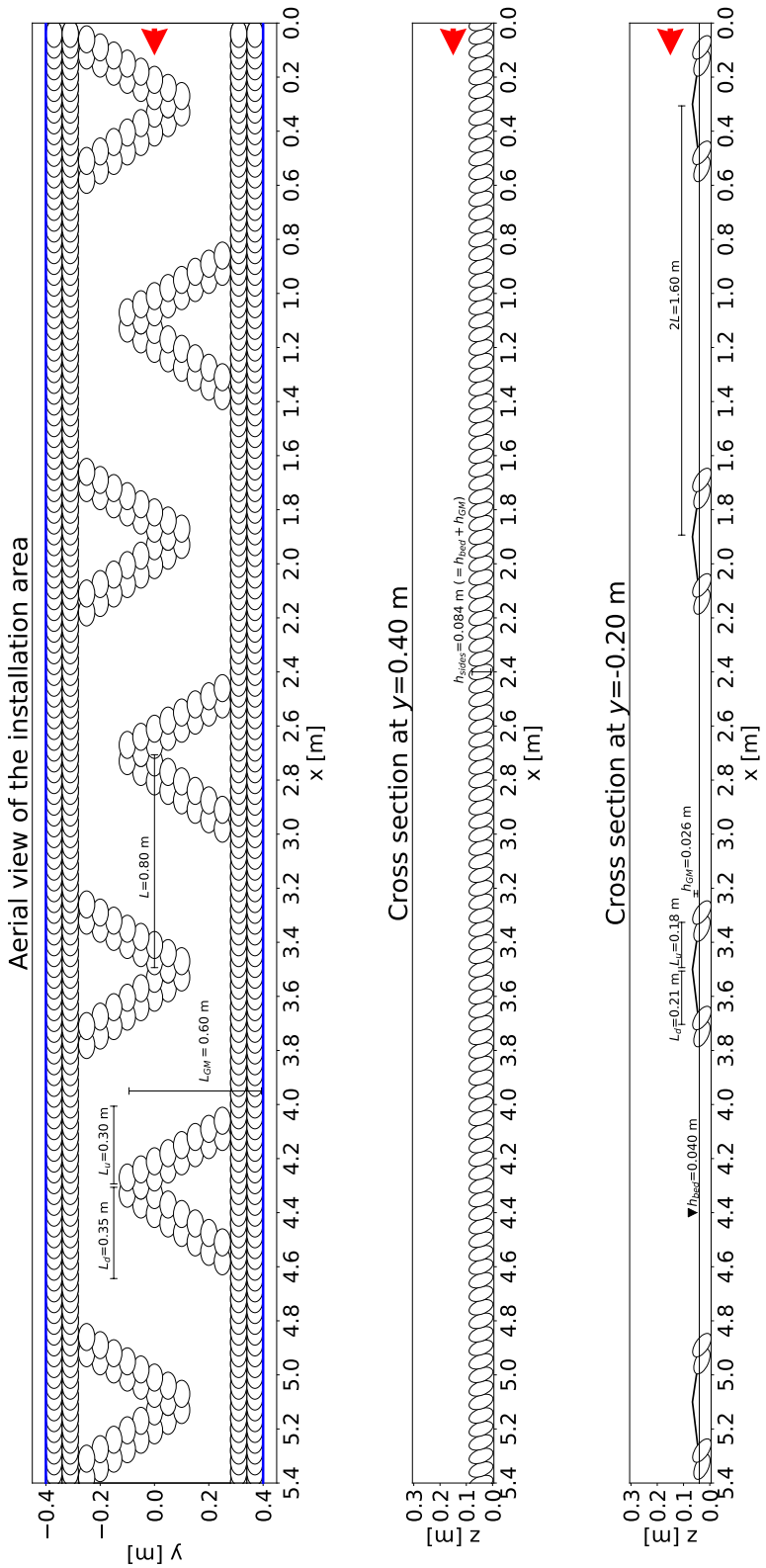

Figure 35: Definition sketch of the installation area for the conducted experiments. The flow direction is given by the red arrow.

4.3 Results and Discussion

4.3.1 Average water depth and Froude number

The average water depth h_{ave} and Froude number Fr are presented for each experiment in Table 12. Both parameters grow because of discharge, with the flow conditions switching from subcritical Fr<1.00 (GM+AB1, GM+AB2 and GM+AB3) to supercritical Fr>1.00 (GM+AB4). The average water depth of both experiments GM+AB1 and GM+AB2 is smaller than the gravel mounts' height h_{GM}=0.0440 m as confirmed visually by Figure 36a, where some boulders are seen emerging above the water. Comparisons are possible between experiments GM2.3, AB4 and GM+AB3 since they all share same height h_{GM}=0.0440 m, channel slope I=0.0100 and discharge Q=0.0588 m^3/s: in experiment GM2.3 (simple triangular gravel mounts) the average water depth is 0.137 m (Table 5); in experiment AB4 (rectangular boulders groynes) it is 0.128 m (Table 9). Both values are larger than what is measured for GM+AB3. This proves that the revised design generate less hydraulic friction with the flow and the addition of assembled boulders and gravel does not necessarily results in a rise in the water level.

Table 12: Flow characteristics above triangular gravel mounts with assembled boulders reinforcement.

	GM+AB1	GM+AB2	GM+AB3	GM+AB4
Q [m^3/s]	0.00370	0.00550	0.0558	0.155
h_{ave} [m]	0.0350	0.0390	0.111	0.145
Fr [-]	0.230	0.290	0.640	1.120

Thanks to the installation of the assembled boulders reinforcements, the model remains stable under all tested discharges. In experiment GM+AB4, widespread gravel shaking and some local erosion is observed. Movement is mostly limited to the top of the gravel mounts, where the gravel is most exposed (Figure 36c). Assembled boulders are never seen moving nor shaking and their critical conditions are expected to happen well above the pump capacity discharge Q=0.155 m^3/s.

(a) Emerging gravel and boulders in model GM+AB1.

(b) Water surface profile over model GM+AB3.

(c) Local gravel erosion at the end of experiment GM+AB4.

Figure 36: Flow conditions above the model under different discharges. In Sub-figures (a) and (b), flow direction is from right to left (left side wall point-of-view).

As shown in Figures 36a, 37a and 37b, in case of small discharge Q≤0.00550 m^3/s the water profile is flat along both the channel's centre part and sides, while some boulder emerges above the flow profile. With increased discharge Q=0.0588 m^3/s (GM+AB3), small waves are formed in the centre part of the channel, while the sides remains flat. The model is now completely submerged. The water level profile resembles what observed in previous experiments such as AB4 (Figure 27d), but the waves amplitude is significantly reduced. Results further confirms the flattening effect of assembled boulders build along the sides of channel. In case of Q=0.155 m^3/s the waves become stronger and now start to appear on the channel's sides as well, although the water surface there can still be classified as generally flat.

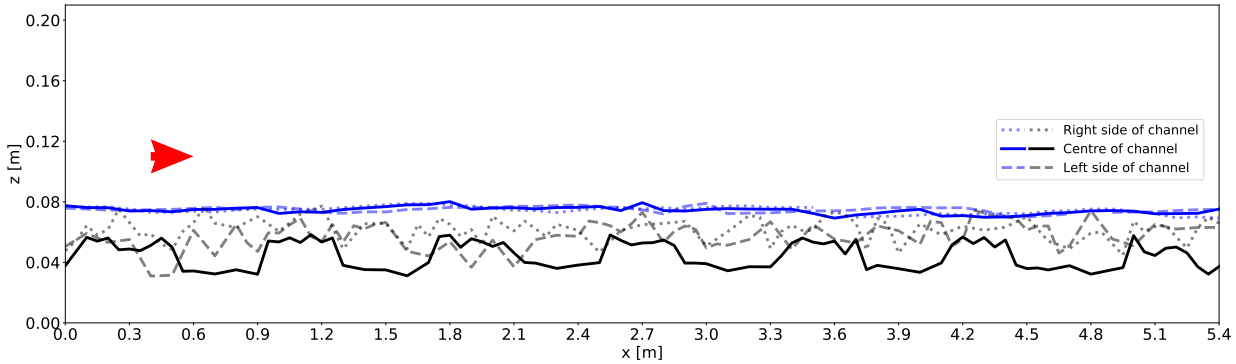

(a) GM+AB1 (Q=0.00370 m^3/s). Measurements at the sides of the channel are taken at y=±0.300 m.

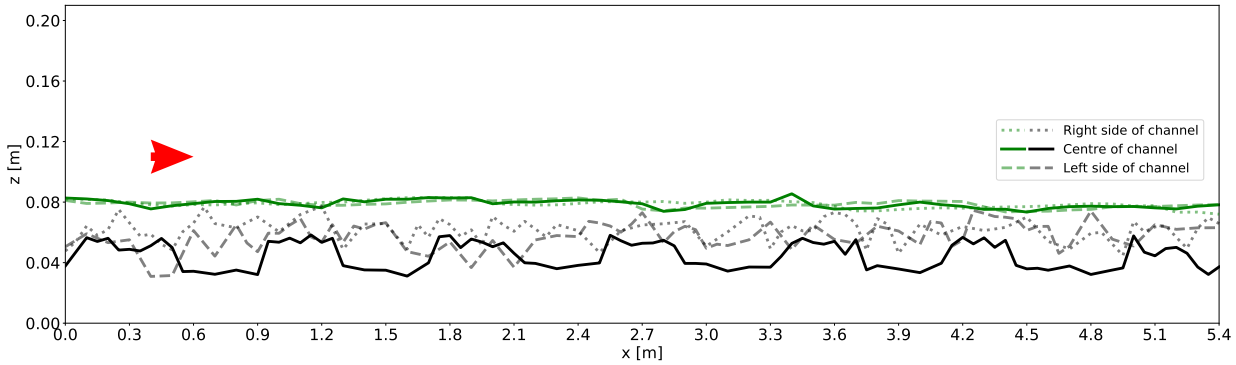

(b) GM+AB2 (Q=0.00550 m^3/s). Measurements at the sides of the channel are taken at y=±0.300 m.

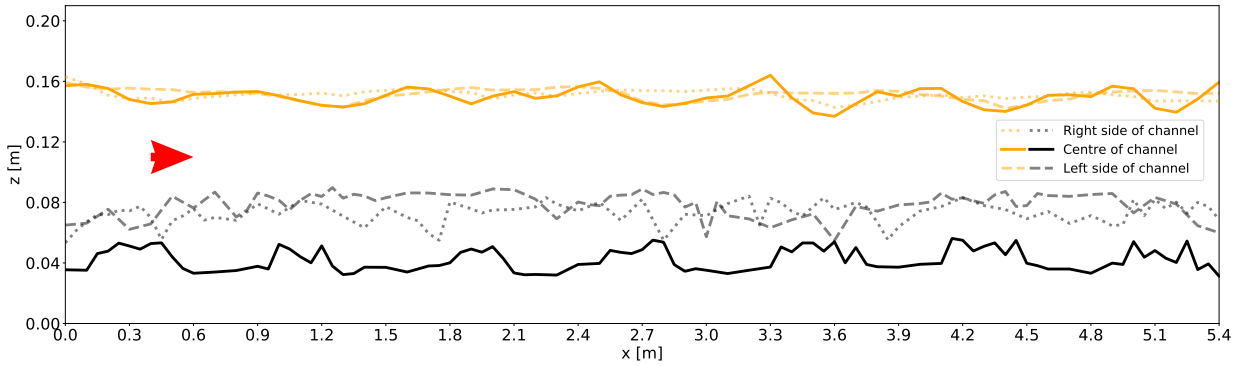

(c) GM+AB3 (Q=0.0588 m^3/s). Measurements at the sides of the channel are taken at y=±0.380 m.

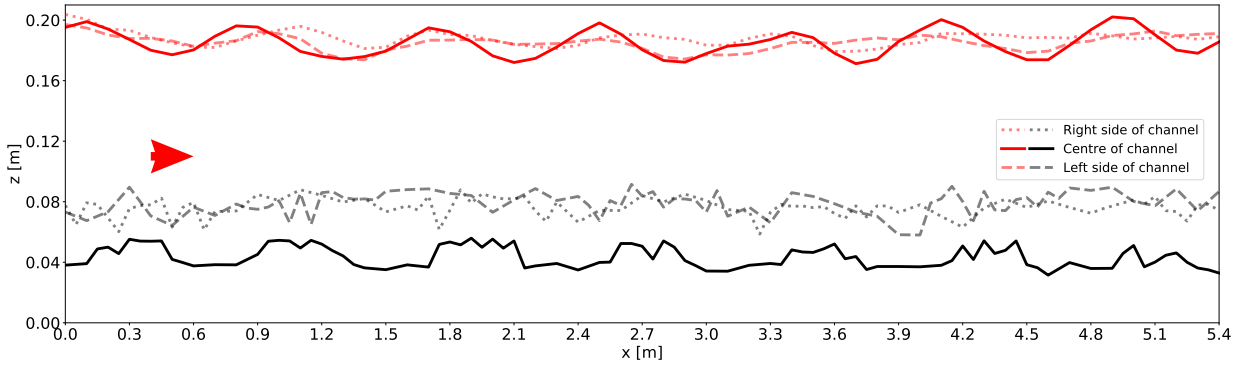

(d) GM+AB4 (Q=0.155 m^3/s). Measurements at the sides of the channel are taken at y=±0.380 m.

Figure 37: Bed and water surface profiles at the centre and the sides of the channel are here presented for this chapter's experiments. The flow direction is given by the red arrow.

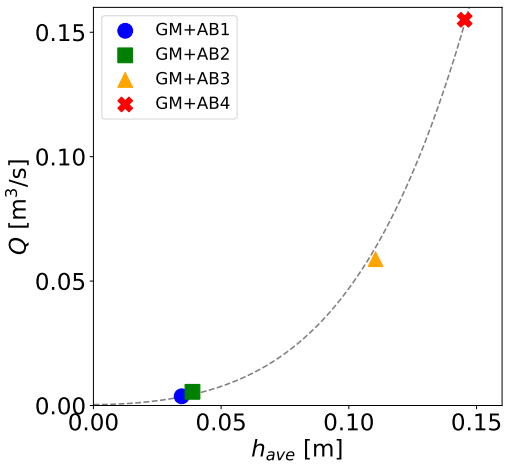

Figure 38: The relationship between average water depth h_{ave} and discharge Q is shown. The dotted gray line represents the trend.

The rise of the average water surface h_{ave} in relationship with discharge Q can be approximated using a 4th polynomial function, as shown in Figure 38. Using this function, it is possible to estimate that the model is fully submerged (i.e. h_{ave}=h_{GM}=0.0440 m) for $Q\geq$0.00580 m^3/s, slightly above what is tested in GM+AB2. The growth of the Froude number with discharge can also be described with a similar plot and another polynomial function of 4th degree. From the latter, it is calculated that critical flow conditions Fr=1.00 are estimated to happen when $Q\cong$0.130 m^3/s.

4.3.2 Vertical velocity profiles

The vertical flow profiles for the different experiments and y-coordinates are shown in Figures 39 to 42. As measurements of the water surface are taken only at the centre and the sides of the channel, the blue line appears each time only in Sub-figures (a) an (d). In experiments GM+AB1 and GM+AB2, measurements at the sides of the channel have been taken at y=±0.300 m (instead of y=±0.380 m as for the other experiments) since the emerging boulders along the sides of the channel made impossible to collect data there. Because a combination of gravel and assembled boulders are used to construct the gravel mounts, it is harder to distinguish each element (and the interstice areas between boulders) from the bed profile's measurements alone. Hence, the total construction area is marked in green-brown stripes without further distinction.

The flat water surface profile observed in experiments GM+AB1 (Figure 39) and GM+AB2 (Figure 40) is shown again. An interruption in the profile due to emerging boulders at y=−0.300 m can be seen in Figure 39d (right). As shown in Figure 37, the increasing discharge creates waves of increasing amplitude primarily in the centre part of the channel and, to a lesser extent, on the sides as well. The formation of refuge able areas is confirmed at least once in every figure, even under the pump capacity discharge of experiment GM+AB4 (Figure 42). The most common places for suitable conditions for refuge to be found are in the right downstream proximity of a gravel mounts or in the sinks inside the mounts' profile where boulders and gravel meet. Similar to what observed around boulders groynes (Chapter 3), not all gravel mounts appear to generate suitable hydraulic conditions for refuge. The measurements' y-coordinate appear to also have a limited effect on the size of the refuge able, contrary to what observed around simple triangular mounts in Chapter 2. The results might be explained by the fact that, from this view angle, the uneven profile of each gravel mount visually looks more similar to a boulders groyne than a triangular gravel mounts. It would make sense for the flow field to behave closer to the former than the latter.

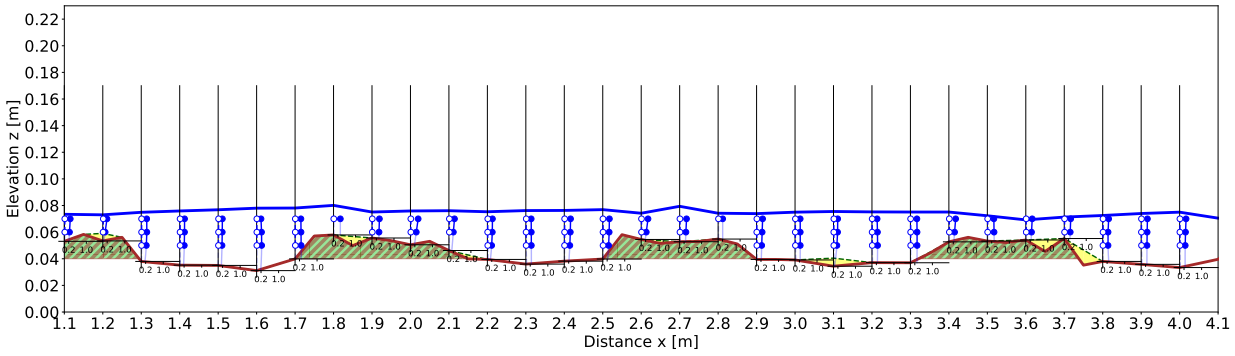

(a) Q=0.00370 m^3/s, y=0.00 m.

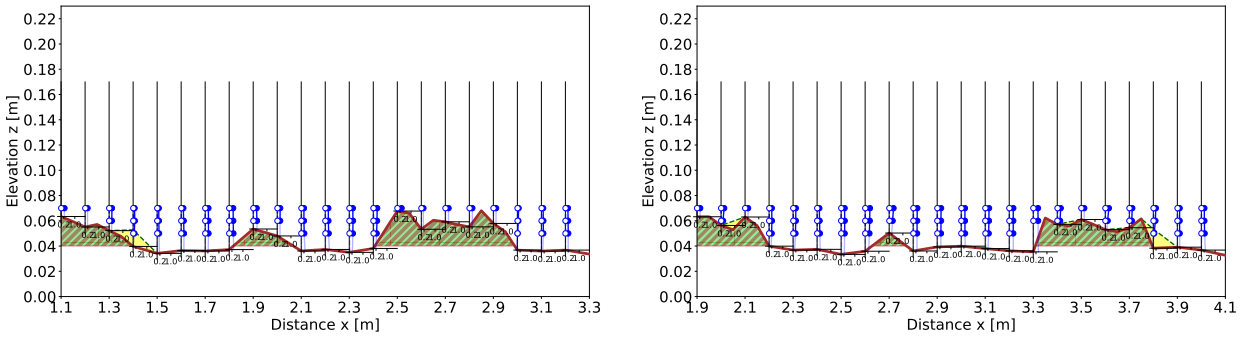

(b) Q=0.00370 m^3/s, y=0.100 m (left) or y=−0.100 m (right). Water surface is not measured here.

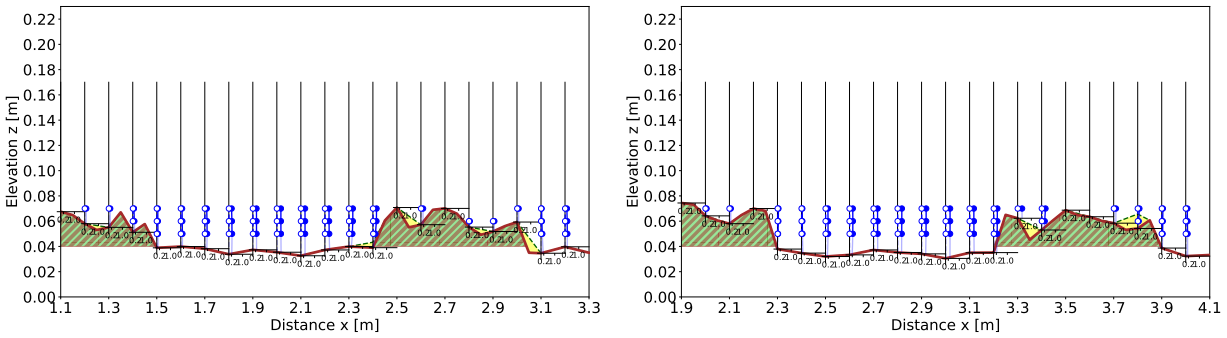

(c) Q=0.00370 m^3/s, y=0.200 m (left) or y=−0.200 m (right). Water surface is not measured here.

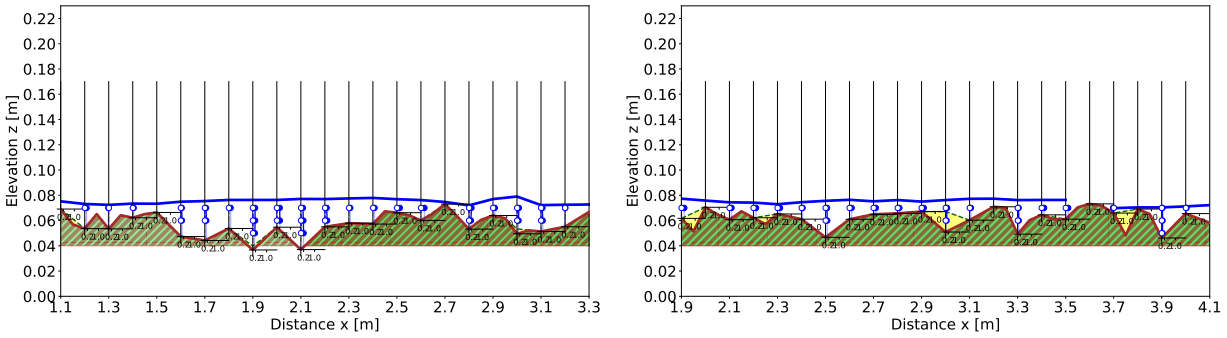

(d) Q=0.00370 m^3/s, y=0.300 m (left) or y=−0.300 m (right).

Figure 39: Vertical profiles of time-averaged velocity (filled markers) and standard deviation of the velocity (empty markers) for experiment GM+AB1. The units of the smaller plots are velocity [m/s] on the x-axis and elevation [m] on the y-axis. The total construction area is coloured brown and green to represent the mounts and interstice areas, respectively. The water surface profile is marked in blue and the refuge able areas are highlighted in yellow.

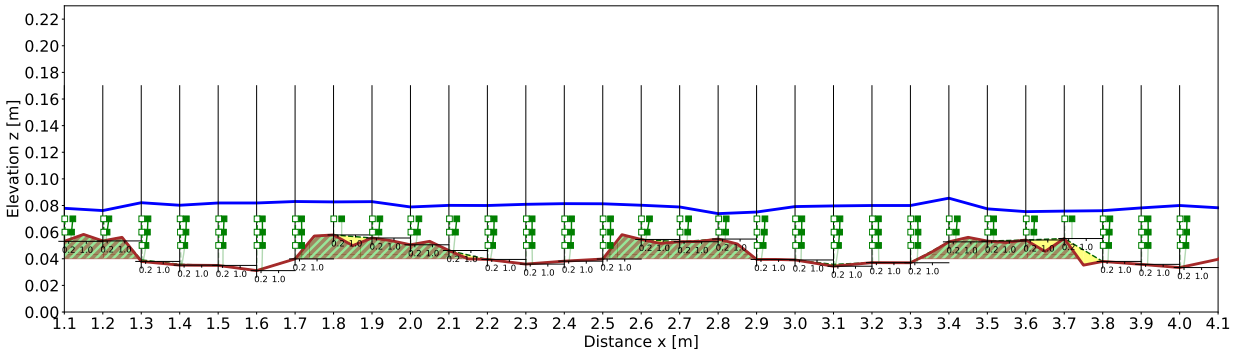

(a) Q=0.00550 m^3/s, y=0.00 m.

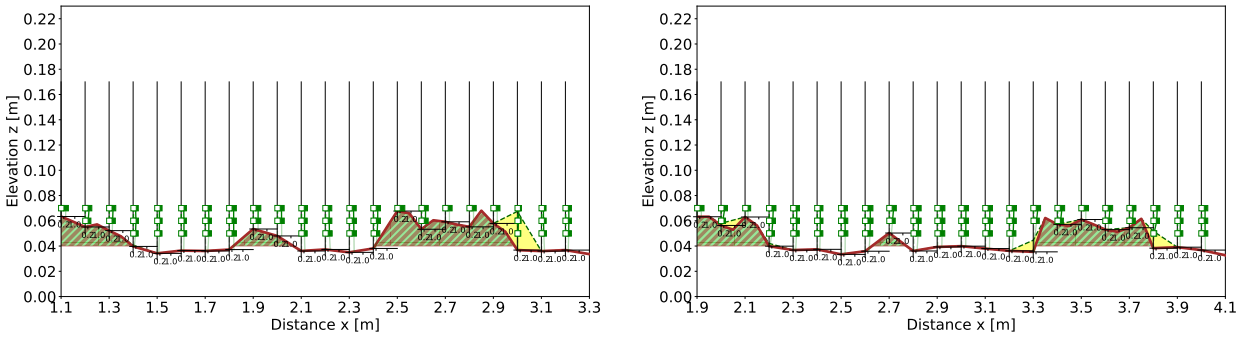

(b) Q=0.00550 m^3/s, y=0.100 m (left) or y=−0.100 m (right). Water surface is not measured here.

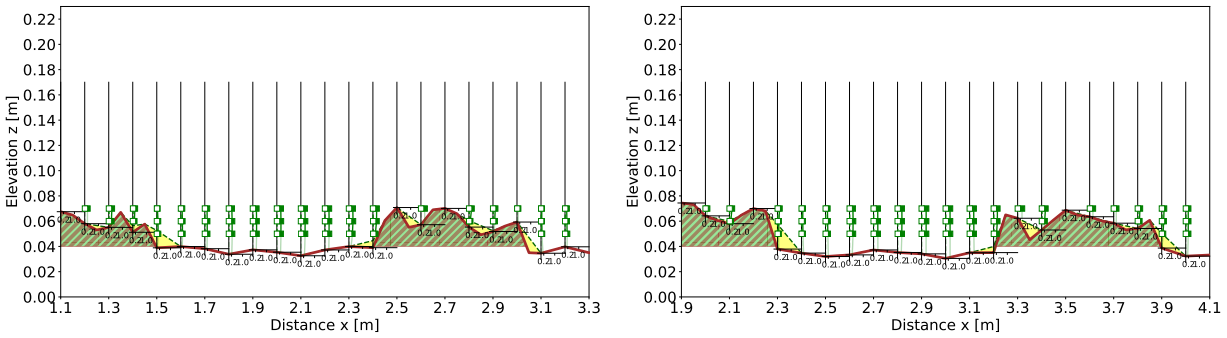

(c) Q=0.00550 m^3/s, y=0.200 m (left) or y=−0.200 m (right). Water surface is not measured here.

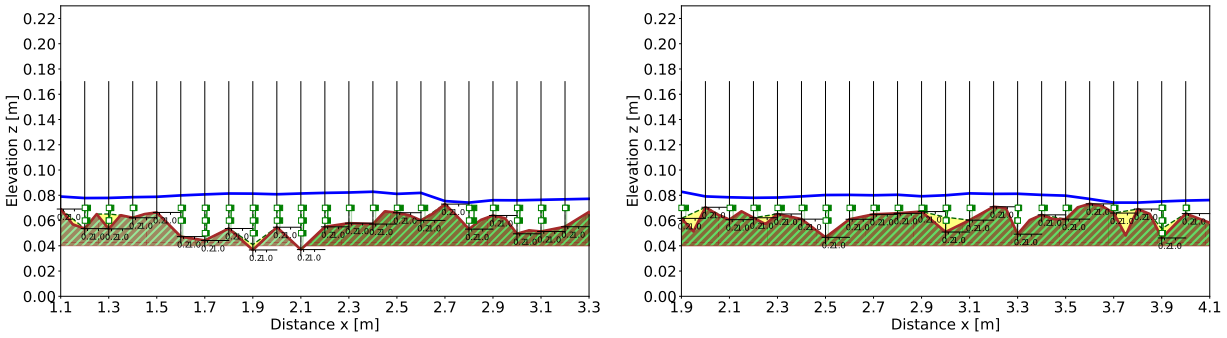

(d) Q=0.00550 m^3/s, y=0.300 m (left) or y=−0.300 m (right).

Figure 40: Vertical profiles of time-averaged velocity (filled markers) and standard deviation of the velocity (empty markers) for experiment GM+AB2. The units of the smaller plots are velocity [m/s] on the x-axis and elevation [m] on the y-axis. The total construction area is coloured brown and green to represent the mounts and interstice areas, respectively. The water surface profile is marked in blue and the refuge able areas are highlighted in yellow.

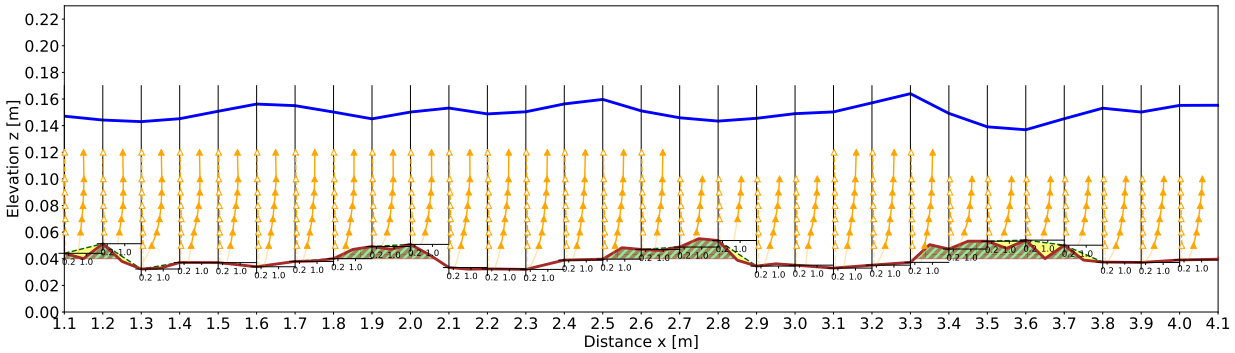

(a) Q=0.0588 m^3/s, y=0.00 m.

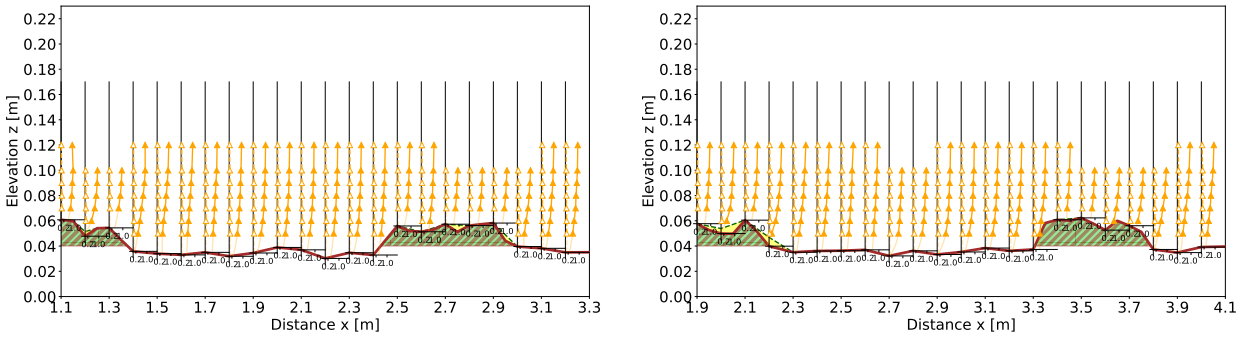

(b) Q=0.0588 m^3/s, y=0.100 m (left) or y=−0.100 m (right). Water surface is not measured here.

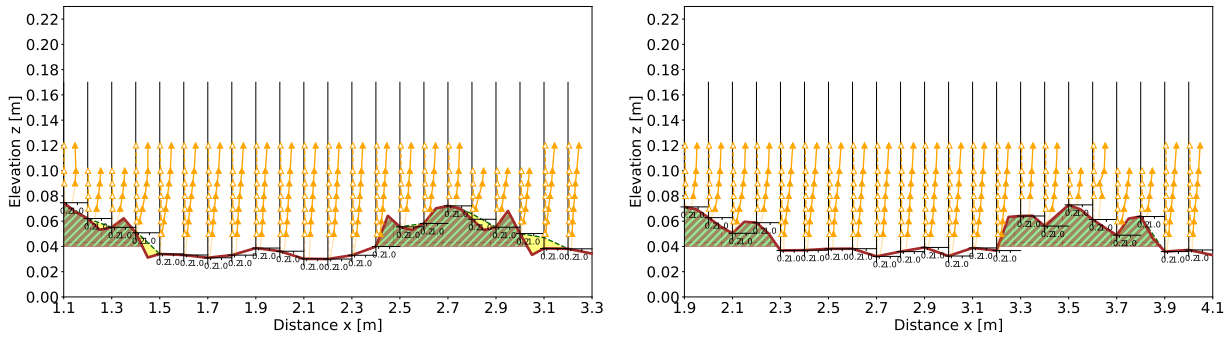

(c) Q=0.0588 m^3/s, y=0.200 m (left) or y=−0.200 m (right). Water surface is not measured here.

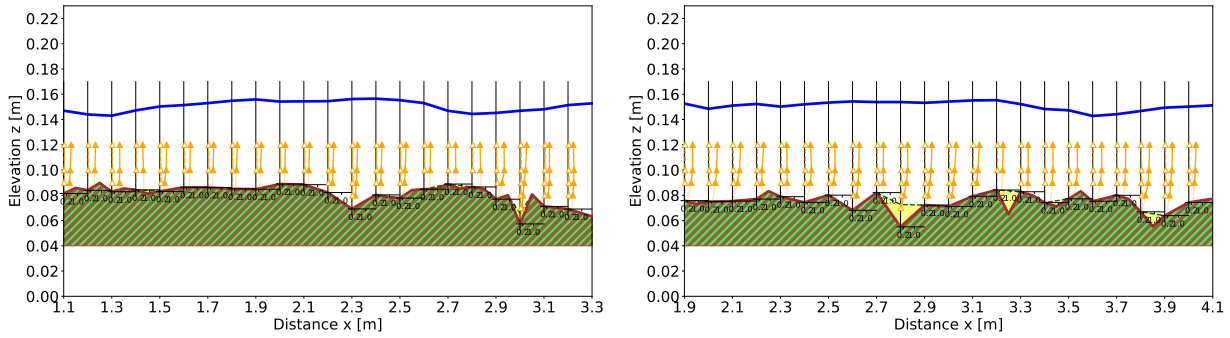

(d) Q=0.0588 m^3/s, y=0.380 m (left) or y=−0.380 m (right).

Figure 41: Vertical profiles of time-averaged velocity (filled markers) and standard deviation of the velocity (empty markers) for experiment GM+AB3. The units of the smaller plots are velocity [m/s] on the x-axis and elevation [m] on the y-axis. The total construction area is coloured brown and green to represent the mounts and interstice areas, respectively. The water surface profile is marked in blue and the refuge able areas are highlighted in yellow.

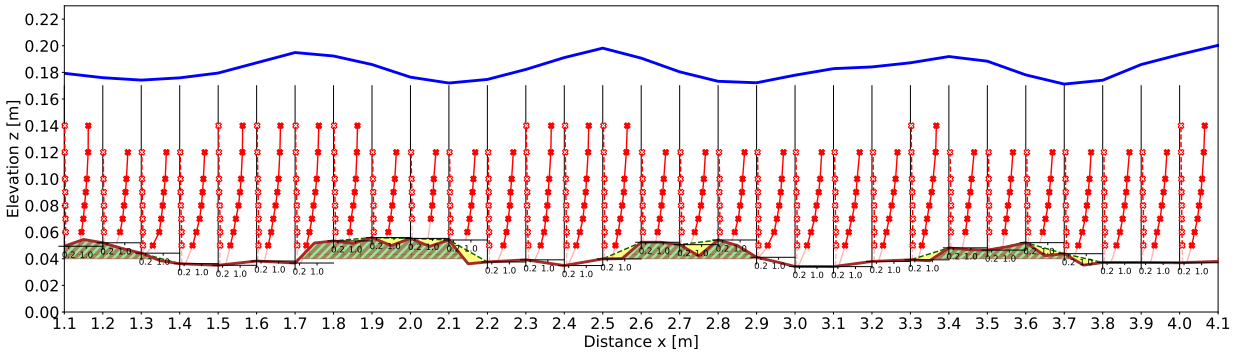

(a) Q=0.155 m^3/s, y=0.00 m.

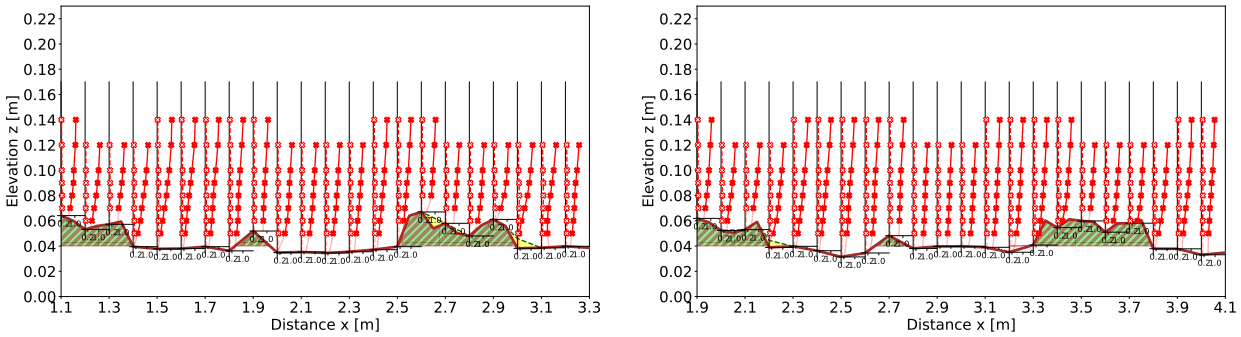

(b) Q=0.155 m^3/s, y=0.100 m (left) or y=−0.100 m (right). Water surface is not measured here.

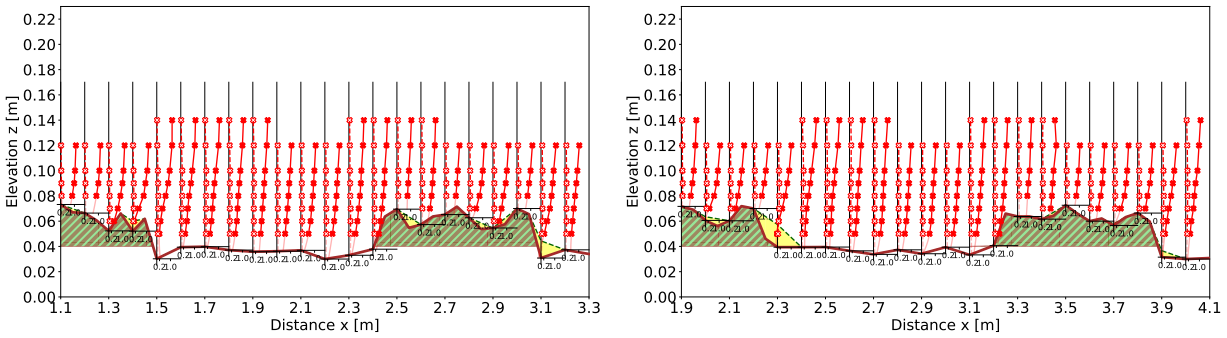

(c) Q=0.155 m^3/s, y=0.200 m (left) or y=−0.200 m (right). Water surface is not measured here.

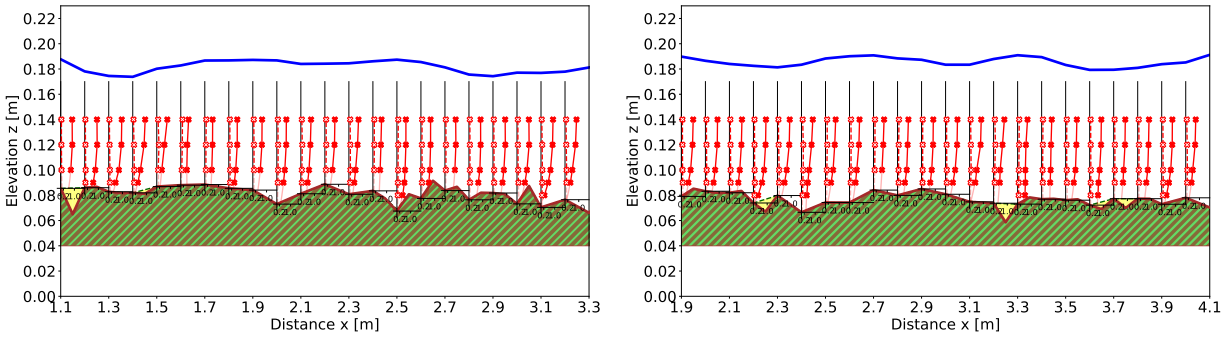

(d) Q=0.155 m^3/s, y=0.380 m (left) or y=−0.380 m (right).

Figure 42: Vertical profiles of time-averaged velocity (filled markers) and standard deviation of the velocity (empty markers) for experiment GM+AB4. The units of the smaller plots are velocity [m/s] on the x-axis and elevation [m] on the y-axis. The total construction area is coloured brown and green to represent the mounts and interstice areas, respectively. The water surface profile is marked in blue and the refuge able areas are highlighted in yellow.

4.3.3 Meandering behaviour

Figures 43 and 44 confirm that the triangular shape of the gravel mounts and their alternated positioning are very important in creating a meandering flow. Areas with slow-flowing areas are visible near the gravel bed behind most gravel mounts. This is another visual representation of the refuge able areas discussed in the previous Sub-chapter 4.3.2. The meandering behaviour is observed in all experiments, although two factors appear to reduce it: measurement elevation and discharge. The flow in Figure 44d looks significantly straighter than what shown in Figure 43a.

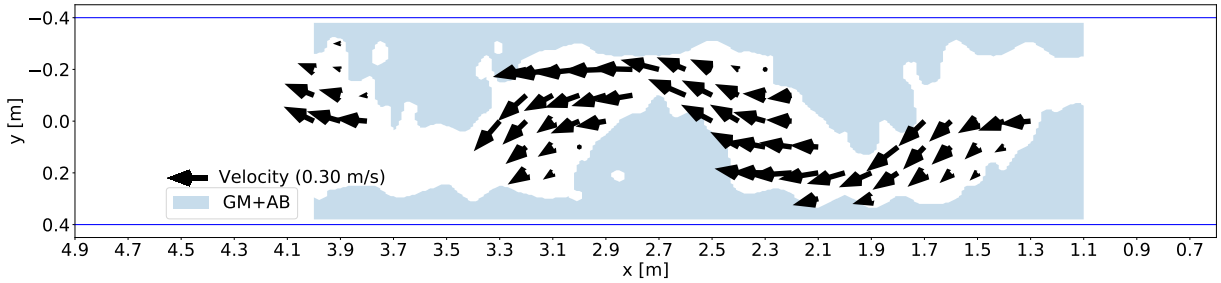

(a) Q=0.00370 m^3/s (GM+AB1), measurement elevation z=0.0500 m.

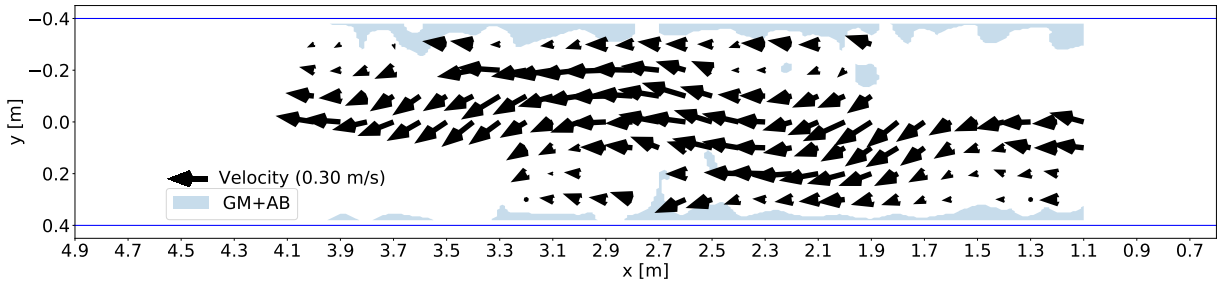

(b) Q=0.00370 m^3/s (GM+AB1), measurement elevation z=0.0700 m.

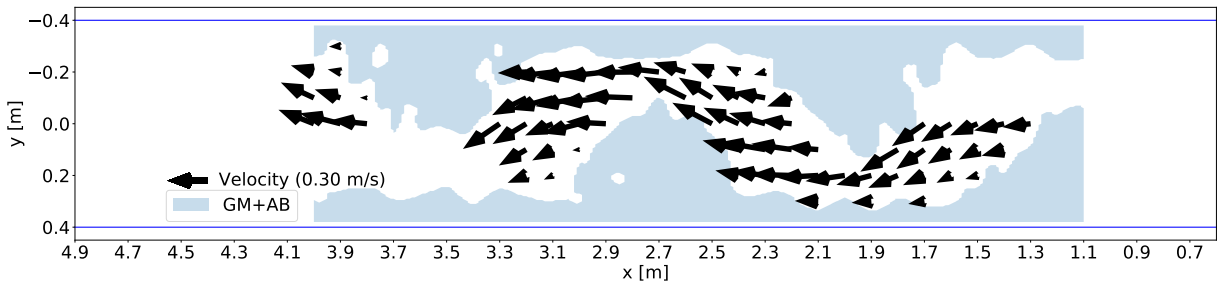

(c) Q=0.00550 m^3/s (GM+AB2), measurement elevation z=0.0500 m.

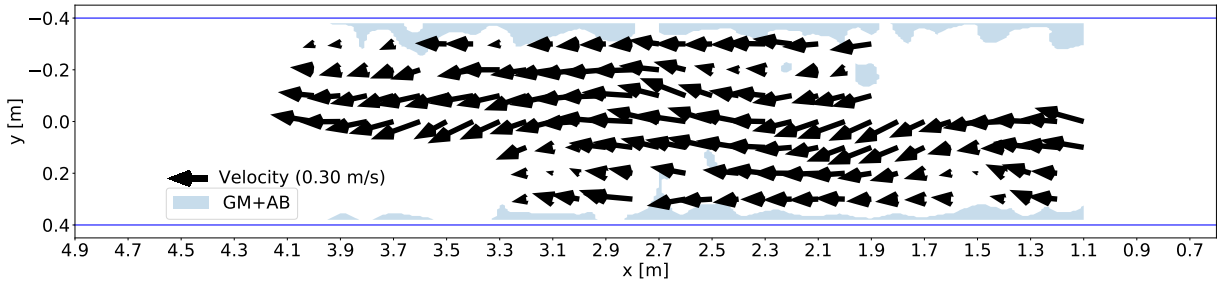

(d) Q=0.00550 m^3/s (GM+AB2), measurement elevation z=0.0700 m.

Figure 43: Horizontal velocity profiles for experiments GM+AB1 and GM+AB2. Each time, the data collected the closest from the gravel bed (a,c) or the water surface (b,d) are shown. Flow direction and its intensity are given by the black quivers (scaled to plot axis, legend for reference), while the total construction area is coloured blue and labelled "GM+AB".

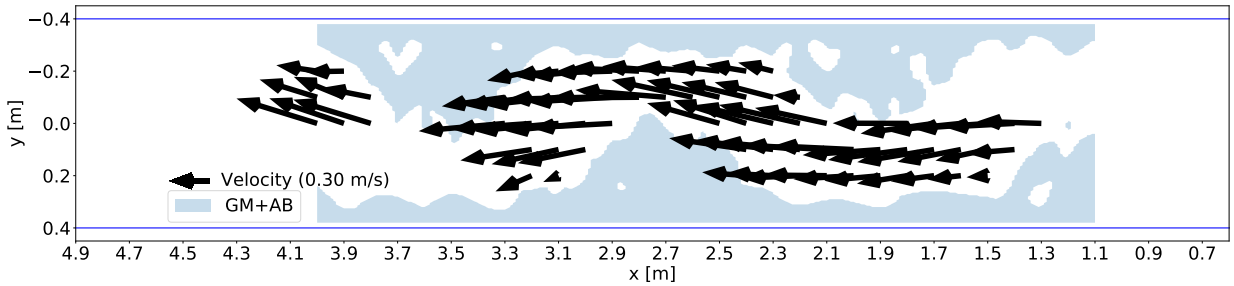

(a) Q=0.0588 m^3/s (GM+AB3), measurement elevation z=0.0500 m.

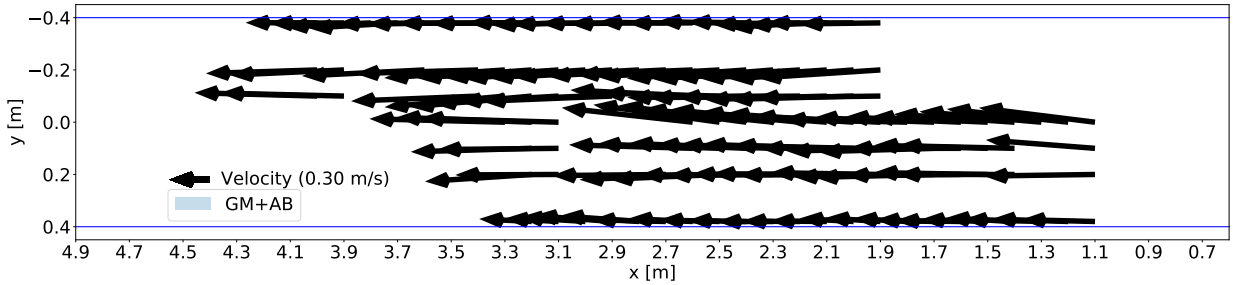

(b) Q=0.0588 m^3/s (GM+AB3), measurement elevation z=0.120 m.

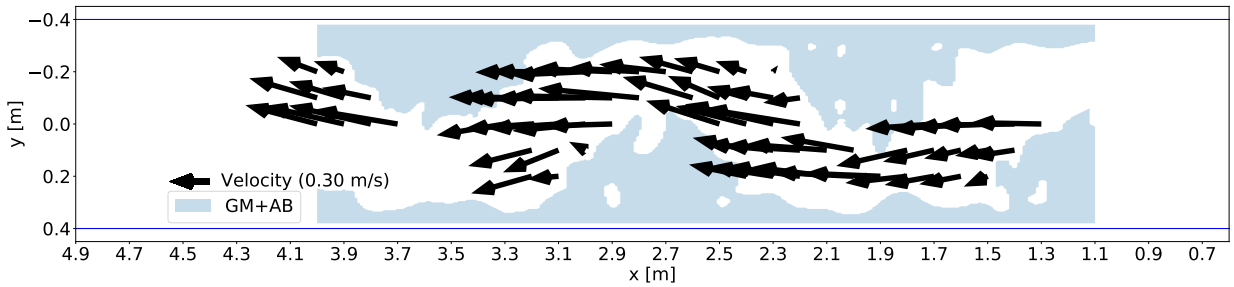

(c) Q=0.155 m^3/s (GM+AB4), measurement elevation z=0.0500 m.

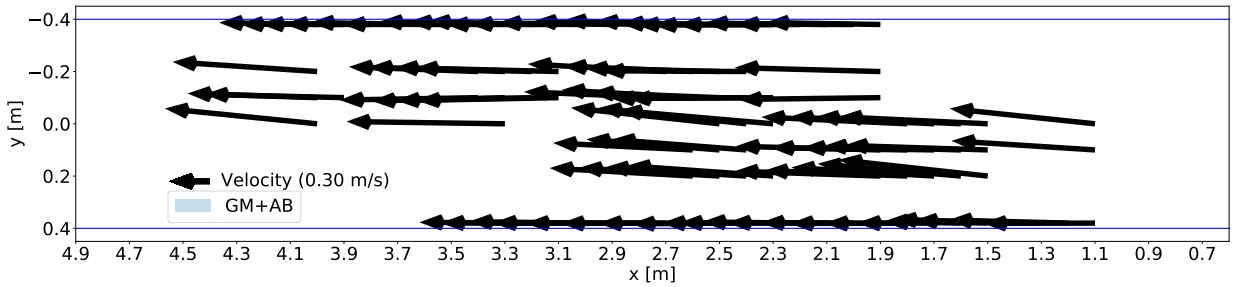

(d) Q=0.155 m^3/s (GM+AB4), measurement elevation z=0.140 m.

Figure 44: Horizontal velocity profiles for experiments GM+AB3 and GM+AB4. Each time, the data collected the closest from the gravel bed (a,c) or the water surface (b,d) are shown. Flow direction and its intensity are given by the black quivers (scaled to plot axis, legend for reference), while the total construction area is coloured blue and labelled ”GM+AB”.

By gathering all velocity measurements in one plot it is possible to extract some trends. As shown in Figure 45, the flow indeed straighten with increasing discharge. This behaviour is stronger in the centre part of the channel since the trend line in Figure 45a (y=0.00 m) is steeper than what observed in Figure 45b ($|y|\geq$0.300 m). The meandering behaviour is expressed as the ratio of the absolute values of the lateral component v [m/s] over the longitudinal u [m/s], as shown in Figure 46. Again, it is clear that the size of the discharge has a straightening effect of the flow. The relationship appear to take the shape of a negative exponential, as the difference between the measurements of GM+AB1 and GM+AB2 is more visible than between GM+AB3 and GM+AB4, despise the discharge difference is 0.00180 m^3/s in the first case and 0.0962 m^3/s in the second.

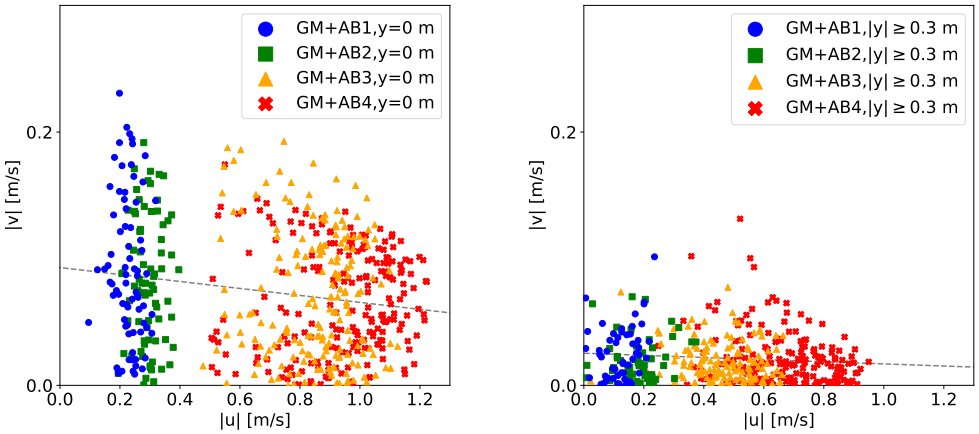

(a) The centre of the channel (y=0.00 m). (b) The sides of the channel ($|y| \geq$0.300 m).

Figure 45: The velocity measurements of all experiments are separated based on their y-coordinate: y=0.00 m (left) and $|y|\geq$0.300 m (right). Both axes are shown in absolute values, while the trend is given by the dotted gray line.

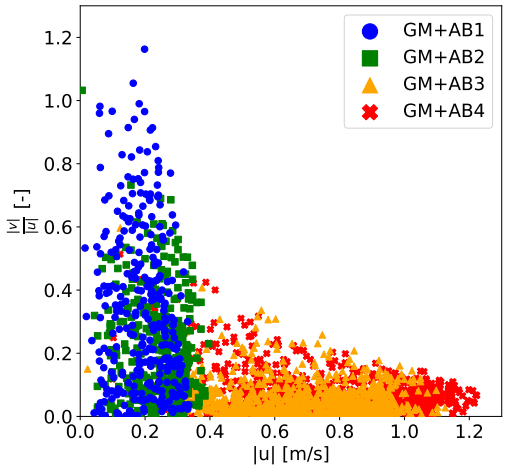

Figure 46: The meandering behaviour is expressed by the ratio of the absolute values of lateral component v [m/s] over longitudinal component u [m/s]. This is then plotted over the absolute value of u [m/s].

4.3.4 Mounts volume, refuge able volume and interstice volume

For each experiment, Table 13 shows the researched volumes: the mounts volume V_{GM}, the refuge able volume V_{RA}, the interstice volume V_I, the relative suitable volume $100 \cdot \frac{V_I+V_{RA}}{V_{GM}}$ and finally the percent of interstice volume over total construction volume $\frac{V_I}{V_{GM}+V_I}$. When calculating V_{GM} and V_I for cases GM+AB1 and GM+AB2, only the gravel and boulders under the average water depth are considered since this is smaller than 0.0440 m, the gravel mounts height.
Because the gravel mounts' morphology is the same for all experiments, V_{GM} $\cong$150.00$\cdot 10^{-4}$ m^3 remains generally constant. This value oscillates a little because each model has been constructed by hand and inaccuracies are therefore generated. The same happens to the interstice volume, which is directly related to the mounts volume. The refuge able volume V_{RA} does not appear to be significantly affected by the increased discharges of experiments GM+AB3 and GM+AB4, thus confirming what speculated in the previous sub-chapters. The relative suitable volumes follow a similar pattern: the smallest value is found in experiment GM+AB1 where the shallow water level is suspected to be the main limiting factor in the formation of suitable habitat. Experiment GM+AB2 results in the largest relative volume (40% of the mounts volume) after which the value stabilizes constant at 38% for both GM+AB3 and GM+AB4. Somewhere between experiments GM+AB2 and GM+AB3, the optimal conditions where sufficiently deep water depth and not-too-large discharge are expected to meet to generate the largest suitable volume possible. Based on the observed results, it can be assessed that each gravel mount with assembled boulders reinforcement can generate a suitable volume around 38% of its own with limiting factors such as shallow water surface and large flood's discharge having only limited effect of this performance. Table 13 also confirms that each gravel mounts has a porosity of n=0.220. This value is constant throughout the experiments and slightly smaller than 0.300, the porosity of simple assembled boulders constructions (Sub-chapter 3.2.1). Future research can use this 22% ratio to calculate the interstice volume directly from the bed surface measurements without going through the calculations of Sub-chapter 4.2.1 again.

Table 13: Mounts volume V_{GM} [10^{-4} m^3], refuge able volume V_{RA} [10^{-4} m^3], interstice volume V_I [10^{-4} m^3], relative suitable volume $100 \cdot \frac{V_I+V_{RA}}{V_{GM}}$ [%] and porosity $\frac{V_I}{V_{GM}+V_I}$ [%] are shown for each experiment.

	GM+AB1	GM+AB2	GM+AB3	GM+AB4
V_{GM} [10^{-4} m^3]	140.00	150.00	150.00	160.00
V_{RA} [10^{-4} m^3]	11.00	18.00	13.00	16.00
V_I [10^{-4} m^3]	42.00	43.00	42.00	44.00
$100 \cdot \frac{V_I+V_{RA}}{V_{GM}}$ [%]	36	40	38	38
$\frac{V_I}{V_{GM}+V_I}$ [-]	0.220	0.220	0.230	0.220

4.4 Conclusions

The new gravel mounts' morphology with assembled boulders reinforcements has shown highly positive results. The stability of the model is guaranteed even under the stress of the pump capacity discharge thanks entirely to the presence of the assembled boulders. They are also instrumental in keeping the water surface flat along both sides of the channel. In the centre part, waves are formed, whose amplitude is directly related to discharge. The average water depth follows a similar behaviour and its relationship with discharge can be approximated using a 4$^{\text{th}}$ polynomial approximation. Full submersion of the model is expected for $Q \geq 0.00580$ m^3/s and the average Froude number should be smaller than 1 for $Q < 0.130$ m^3/s, above which the flow turns supercritical. For same constructions' height, discharge and slope, the average water depth above the here tested models is the smallest between all studied designs of this thesis. The triangular shape of the gravel mounts is important to create a meandering flow and to generate areas with slow flowing water near the gravel bed behind

each gravel mount. Other important spots where refuge able areas can be generated are the inward side of the assembled boulders reinforcements (where boulders and gravel meet) and the sinks in the profile of the boulders build along the sides of the channel. By increasing the discharge, the flow tend to straighten, particularly around the centre part of the channel and/or close to the water surface. However, this does not significantly affect the flow characteristics near the gravel bed, where both the meandering flow and the refuge able areas continue to be observed even under pump capacity discharge. Shallow water conditions also appear not to significantly affect the creation of refuge able areas. Based on the gathered results, it can be confidently assessed that each triangular gravel mount with assembled boulders reinforcement can generate a total suitable volume (refuge able volume plus interstice volume) around 38% of its own. Also, calculations have discovered that 22% of the space occupied by each gravel mounts is empty (i.e. the mounts' porosity is n=0.220). Since gravel is here used together with boulders, this value is smaller than 0.300, the porosity of simple assembled boulders constructions.
The main discoveries of this chapter are summarized here:

- Thanks to the installation of the assembled boulders reinforcement, the stability of the gravel mounts is confirmed for all studied discharges, even at pump capacity;
- The water surface is flat in case of small discharge, but waves of each time larger amplitude are formed in the centre part of the channel when the discharge is increased;
- The assembled boulders built along the sides of the channel successfully keep the water surface flat there;
- The proposed design measures the smallest average water surface between all experiments tested in this thesis that have same mounts' height, discharge and channel slope;
- The average water surface grow with discharge following a 4^{th} polynomial function and full submersion of the model is expected for $Q \geq 0.00580$ m^3/s;
- The flow is subcritical for $Q < 0.130$ m^3/s, above which it becomes supercritical;
- The triangular shape of the gravel mounts forces the flow to meander. This behaviour is observed under all tested discharges and it is at its strongest near the gravel bed;
- The flow straighten with increasing discharge and this process is faster near the water surface and/or in the centre part of the channel;
- Refuge able areas are found mostly near the gravel bed behind the gravel mounts, although this is not observed everywhere;
- Other common places where the suitable conditions for refuge are met are: inside the sinks of the boulders' profile or the inward side of the assembled boulders reinforcements where the boulders meets the gravel of the mounts;
- Gravel mounts with assembled boulders reinforcement have a porosity of n=0.220 (i.e. the interstice volume is 22% of the total constructions volume). This value is smaller than 0.300 observed inside constructions that use only assembled boulders;
- Each triangular gravel mounts can generate a total suitable volume around 38% of its own, with limiting factors such as shallow water and large discharge having little effects on this performance.

5 Further experiments conducted besides the main research

5.1 Multi-layered gravel bed

The experiments presented in Chapter 2 highlighted serious stability concerns for triangular gravel mounts built over a single-layered gravel bed. To address this problem, the first model using a multi-layered gravel bed was constructed on September 7$^{\text{th}}$, 2020. The installation's length is 4.70 m with bed thickness h_{bed}=0.0400 m and flat surface (Figure 47a). A metal bar is installed at the downstream end of the model and the channel slope is set at I=0.0100. Four discharges are tested: Q=0.0590, 0.0840, 0.114, 0.143 m^3/s. In the latter case, flow velocity is measured at three coordinates x=0.900, 2.30, 3.50 m at the centre of the channel (y=0.00 m) every 0.0100 m in z-direction from the gravel bed to the water surface. At x=3.50 m further velocity measurements are taken at y=−0.200, −0.300, −0.380 m also every 0.0100 m in z-direction. After one hour, the metal bar is removed and the erosion process observed. The results of this experiment have been published in Yasuda (2021) [32]).
In case of Q=0.0590 m^3/s, the water surface can be described as flat. Frequent shaking of the grains on the bed surface is observed, although movement is rare and erosion downstream of the installation area is negligible. For Q=0.0840 m^3/s, the water surface remains flat, while slightly more gravel movement and erosion is observed. Stronger discharge Q=0.114 m^3/s causes more grain shaking, but transport is still negligible. In case of Q=0.143 m^3/s, the first signs of scouring are observed at the upstream end of the model, where 0.150 m long dent is formed (Figure 47b). Slightly more gravel activity is also observed on the bed surface, but the situation generally stabilize itself after around 20 minutes from the discharge increase. No further remarkable changes are noticed for the following couple of hours. Velocity measurements can be taken until a maximal elevation of z=0.100 m before the air bubbles generated by the water crashing on the sensor holder make data collection impossible. To measure the surface velocity component u (i.e. in longitudinal direction), a propeller-type current meter (KENEK Co. model VR-301 [47]) is used in the centre part of the channel. The resulting surface velocities are: u≅1.25 m/s in the upstream area of the model (precise x-coordinate not recorded), u≅1.35 m/s in the middle area and u≅1.45 m/s in the downstream area. These values confirm what measured by the electrical-magnetic current meter shown in Figure 48 where the time-averaged velocity swings from $\overline{V}$ ≅0.700 m/s near the gravel bed to $\overline{V}$ ≅1.20 m/s at z=0.100 m. Similar to what observed in the other experiments with flat gravel bed morphology (i.e. GM1.1, GM2.1 and AB1), the vertical flow velocity profiles show little heterogeneity in both longitudinal and lateral directions. The standard deviation of the velocity remains constant at *std(V)*≅0.100 m/s in all three dimensions. Since both parameters are well above the thresholds for refuge, the total suitable volume in this model is expected to be 0.00 m^3.

(a) Model set-up with 0.0400 m thick, flat gravel bed.

(b) Upstream scouring in case of Q=0.143 m^3/s.

(c) Gravel erosion in case of Q=0.143 m^3/s.

Figure 47: Experimental set-up (left) and model condition in case of Q=0.143 m^3/s, before the downstream metal bar is removed (centre and right). Flow direction from right to left.

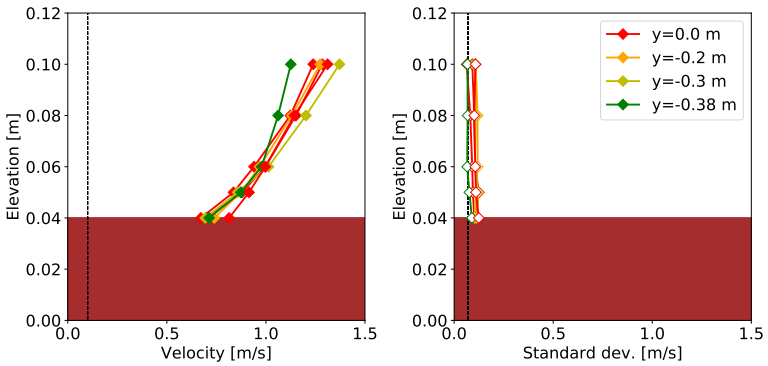

Figure 48: Vertical profiles of time-averaged velocity $\overline{V}$ and standard deviation of the velocity $std(V)$ above 0.0400 m thick flat gravel bed and Q=0.143 m^3/s. The thresholds for refuge are marked by the dotted line. The brown area represents the bed profile.

After the removal of the downstream metal bar, significant erosion is observed almost immediately, as shown in Figure 49. In the upstream side of the model, the scouring dent increases to 0.200 m in length within the first 15.00 s. The gravel bed reorganizes in anti-dunes with a general height of around 0.0500-0.0600 m and distance between one another of around 0.800 m. Strong waves are formed on the water surface. Their length and amplitude appear to be uniform along both x- and y-axis and each top is around 0.210 m high. In total, 3.40 kg of gravel are collected downstream of the model at the end of the experiment (this mass considers also the erosion occurred under smaller discharge conditions, although their contribution is considered negligible). With a total model mass estimated at 140.60 kg, results suggest that 2.4% of the gravel mass has been eroded during the experiment.
In conclusion, this experiment confirms the importance of a multi-layered bed thickness and the installation of the metal bar at the downstream end of each model for the creation of a stable gravel bed that could resist multiple hours under the stress of discharges close to the pump capacity conditions. Based of these remarks, a bed thickness of 0.0400 m has been preferred for all the following experiments presented from Chapter 3 onward.

(a) Grains transport from one anti-dune to another.

(b) Anti-dunes are visible under the wavy water surface.

(c) Gravel erosion after the removal of the downstream metal bar.

Figure 49: Model condition in case of Q=0.143 m^3/s after the downstream metal bar is removed. Flow direction from right to left.

5.2 Living eels and prototype-scaled boulders

On July 7th, 2020, an experiment was conducted releasing Japanese eels (*Anguilla japonica*) around prototype-scaled assembled boulders. The results have been published in Yasuda (2021) [32]).
Firstly, the channel is filled with boulders (average diameter around 0.250 m, mostly round-shaped, exact grain distribution unknown) assembled on top of each others for a total model length of 4.15 m. In two points (x=0.650, 2.95 m), a second line of boulders is placed over the assembled construction, to create a structure similar to a ramp (Figure 50). The channel slope is set at I=0.0100 and two

metal nets are placed at both ends of the experimental channel to avoid eels wandering off or getting flushed down the water tank. The experiment begins by filling the model at discharge Q=0.0582 m^3/s. The eels are then released in the channel and left to adapt to the new environment for one day. On the second day (July 8$^{\text{th}}$), the discharge is increased to Q=0.151 m^3/s.

(a) Prototype-scaled boulders with the author's hand for reference.

(b) Side view of one of the ramps (left side wall).

(c) The model is viewed from upstream.

Figure 50: The experimental set-up before the release of eels.

Under discharge Q=0.0582 m^3/s, eels are occasionally seen swimming around (Figure 51b), although the majority of the time, they lay between the assembled boulders as shown in Figure 51c. Based on the observed behaviour, eels do not appear to be in danger of being flushed under this discharge.

(a) The eels before being released inside the channel.

(b) An eel return inside the assembled boulders (flow from right).

(c) An eel lays inside the assembled boulders (flow from right).

Figure 51: The experimental conditions for Q=0.0582 m^3/s.

The sudden increase of the discharge to Q=0.151 m^3/s causes two eels to crash against the downstream net. Later, two more eels were flushed downstream after having leapt outside the assembled boulders. Although injured, all four individuals are safely removed from the experiment. One individual was collected upstream of the model having slipped thought the net while trying to conduct an upstream migration. Besides these, the majority of the eels laid in groups inside the assembled boulders for the entire duration of the experiment (Figures 52a and 52b).

(a) An eels on the move.

(b) Group of eels between boulders.

(c) The water surface.

Figure 52: The experimental conditions for Q=0.151 m^3/s (flow direction from right to left).

5.3 Combination of gravel and boulders with scale factor S=2.5

Between April 19th and 22nd, 2022, the flow characteristics were researched inside one section of a S=2.5 scaled model of the triangular gravel mounts with assembled boulders reinforcement presented in Chapter 4. The aim of the experiment is to study the vertical velocity flow profile inside the gravel or boulders constructions, unreachable areas by the usual experimental scale. Since the scaled width would measure 2.00 meters and do not fit in the 0.800 m wide experimental channel, only the left section is constructed as a 6.00 m long model with two gravel mounts built 4.00 m apart and each time 1.00 m from the upstream and downstream ends of the model. Both mounts are 1.62 m wide at the left side wall with theoretical upstream and downstream widths of 0.750 m and 0.870 m, respectively. For simplicity, both sides are constructed equally long 0.810 m in practice. The triangular shape was maintained resulting in the mounts' width decreasing to 0.580 m on the right side wall of the channel (due to the scale of the model, the gravel mounts' toes do not fit in the experimental channel). Along the left side wall, the assembled boulders are placed with same height as the mounts' top in two layers running along the entire model's length. Their transverse width is around 0.180-0.200 m. Firstly, coarse gravel G1 (d_{50}=0.0170 m) is used as foundation and deposited along the left side of the channel or inside the mounts' perimeter. The rest of gravel bed is constructed using medium boulders B1 (d_{50}=0.0630 m), assembled like fallen dominoes facing downstream with an angle of 60°-70° from the horizontal. The bed thickness is uniform at 0.100 m. The same material is used to build the core of the two gravel mounts. The triangular profile is maintained with linearly decreasing height: from 0.210 m at the left side wall to 0.140 m at the right. The scaled assembled boulders are simulated using coarse boulders B2 (d_{50}=0.0920 m), again placed on top of each others like fallen dominoes facing downstream with an angle of 60°-70° from the horizontal. Pictures of the construction process are shown in Figure 53. The channel slope and discharge are I=0.0100 (scale independent) and $Q_{S=2.5}$=0.144 m^3/s (equal to $Q\cong$0.0150 m^3/s in the usual experimental scale). Bed surface and water level are collected every 0.100 m in x-direction along the entire model's length and y=−0.380, −0.300, −0.200, −0.100, 0.00, 0.100, 0.200, 0.300, 0.380 m for the former and y=−0.380, 0.00, 0.380 m for the latter, respectively. Velocity measurements are conducted at specific points each time every 0.0100 m in z-direction from the lowest allowed elevation inside the gravel or boulders construction to the water surface. In total, 3 measurements points are chosen inside the gravel mounts; 17 points inside the assembled boulders around the mounts; 3 points inside the assembled boulders along the left side wall and finally 2 more points inside the gravel bed.

(a) Construction of one scaled gravel mount.

(b) Composition of the assembled boulders along the side wall.

(c) The completed model scaled 2.5 times viewed from upstream.

Figure 53: Construction of the scaled gravel mounts with assembled boulders reinforcement.

The studied discharge $Q_{S=2.5}$=0.144 m^3/s is too small to generate any movement in the model, as proved by the fact that the scaled model remains completely immobile. The water surface has different characteristics depending on the side: along the left side wall (where the assembled boulders are places) the profile is flat and the water appear to flow slower than on the right side, where strong waves are formed. The efficacy of assembled boulders along the sides of the channel is once more confirmed. The average water surface is $h_{ave,S=2.5}$=0.230 m (equal to h_{ave}=0.0900 m in experimental

scale). The scaled thresholds for the definition of refuge are $\overline{V}$=0.160 m/s and $std(V)$=0.110 m/s. Figure 54 presents a selection of the conducted measurements: two points are taken inside the gravel mounts' reinforcement, the third is taken inside the gravel bed, while the forth is taken inside a gravel mount. In all four plot, there is a clear separation between the flow conditions below or above the model surface (defined by the brown area). Inside gravel or boulders constructions, both time-averaged velocity and standard deviation of the velocity are lower than the scaled thresholds for the definition of refuge. This confirms the assumption that the empty space between stones can be defined as interstice volume. The model surface appear to act as transition layer above which the vertical velocity profiles recover their usual parabolic vertical profile. In none of the shown plots the thresholds for refuge are met above the model's surface and the refuge able volume would be expected to be 0.00 m^3. Figures 54c and 54d confirm that interstice volume is generated between the gravel grains as well, although this has been neglected in this thesis since the holes are unusable for the target small-sized fishes.

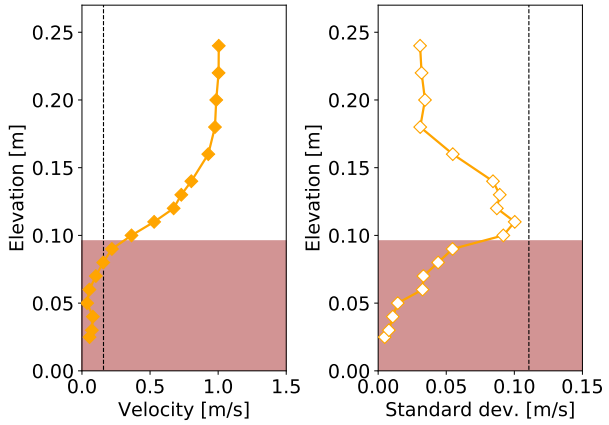

(a) x=1.25 m, y=0.217 m.

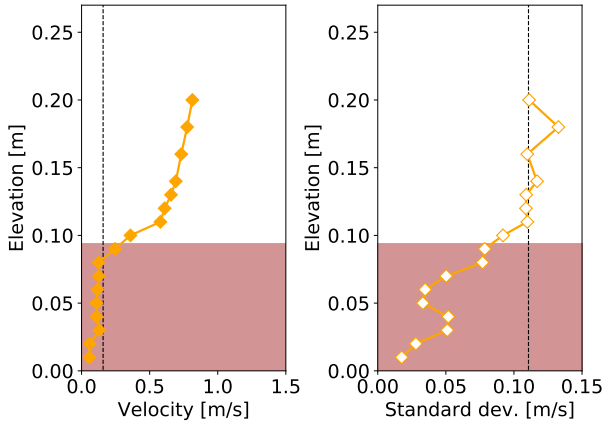

(b) x=5.05 m, y=0.138 m.

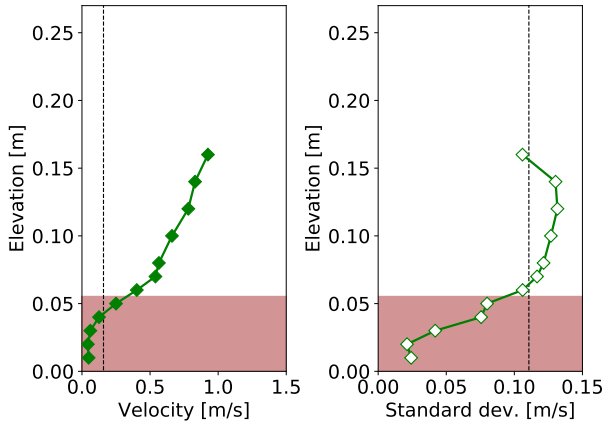

(c) x=4.12 m, y=−0.202 m.

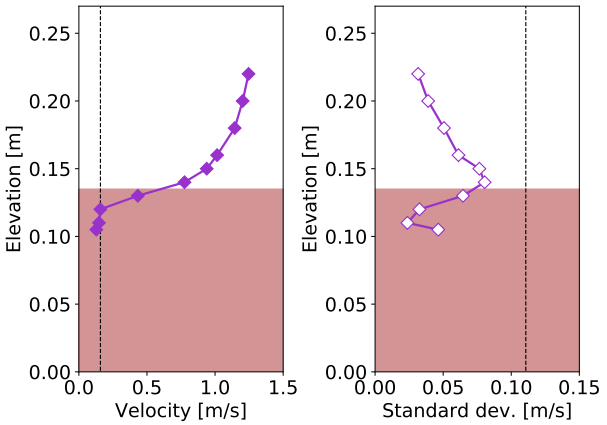

(d) x=1.61 m, y=0.0280 m.

Figure 54: Vertical velocity profile in four measurements point for $Q_{S=2.5}$=0.144 m^3/s. Sub-figures (a) and (b) are collected inside assembled boulders reinforcement, Sub-figures (c) and (d) between the gravel composing the bed or a gravel mount, respectively. The model area at specific coordinate is shown in brown. The dotted lines represents the scaled thresholds for refuge.

5.4 Living fishes

On August 8th-9th, 2022, 100 small-sized fishes were released inside the experimental channel. This has been the second experiment of this kind, after the one conducted in the Summer of 2020 and presented in Beretta Piccoli, Yasuda and Boes (2020) [7] (and (2019, unpublished) [34]). This time,

a 2.00 m long wooden platform is placed in the upstream part of the channel. At its downstream end there is a wooden stairs composed by seven steps, each 0.200 m wide and 0.100 m lower than the previous one. Coarse boulders B2 (d_{50}=0.0920 m) are assembled over the wooden steps along the entire channel's width. Once reached the channel's metal surface, the central area is kept empty and the assembled boulders are placed only at the sides (each arm having a general width of 0.200 m), thus creating a U-shaped structure. In total, the model is 5.79 m long and the top of the stairs is considered its upstream end. A metal bar is placed at the downstream end of the model while two metal grids block both ends of the experimental channel preventing wondering fishes from hurting themselves. Because real-sized fishes are used, this experiment has prototype scale S=15 (Sub-chapter 1.9). The channel slope and the discharge are I=0.0100 and $Q_{S=15}$=0.155 m^3/s (Q≅0.000200 m^3/s in the usual experimental scale), respectively. Bed elevation is measured every 0.100 m in x-direction and y=−0.380, −0.300, −0.200, −0.100, 0.00, 0.100, 0.200, 0.300, 0.380 m along the entire model's length. The water surface is measured every 0.200 m along the x-axis for y-coordinates y=−0.380, 0.00 m. Velocity measurements are taken using the electrical-magnetic current meter at seven specific points inside the boulders structures always at y=0.390 m. Six of these are chosen because fishes are observed using these specific space for refuge (i.e. staying there longer than 2.00 s as defined by Johnasen, Bellwood and Fulton (2008) [17]). One extra unused point is taken for comparative purposes to understand why it was not chosen by the aquatic animals. A precise list of the species released in the experimental channel is here presented:

- 25 Ayu fish (*Plecoglossus altivelis*);
- 18 pale chubs (*Opsariichthys platypus*);
- 16 Japanese crucian carp (*Carassius cuvieri*);
- 15 Japanese rice fishes (*Oryzias latipes*);
- 7 dark chubs (*Nipponocypris temminckii*);
- 6 freshwater goby (*Rhinogobius sp. OR*);
- 6 pond loaches (*Misgurnus anguillicaudatus*);
- 6 stone moroko (*Pseudorasbora parva*);
- 1 Japanese barbel (*Hemibarbus barbus*).

(a) The assembled boulders at the bottom of the wooden stairs.

(b) The water profile at the upstream end of the model.

(c) The water profile at the downstream end of the model.

Figure 55: Experimental set-up before the release of the fishes. Flow direction from right to left.

(a) Two small-sized fishes hide between boulders.

(b) A benthic fish lays near the downstream end of the channel.

(c) Another benthic fish hides inside the assembled boulders.

Figure 56: Experimental conditions after the release of the fishes. Flow direction from right to left.

The model stays perfectly still for the entirety of the experiment with discharge $Q_{S=15}$=0.155 m^3/s (Figure 55a). The water surface is wavy and shallow above the upstream wooden stairs (Figures 55b and the water depth is around 0.150 m there. Moving downstream, the surface become increasingly flatter (Figure 55c) and the water depth increases to around 0.210 m at the model's end. Fishes are observed swimming upstream and downstream of the model (Figure 56a) with many inhabiting the holes between the assembled boulders (Figure 56b). As shown in Figure 56c, these spaces are suitable also for individuals larger than the 0.200 m body length threshold used in this research to define small-sized fishes. This shows the potential for the study on refuge beyond this research's boundaries. Based on the observed behaviour, fishes do not appeared stressed by the flow conditions.
The vertical velocity profiles of four measurement points are shown in Figure 57. Inside the assembled boulders both time-averaged velocity and standard deviation of the velocity are very low and generally homogeneous. Above the model's surface, the velocity increases quickly, while the standard deviation only slightly. The plots are similar to what observed in Figure 54 when the model scale was S=2.5 (Sub-Chapter 5.3). At current prototype scale S=15, the thresholds for refuge are: $\overline{V}$=0.390 m/s and $std(V)$=0.270 m/s. In all the studied points both parameters are well within these thresholds. For what can be observed here, the vertical velocity profiles of the only coordinate not used by fishes (Figure 57b) do not appear to differ from the other studied points.

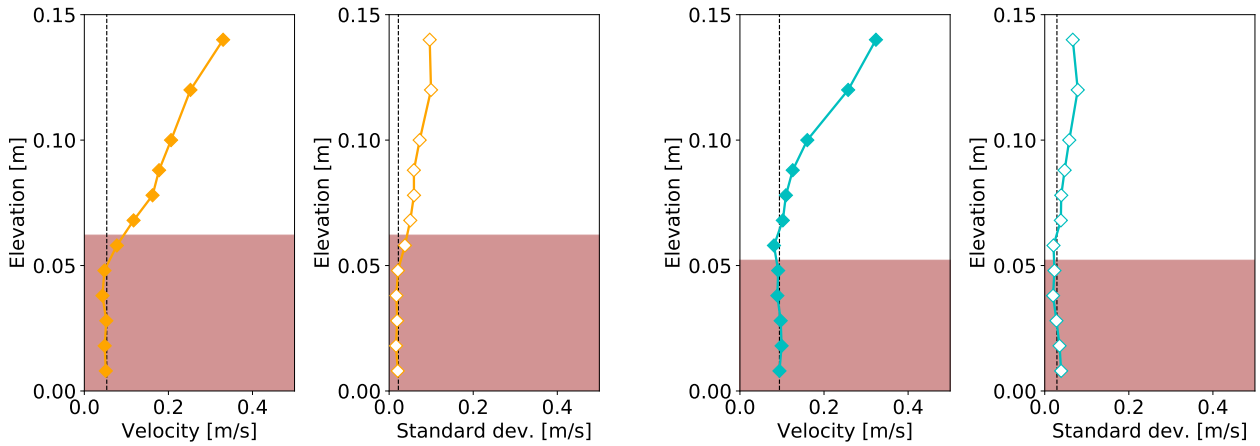

(a) x=2.03 m, y=0.390 m (used by fishes).

(b) x=3.03 m, y=0.390 m (not used by fishes).

(c) x=3.30 m, y=−0.390 m (used by fishes).

(d) x=4.77 m, y=0.390 m (used by fishes).

Figure 57: Vertical velocity profile in four measurements point for $Q_{S=15}$=0.155 m^3/s. Fishes are observed using the coordinates of Sub-figures (a), (c) and (d) for refuge, while Sub-figure (b) is left empty. The assembled boulders area at specific coordinate is shown in brown, while the dotted lines represents the average of the measurements inside the model (i.e. elevation is lower than the boulders).

For each coordinate, the average of the measurements inside the model's area (i.e. with an elevation smaller than the assembled boulders' surface) are plotted in Figure 58. This plot confirms that the flow conditions inside the assembled boulders are well weaker than the maximal thresholds for refuge. Again, the unused point at (x,y)=(3.03,0.390) does not appear to have characteristics that would clearly explain why it is avoided by fishes. Both time-averaged velocity and standard deviation of the velocity are larger than the average of all used points, but at coordinates (x,y)=(1.46,0.390) fishes choose a place with similar time-averaged velocity but much stronger standard deviation.

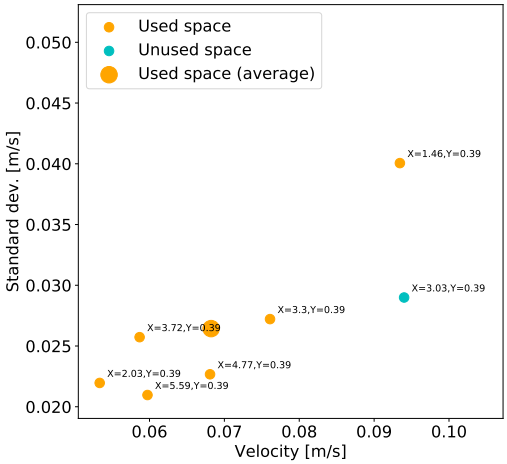

Figure 58: For each point, the average of all the measurements taken inside the assembled boulders are plotted. Points are coloured depending if the fishes had been observed using that coordinate (orange) or not (cyan). The larger point represents the average of the used points.

For each coordinate, the entire 30.00 s interval of each measurement inside the assembled boulders is presented in Figure 59. To smooth the raw data, a 4-point moving average is applied. Again, there are no significant difference between data from used or unused coordinates. For both velocity components, the largest time-averaged velocities are recorded somewhere fishes have visited.

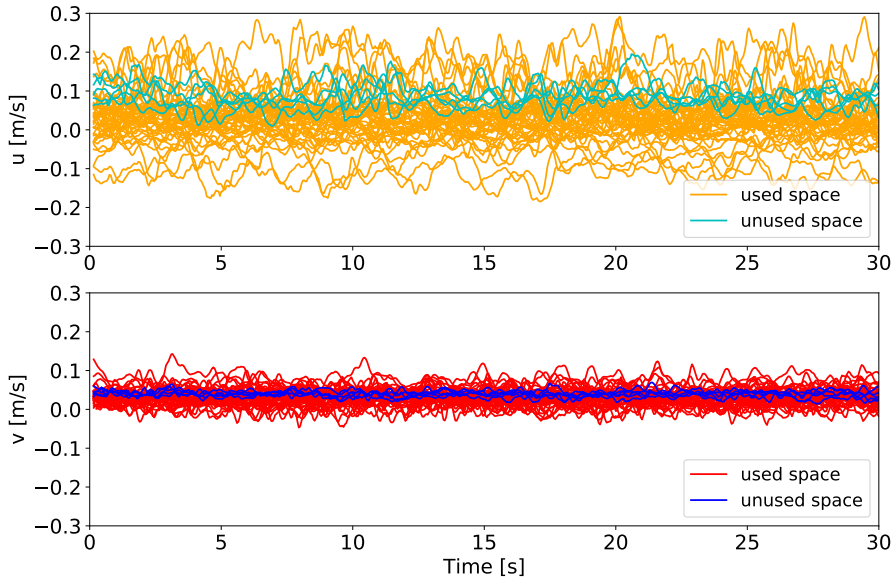

Figure 59: For each measurement taken inside the assembled boulders, the point values of both velocity component u (x-direction) and v (y-direction) are shown using a 4-points moving average. Measurements are coloured differently depending if their coordinates have been used by fishes or not.

Lastly, a Fast Fourier Transform (FFT) is conducted on these same measurements to assess their wave behaviour. Because of systematic error caused by the sensor being placed just 0.0100 m from the left side wall, frequencies above 4.50 are discarded. As shown in Figure 60, the unused coordinate does not differ from the rest of the data set. Based on the analysed results, it is suggested that coordinates (x,y)=(3.03,0.390) have been avoided by fishes not because its flow conditions are unsuitable, but rather because there has been no need to use it. It is believed that the flow field has generated a surplus of suitable places for the size of the fish school and, had the experiment lasted longer, some fish would have eventually used that space as well.

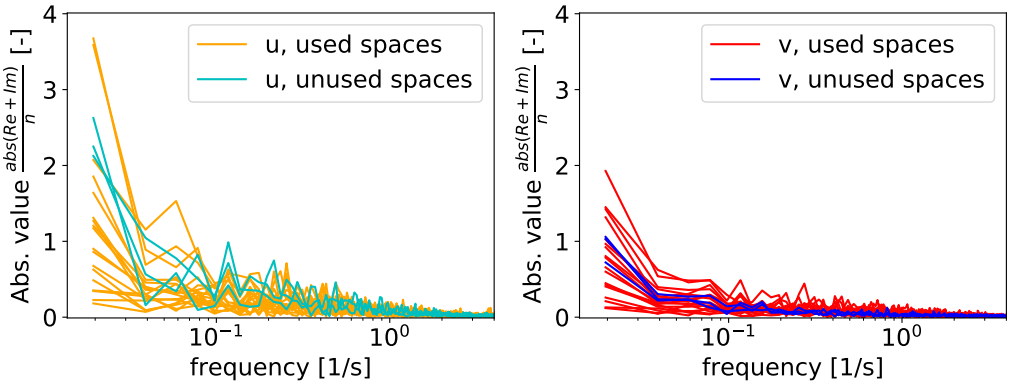

Figure 60: Results of the FFT on the measurements inside the assembled boulders for both velocity components. The sum of the real and imaginary parts in absolute value is divided by N=601, the number of point measurements. This is plot over the frequency in the x-axis. Measurements are coloured differently depending if fished have been seen there (orange and red) or not (cyan and blue).

In conclusion, this experiment confirms that fishes can and do use the holes inside assembled boulders for refuge. This behaviour is even present for species larger than the small-sized fishes targeted with this research and future experiments could start considering the possibility of expanding the biological study. The velocity measurements show that the flow conditions inside the prototype fit the definition of refuge, while the flat water surface along the sides of the channel proves once more the efficacy of boulders structures there.
Although a general success, this experiment fails to put the fishes under stressful swimming conditions. No information can be gathered regarding their behaviour during flood stages, nor could the thresholds for the definition of refuge (i.e. $\overline{V}$=0.390 m/s and $std(V)$=0.270 m/s) be tested on this prototype scale. Given the pump capacity limitations of the experimental channel, it might be necessary to consider the construction of a full-sized prototype inside a real channelized river to reach such conditions.

6 Conclusions

6.1 Conclusions to the research

Through a long trial-and-error process, this thesis was able to find the optimal design to construct gravel mounts in straight channelized rivers. It was proved that neither coarse gravel nor medium boulders are suitable materials to build a proper model if they are used alone. Together, the resistance of assembled boulders and the low hydraulic friction formed around triangular gravel mounts can be combined to create highly satisfactory results.
Based on the experimental discoveries collected in this thesis, it is possible to prepare the first prototype proposal. Inside a theoretical straight, 12.00 m wide, rectangular channel (defined scale factor S=15), the triangular gravel mounts should be built every L=12.00 m on alternated sides of the channel using coarse gravel with a characteristic diameter of around d_{50} ≅0.250 m. To maximise their performance, each mount should have the following characteristics: the height should be h_{GM}=0.660 m (linearly decreasing from the riverbank to the mount's toe) and the upstream and downstream widths are recommended to be L_d=5.25 m and L_u=4.50 m, respectively. To ensure the constructions' stability, the channel bed should have a multi-layered gravel armouring (recommended thickness of at least h_{bed}=0.600 m) and a metal bar should be placed across the channel's width on the downstream end of the installation area. Medium boulders (d_{50} ≅0.950 m) are necessary to further strengthen the prototype's overall stability and to flatten the water surface. Experimental results show that two layers around each mount's shape and two more along both sides of the channel, are sufficient to obtain the desired effects, but the height of the boulders must be adjusted to the gravel mounts' profile. If these directives are followed, it is expected that suitable space around 38% of the mounts volume will be generated inside the channelized river, independently from limiting factors such as large discharge or shallow water conditions. The prototype's performance might even increase if it would be constructed inside rivers with a channel slope smaller than the tested 1% (I=0.0100). As learned in Chapter 2, steepness makes the flow conditions harsher.
Since the experiments could not find the erosion conditions of the proposed prototype, it is impossible to provide a precise prediction of its applicability ranges. Based on the collected results, damages are not expected to occur to the installation area in case of discharges with return period smaller than 10 years. After larger flood stages, the restoration of the mounts' tops might be necessary, as these are the most exposed gravel areas and the first to erode. Total collapse of the installation area is not expected during flood stages with return periods smaller than 30 years, although, in case of large flood stages, the exponentially increasing average water depth is considered the biggest risk factor. When constructed inside a prototype river, it must be confirmed with certainty that the alternated gravel mounts with assembled boulders reinforcement do not reduce the channel's capacity, consequently increasing the risk of overspilling. If that were the case, other countermeasures might be required (e.g. lower the channel bed elevation). The average water depth is considered to be a good parameter for the assessment of the water surface rise, as large waves along the sides of the channel are prevented from forming by the assembled boulders constructions there. Finally, the conducted research can not provide any prediction about the installation and maintenance costs that the proposed prototype will require, as economical aspects were not discussed in this thesis.

6.2 From this point onward

Following the highly positive results, the experimental side of the research can be considered satisfactory. The collected knowledge has established the potential of alternated gravel mounts as simpler, but equally effective, alternative to more established river restoration strategies within the experimental scale. At the current state, there is no way to know if the same positive performances can be repeated in the real world as well. It is the author's suggestion, that, from this point onward, the priority for future research should be put on moving toward a more prototype-based methodology.

Tokyo, January 2024

The final goal should be the construction of a real-life-scaled gravel and boulders installation inside an existing straight channelized river based on the proposal described in the previous Sub-chapter 6.1. This phase is expected to be more difficult and time consuming, as it will require the collaboration with other entities external to the university (e.g. public offices must be consulted to obtain the construction permits). To minimize risks, non-urban areas without valuable lands in their proximity might be recommended to conduct the first try. Between planning, construction and early success control, at least the equivalent of another PhD thesis is expected to be necessary (i.e. a minimum period of 3 years). An even longer time frame will probably be required to complete a success control (expected period of 5-10 years). Bachelor or Master students could profit of this time to conduct their graduation work, as the repetition of the data gathering process would provide the best opportunity for them to gather in-field experiences and to showcase the performance of gravel mounts over the years. The experience already collected by the Laboratory on prototype-scaled assembled boulders groynes inside Japanese channelized river will be of great help (Yasuda, Yasuda and Beretta Piccoli (2023) [31], Yasuda (2021) [32] and Yasuda and Beretta Piccoli (2020) [33]).
On the other hand, the laboratory research will always remain important, as many unknown are left. As mentioned before, there is no information regarding the erosion process of assembled boulders and without this knowledge, it is impossible to set accurate applicability ranges for the proposed model. Future experiments could consider reducing the model scale so that the pump capacity discharge Q=0.155 m^3/s might represent an even higher return period. Furthermore, it might be helpful to consider if the model resilience is maintained when the flow is full of sediment or carrying large object such as detached logs. So far, only clear-water flow conditions have been studied. It would be interesting to discover what processes (sedimentation, transport or erosion) are taking place where around the alternated gravel mounts. Would sedimentation reduce the gravel mounts' performance as it happens to reservoirs created by dams (Boes (2017) [36])? Also, in this research it has been assumed that all the interstice volume is suitable and the results obtained in the scaled models presented in Sub-chapters 5.3 and 5.4 appear to validate this assumption. This said, the precise flow field inside assembled boulders construction can be researched further. A new experiment specifically focused on mapping the water movement inside the interstices should solve this problem. The same set-up as Sub-chapter 3.2.1 could be repeated here. As described in the previous Sub-Chapter 6.1, the with discharge exponentially increasing average water surface might reduce the cross sectional capacity of the channel. As the risk of overspilling must not be increased, further research on the water surface rise is recommended. It would be interesting to study the flow conditions around gravel mounts with assembled boulders reinforcement in the case of low-flows as well.
On the ecological side, the study of the suitable habitats should be continued and deepened. From the current stand point, several path are open to exploration: the definition for refuge could grow in complexity, the requirements for spawning could also be taken into account or the target species' definition could be expanded to include other aquatic species. In the former case, other variables other than the time-averaged velocity and the standard deviation could be introduced and calibrated. Early suggestions for new parameters are: water depth, water temperature or sediment concentration. The second path would allow to discover if the alternated gravel mounts could provide suitable hydraulic conditions for eggs laying and hatching besides the already studied utilizations as refuge against flooding. If it were to follow the third path, the research could target smaller (e.g. micro-organisms, aquatic insects) or larger (e.g. fishes with a body length bigger than 0.200 m) riverine animals. Since they stand at the bottom of the food chain, algae should also be considered when talking about environmental improvements. It would be interesting to know if rooting could take place inside the spaces between the gravel grains.

References

Published papers

[1] P. Beretta Piccoli, Y. Yasuda, *Formation of Refuge Able Areas around different Gravel Mounts' Designs*, Proceedings the 40th IAHR World Congress, pp. 1310-1316, ISSN (online) 2521-7119, Austria, 2023. DOI: https://www.doi.org/10.3850/978-90-833476-1-5_iahr40wc-p0056-cd

[2] P. Beretta Piccoli, Y. Yasuda, *Alternated Gravel Mounts with Artificial Assembled Boulders Reinforcement inside Channelized Rivers*, Journal of Environmental Science Studies, vol. 6, no. 1 (2023), pp. 26-35, July Press, ISSN 2591-779X, E-ISSN 2630-4821, Singapore, 2023. DOI: https://www.doi.org/10.20849/jess.v6i1.1352

[3] P. Beretta Piccoli, Y. Yasuda, *Experimental analysis on the stability of alternative gravel mounts during flood stages in channelized rivers*, presented at the 11th International Conference on Fluvial Hydraulics - River Flow 2022, to be published in the Proceedings, Canada, 2022.

[4] P. Beretta Piccoli, Y. Yasuda, *The stability of alternative gravel mounts with stacked boulders during major flood stages inside channelized rivers*, presented at the 77th Annual Conference of the Japanese Society of Civil Engineers, Japan, 2022.

[5] P.Beretta Piccoli, Y. Yasuda, *Experimental analysis on the formation of refuge areas for fishes behind alternative gravel mounts in channelized rivers during flood stages*, Proceedings of the 39th IAHR World Congress, pp. 2290-2299, Spain, 2022. DOI: https://doi.org/10.3850/IAHR-39WC252171192022679

[6] P. Beretta Piccoli, Y. Yasuda, *Formation of refuge areas behind alternative gravel mounts for fishes during flood stages*, Modern Environmental Science and Engineering Journal, vol. 11, 2021, pp. 1021-1031, Academic Star Publishing, ISSN 2333-2581, USA, 2021. DOI: https://www.doi.org/10.15341/mese(2333-2581)/11.07.2021/001

[7] P. Beretta Piccoli, Y. Yasuda, R. Boes, *Installation of alternative gravel mounts in channelized rivers*, Proceedings of the 22nd IAHR-APD Congress Conference, Japan, 2020.

[8] T.C. Blair, J. G. McPherson, *Grain-size and textural classification of coarse sedimentary particles*, Journal of Sedimentary Research, vol. 69, pp. 6-19, USA, 1999. DOI: https://www.doi.org/10.2110/jsr.69.6

[9] M. Church, M. A. Hassan, J. F. Wolcott, *Stabilizing self-organized structures in gravel-bed stream channels: Field and experimental observations*, Water Resources Research, vol. 34, no. 11, pp. 3169-3179, USA, 1998.

[10] A. J. H. Davey, D. J. Kelly, B. J. F. Biggs, *Refuge-use strategies of stream fishes in response to extreme low flows*, Journal of Fish Biology, vol. 69, pp. 1047–1059, Wiley-Blackwell Publishing, USA, 2006. DOI: https://www.doi.org/10.1111/j.1095-8649.2006.01180.x

[11] E. A. Edwards, K. A. Twomey, *Habitat suitability index models: Common carp*, U.S. Dept. Int. Fish Wildl. Serv., FWS/OBS-82/10.12., USA, 1982.

[12] European Environmental Agency, *EEA Report 2016: Rivers and lakes in European cities - Past and future challenges*, Publications Office of the European Union, ISBN 9789292138219, ISSN 19778449, Luxembourg, 2016. DOI: https://www.doi.org/10.2800/516136

[13] V. Felten, S. Dolédec, B. Statzner, *Coexistence of an invasive and a native gammarid across an experimental flow gradient: flow-refuge use, -mortality, and leaf-litter decay*, Fundamental and Applied Limnology, Archiv für Hydrobiologie, vol. 172/1, pp. 37–48, Schweizerbart'sche Verlagsbuchhandlung, Germany, 2008. DOI: https://www.doi.org/10.1127/1863-9135/2008/0172-0037

[14] C. L. Gerstner, *Use of substratum ripples for flow refuging by Atlantic cod, Gadus morhua*, Environmental Biology of Fishes, vol. 51, pp. 455–460, Kluwer Academic Publishers, Netherlands, 1998.

[15] E. Graynoth, D. Booker, *Biomass of longfin eels in medium to large rivers*, New Zealand Fisheries Assessment Report 2009/44, ISSN 1175-1584, New Zealand, 2009.

[16] D. D. Hart, R. A. Merz, *Predator-prey interactions in a benthic stream community: a field test of flow-mediated refuges*, Oecologia, vol. 114, pp. 263-273, Springer-Verlag, Germany, 1998.

[17] J. L. Johansen, C. J. Fulton, D. R. Bellwood, *Coral reef fishes exploit flow refuges in high-flow habitats*, Marine Ecology Progress Series, vol. 360, pp. 219–226, Germany, 2008. DOI: https://www.doi.org/10.3354/meps07482

[18] J. L. Johansen, C. J. Fulton, D. R. Bellwood, *Avoiding the flow: refuges expand the swimming potential of coral reef fishes*, Coral Reefs, vol. 26, pp. 577–583, Springer-Verlag, Germany, 2007. DOI: https://www.doi.org/10.1007/s00338-007-0217-y

[19] J.-Y. Lin, Y.-C. Chen, E. H. Tsao, H.-C. Yang, *Refuge-use strategies of stream fishes in response to extreme low flows*, Doboku Gakkai Ronbunshuu B, vol. 62, Nr. 4, pp. 320-329, Taiwan, 2006.

[20] I. Logar, R. Brouwer, A. Paillex, *Do the societal benefits of river restoration outweigh their costs? A cost-benefit analysis*, Journal of Environmental Management, vol. 232, pp. 1075-1085, Elsevier, Switzerland, 2019. DOI: https://www.doi.org/10.1016/j.jenvman.2018.11.098

[21] 中村俊六 (S. Nakamura), 石川雅朗 (M. Ishikawa), 月崎正美 (M. Tsukisaki), 東信行 (N. Azuma), 中村緩徳 (Y. Nakamura), 河川における魚類生息環境評価 *(IFIM適用)*のための基礎調査 *(Field Research to Obtain the IFIM's Preference Curves for Japanese Fresh Water Fishes)*, 第 2回河道の水理と河川環境シンポジウム, pp. 127-134, Japan, 1995. [in Japanese]

[22] 鬼束幸樹 (K. Onitsuka), 永矢貴之 (T. Nagaya), 白石芳樹 (Y. Shiraishi), 筌瀬明日香 (A. Kakase), 東野誠 (M. Higashino), 高見徹 (T. Takami), 横峯正二 (S. Yokomine), 秋山壽一郎 (J. Akiyama), 小野篤志 (A. Ono), 芹川泰介 (T. Serikawa), アユに関する流速の選好曲線の提案 *(A Proposal of Preference Curves of Velocity for Ayu)*, Kyushu Institute of Technology, Japan, 2009. [in Japanese]

[23] 鬼束幸樹 (K. Onitsuka), 永矢貴之 (T. Nagaya), 東野誠 (M. Higashino), 高見徹 (T. Takami), 大塚法晴 (N. Otsuka), 秋山壽一郎 (J. Akiyama), 尾関弘明 (H. Ozeki), 白石芳樹 (Y. Shiraishi), アユの産卵および生息に適した水理環境に関する検討 *(Study on suitable hydraulic condition for spawning and living of Ayu)*, 水工学論文集 2005, 49 巻, pp. 1471-1476, ISSN (online) 1884-9172, ISSN (print) 0916-7374, Japan, 2005. [in Japanese]

[24] A. Raudkivi, R. Ettema, *Stability of armour layers in rivers*, Journal of the Hydraulics Division 108, pp. 1047-1057, American Society of Civil Engineers, USA, 1982. DOI: https://www.doi.org/10.1061/JYCEAJ.0005903

[25] D. Rickenmann, A. Recking, *Evaluation of flow resistance in gravel-bed rivers though a large field data set*, Water Resources Research, vol. 47, USA, 2011. DOI: https://www.doi.org/10.1029/2010WR009793

[26] W. J. Stewart, F.-B. Tian, O. Akanyeti, C. J. Walker, J. C. Liao, *Refuging rainbow trout selectively exploit flows behind tandem cylinders*, Journal of Experimental Biology, vol. 219, pp. 2182-2191, The Company of Biologists, UK, 2016. DOI: https://www.doi.org/10.1242/jeb.140475

[27] D. L. Strayer, *Use of Flow Refuges by Unionid Mussels in Rivers*, Journal of the North American Benthological Society, vol. 18, no. 4, pp. 468-476, JSTOR Publishing, USA, 1999.

[28] Wildlife Division, *The wildlife in Japan*, informative pamphlet, Nature Conservation Bureau and Japan Wildlife Research Center and the Ministry of Environment, Japan, 2015.

[29] WWF, *Bending the curve of biodiversity loss: a deep dive into freshwater*, Living Planet Report 2020, R. Almond, M. Grooten, T. Petersen (Eds), WWF, Switzerland, 2020.

[30] 山本亮介 (R. Yamamoto), 本田晴朗2 (H. Honda), 短期的な流況変動に起因するアユ産卵環境の変動予測 *(Numerical prediction for the impact of short-time variations or river flow on the spawning environment of Ayu)*, 水工学論文集, 2005, 49 巻, pp. 1483-1488, 公開日 2011/06/27, ISSN (online) 1884-9172, ISSN (print) 0916-737, Japan, 2005. [in Japanese]

[31] Y. Yasuda, K. Yasuda, P. Beretta Piccoli, *Balance between flood control and preservation of aquatic habitat through consecutively assembled boulders*, Eel Science by K. Tsukamoto, M. Kuroki, S. Watanabe, part of Fisheries Science Series, pp. 293-302, Springer Publishing Company, ISSN 2522-0470, ISSN (online) 2522-0489, USA, 2023. DOI: https://www.doi.org/10.1007/978-981-99-5692-0_22

[32] Y. Yasuda, *Improvement of flow condition in channelized river due to stacked boulders*, IOP Conf. Series: Earth and Environmental Science 626 (2021), IOP Publishing, UK, 2019. DOI: https://www.doi.org/10.1088/1755-1315/626/1/012001

[33] Y. Yasuda, P. Beretta Piccoli, *Installation of ground sill with stacked boulders in channelized river*, Proceedings of the 22nd IAHR-APD Congress Conference, Japan, 2020.

Unpublished papers and academic lectures

[34] P. Beretta Piccoli, *Optimal river cross section in terms of flood control and aquatic habitat*, Master thesis, supervised by Prof. Dr. R. Boes and Prof. Dr. Y. Yasuda, Versuchsanstalt für Wasserbau, Hydrologie und Glaziologie Zürich (Zürich,Switzerland) and Laboratory for Ecological Hydraulic, College of Science and Technology, Nihon University, Japan, 2019.

[35] G. R. Bezzola, *Flussbau Vorlesungsskript*, Lecture Script, SS 2017, Versuchsanstalt für Wasserbau, Hydrologie und Glaziologie, ETH Zürich, Switzerland, 2017. [in German]

[36] R. Boes, *Wasserbau 1 Vorlesungsskript*, Lecture Script, SS 2017, Versuchsanstalt für Wasserbau, Hydrologie und Glaziologie, ETH Zürich, Switzerland, 2017. [in German]

[37] R. Boes, *Wasserbau 2 Vorlesungsskript*, Lecture Script, SS 2017, Versuchsanstalt für Wasserbau, Hydrologie und Glaziologie, ETH Zürich, Switzerland, 2017. [in German]

[38] W. Kinzelbach, *Skript zur Vorlesung Hydraulik I*, Lecture Script, SS 2015, ETH Zürich, Switzerland, 2011. [in German]

[39] H. Fuchs, L. Schmocker, I. Albayrak, *Hydraulics of Engineering Structures (101-1249-00L)*, Lecture material, SS 2016, Versuchsanstalt für Wasserbau, Hydrologie und Glaziologie, ETH Zürich, Switzerland, 2016.

[40] R. Stocker, V. Fernandez, *Ecohydraulic and habitat modelling (102-0259-00L)*, Lecture material, SS 2018, Department of Civil, Environmental and Geomatic Engineering, ETH Zürich, Switzerland, 2018.

[41] V. Weitbrecht, M. Detert, M. Koksch, C. Weber, *Revitalisierung von Fliessgewässern (101-0259-00L)*, Lecture material, SS 2018, Versuchsanstalt für Wasserbau, Hydrologie und Glaziologie, ETH Zürich, Switzerland, 2018. [in German]

Web pages

[42] AND CO., Scale model SJ-20k, Japan. Product information sheet (no date): `https://www.aandd.co.jp/pdf_storage/manual/balance/m_sj.pdf` [in Japanese, last visited: 2022.07.05]

[43] Fish species' information platform: `http://www.biokids.umich.edu/` [last visit: 2022.07.15]

[44] Food and Agriculture of the United Nations, Fisheries and Aquaculture Department website: `http://www.fao.org/fishery/en` [last visit: 2022.07.15]

[45] Fish species' online database: `http://www.fishbase.org` [last visit: 2022.07.15]

[46] KENEK CO. LDT, Electromagnetic Current Meter: model VM-806H/VMT2-200-04P, Japan. Product information sheet (no date): `http://www.kenek-co.com/english/pdf/VM806H.pdf` [last visited: 2022.07.05]

[47] KENEK CO. LDT, Propeller-type Current Meter: model VR-301, Japan. Product information sheet (no date): `https://www.kenek-co.com/vr301.html` [last visited: 2023.06.26]

[48] Ibaraki Prefectural Government, Land Development Department, River Policy Division official website: `http://www.pref.ibaraki.jp/doboku/kasen/shomu/kasentop.html` [last visit: 2022.07.14]

[49] Online forum for programming with LaTeX: `https://tex.stackexchange.com/` [last visit: 2023.09.19]

[50] Nagasaki Prefectural Government, River Policy Division official website: `https://www.pref.nagasaki.jp/section/kasen/` [last visit: 2022.07.14]

[51] South Caroline Department of Natural Resources, information on common carp: `http://www.dnr.sc.gov/fish/species/commoncarp.html` [last visit: 2022.07.15]

[52] Online forum for programming with Python: `https://stackoverflow.com/` [last visit: 2023.09.19]

[53] United Nation webpage on climate change, `https://www.un.org/en/climatechange/science/causes-effects-climate-change` [last visited: 2023.09.15]

[54] Online knowledge archive: `https://en.wikipedia.org/wiki/Main_Page` [last visit: 2023.09.19]

Appendices

A Introduction to the research

A.1 Measurement instruments

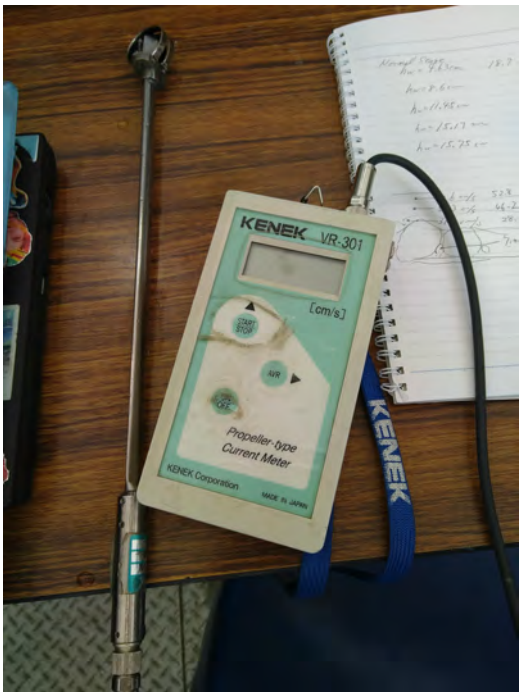

Figure 61: Propeller-type current meter KENEK Co. model VR-301.

A.2 Scale, prototype river and discharge

Two Japanese rivers have similar characteristics with the theoretical prototype of the experimental channel scaled $S = 15$. They are: the Edokami river, 江戸上川, in Ibaraki Prefecture (170 km north from Tokyo, trapezoidal cross section, width 12.00-24.00 m, slope 0.0100, rainfall-based flood statistics) and the Kawatana river, 川棚川, in Nagasaki Prefecture (Kyushu Island, trapezoidal cross section, width 7.80-10.20 m, slope 0.0100, discharge-based flood statistics). The data to build the flood curve for Edokami river come from the Ibaraki Prefectural Government, Land Development Department, River Policy Division [48], while Kawatana river's information are given by the Nagasaki Prefectural Government, River Policy Division [50].

(a) Edokami river.

(b) Kawatana river.

Figure 62: The prototype rivers. The flow direction is given by the red arrow.

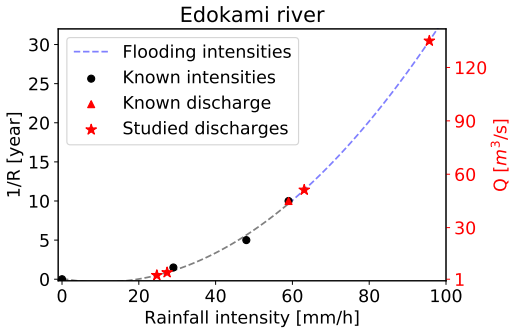

(a) Edokami river.

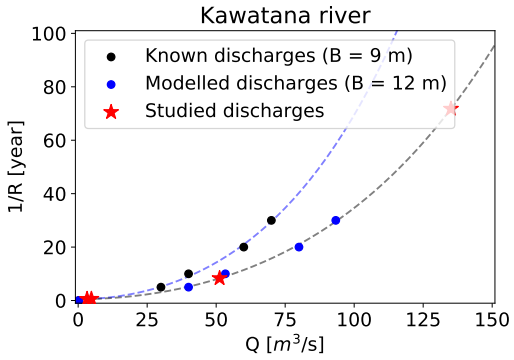

(b) Kawatana river.

Figure 63: The flood curve of the Edokami river is build from rainfall data, while discharge data is used in the case of the Kawatana river (scaled to the appropriate width B=12.00 m).

A.3 Gravel

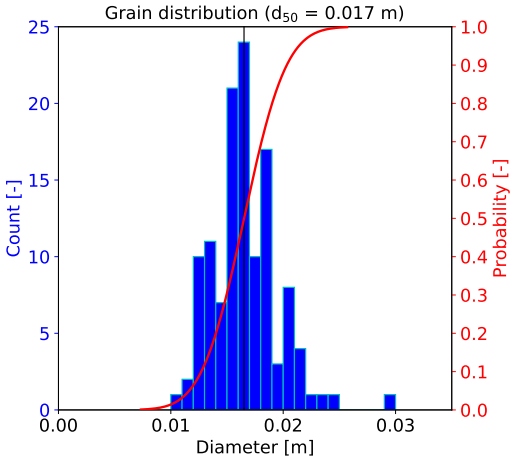

(a) Coarse gravel G1.

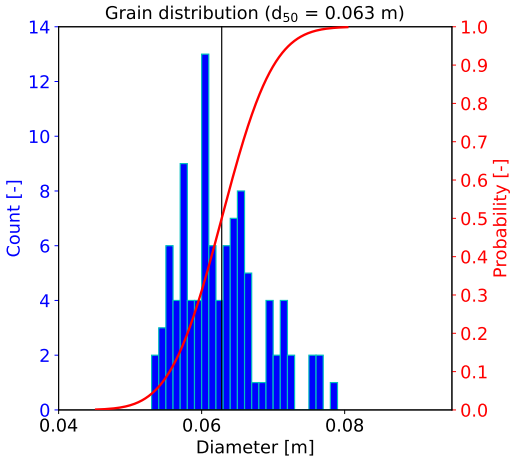

(b) Round medium boulders B1.

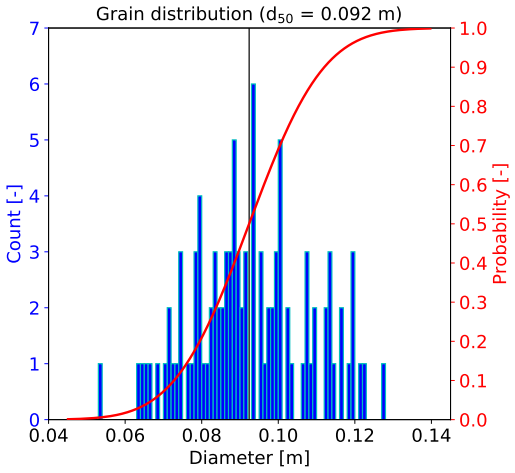

(c) Coarse boulders B2.

Figure 64: Grain distribution for the three stones types used in the research (one kind of gravel and two of boulders). The pyramid of the sorted grains is shown in blue, while the fitted probability distribution is shown in red.

A.4 Target species

(a) Common carp *Cyprinus carpio* (Source: https://fishesofaustralia.net.au/home/species/3964).

(b) Atlantic cod *Gadus morhua* (Source: https://en.wikipedia.org/wiki/Cod).

(c) Formosan landlocked salmon *Oncorhynchus masou formosanus* (Source: https://it.wikipedia.org/wiki/Oncorhynchus_masou).

(d) Longfin eel *Anguilla dieffenbachii* (Source: https://www.doc.govt.nz/nature/native-animals/freshwater-fish/eels/freshwater-eels-in-new-zealand/).

(e) Rainbow trout *Oncorhynchus mykiss* (Source: https://www.fisheyeguyphotography.com/).

(f) Pearly wrasse *Halichoeres margaritaceus* (Source: https://fishesofaustralia.net.au/home/species/234).

Figure 65: Pictures for the other species taken into consideration in this research besides Ayu fish *Plecoglossus altivelis*.

(g) Whitetail damsel *Pomacentrus chrysurus* (Source: `https://www.fisheyeguyphotography.com/`).

(h) Surge damselfish *Chrysiptera brownriggi* (Source: `https://fishesofaustralia.net.au/home/species/234`).

(i) Canterbury galaxias *Galaxias vulgaris* (Source: `https://en.wikipedia.org/wiki/Common_river_galaxias`).

(j) Upland bully *Gobiomorphus breviceps* (Source: `https://en.wikipedia.org/wiki/Upland_bully`).

Figure 65: Pictures for the other species taken into consideration in this research besides Ayu fish *Plecoglossus altivelis*.

B Optimal height of the gravel mounts

B.1 Average water depth and Froude number

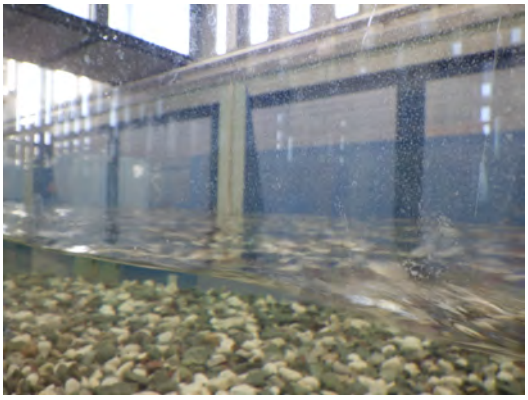

(a) GM1.1.

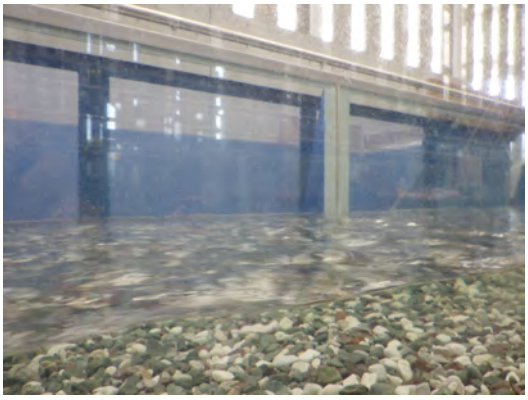

(b) GM1.2.

(c) GM1.3.

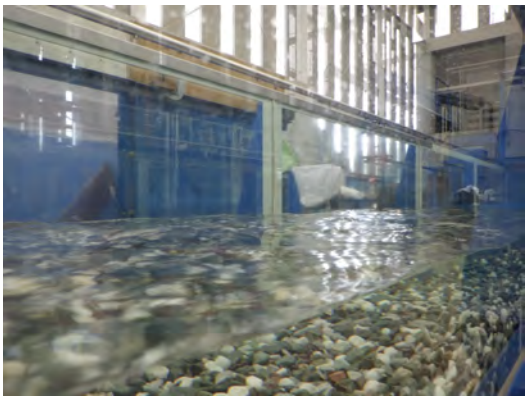

(d) GM1.3bis.

(e) GM1.4.

Figure 66: Water surface for the different experiments at discharge Q=0.0588 m^3/s and slope I=0.00200. The flow direction is always from right to left.

(f) GM2.1.

(g) GM2.3.

(h) GM2.4.

(i) GM2.5.

Figure 66: Water surface for the different experiments at discharge Q=0.0588 m^3/s and slope I=0.0100. The flow direction is always from right to left.

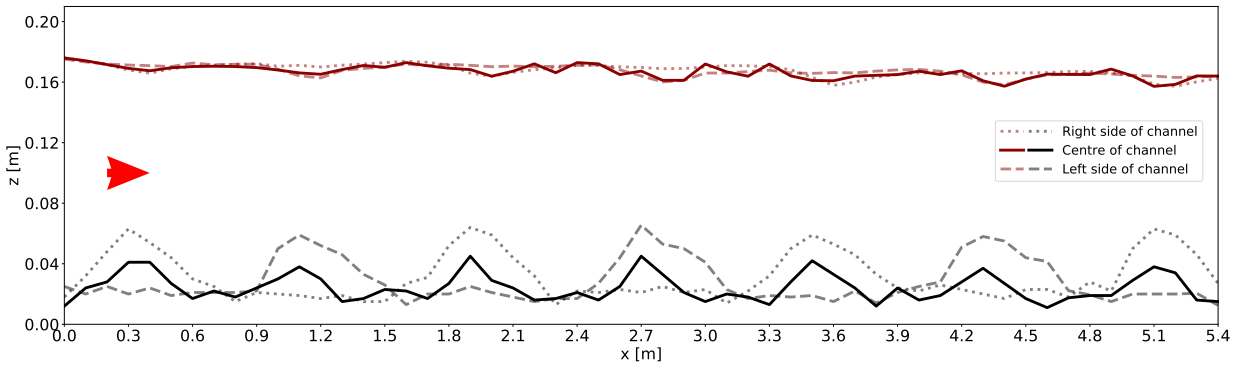

(a) h_{GM}=0.0440 m, L_u=0.200 m (GM1.3bis).

Figure 67: Bed and water surface profiles at the centre and the sides of the channel are here presented for experiment GM1.3bis (discharge Q=0.0588 m^3/s, channel slope I=0.0100). The flow direction is given by the red arrow.

B.2 Horizontal velocity profiles

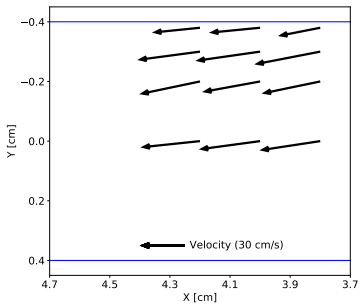

(a) GM1.1, measurement elevation z=0.0300 m.

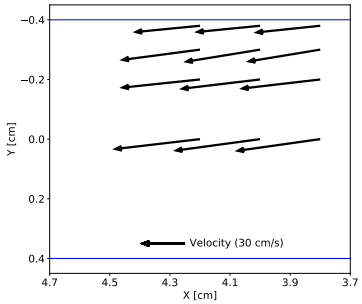

(b) GM1.1, measurement elevation z=0.140 m.

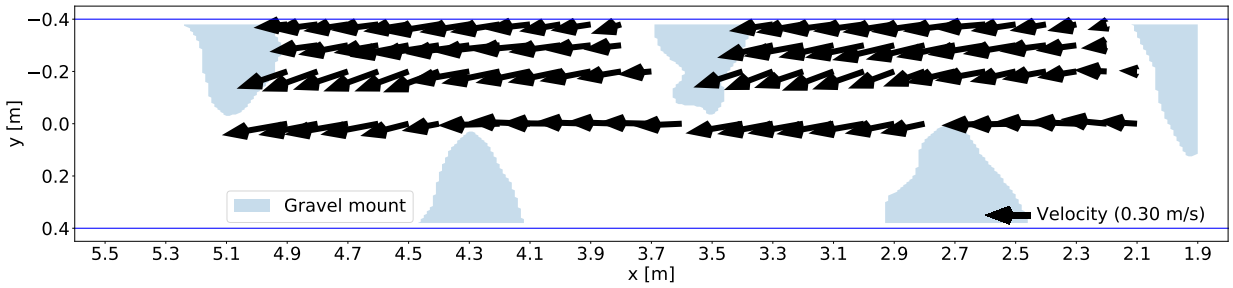

(c) GM1.2, measurement elevation z=0.0300 m.

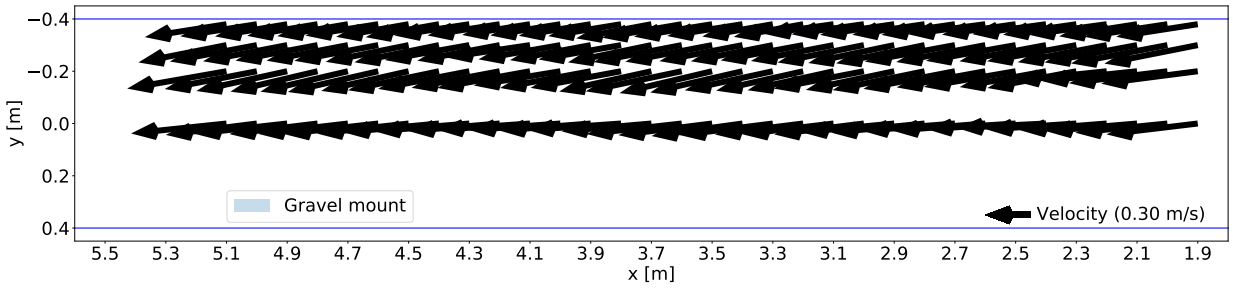

(d) GM1.2, measurement elevation z=0.140 m.

Figure 68: Horizontal velocity profiles for experiments GM1.1 and GM1.2 (slope I=0.00200 and discharge Q=0.0588 m^3/s). Each time, the data collected the closest from the gravel bed (a,c) or the water surface (b,d) are shown. Flow direction and its intensity are given by the black quivers (scaled to plot axis, legend for reference), while the mounts area is coloured blue and labelled "Gravel mount".

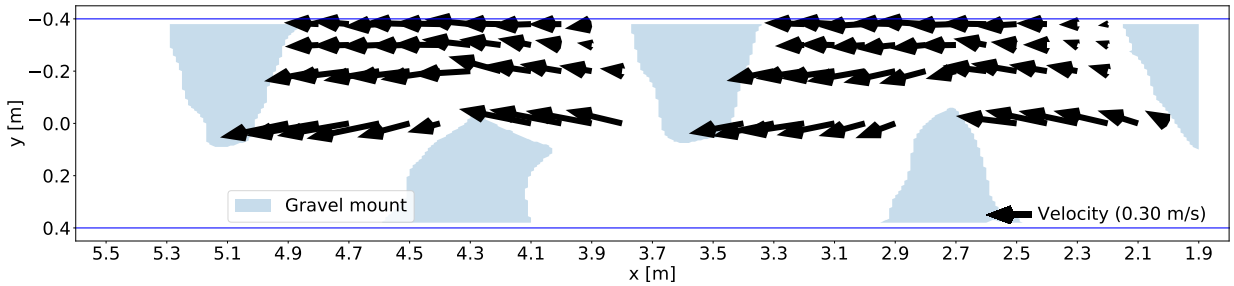

(a) GM1.3, measurement elevation z=0.0300 m.

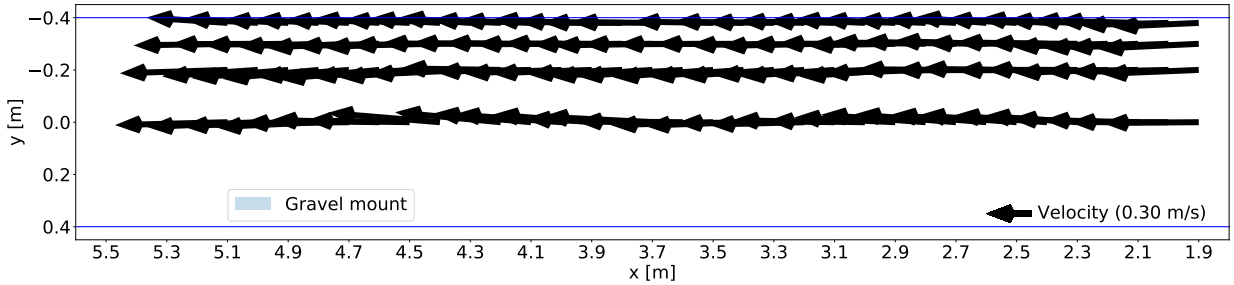

(b) GM1.3, measurement elevation z=0.140 m.

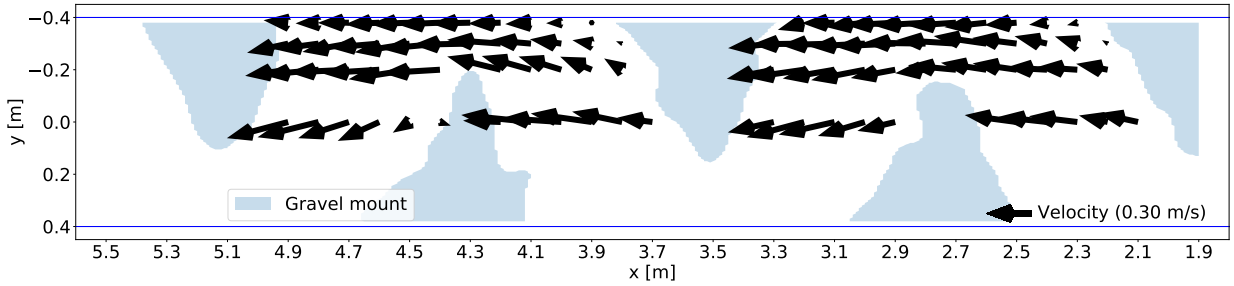

(c) GM1.3bis, measurement elevation z=0.0300 m.

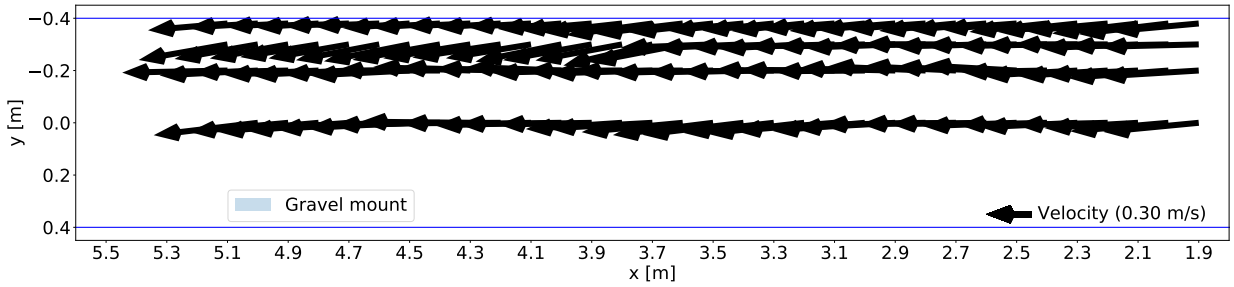

(d) GM1.3bis, measurement elevation z=0.140 m.

Figure 69: Horizontal velocity profiles for experiments GM1.3 and GM1.3bis (slope I=0.00200 and discharge Q=0.0588 m^3/s). Each time, the data collected the closest from the gravel bed (a,c) or the water surface (b,d) are shown. Flow direction and its intensity are given by the black quivers (scaled to plot axis, legend for reference), while the mounts area is coloured blue and labelled "Gravel mount".

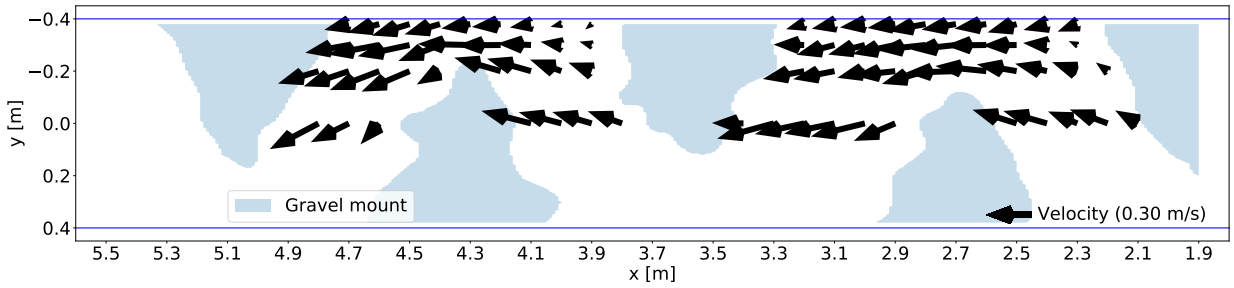

(a) GM1.4, measurement elevation z=0.0300 m.

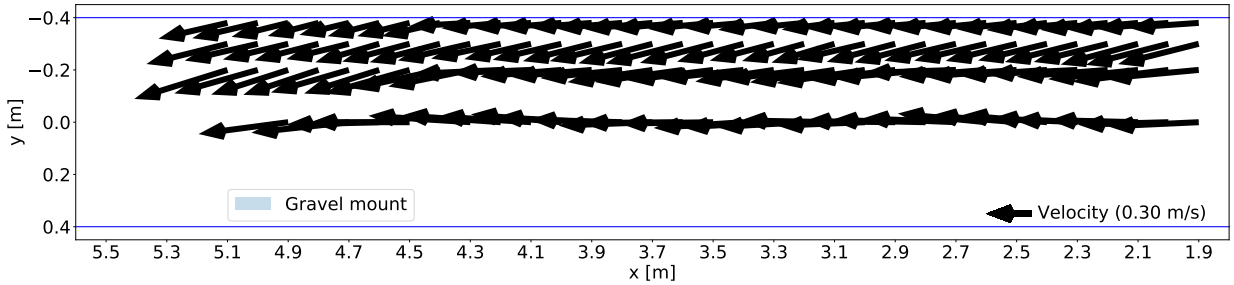

(b) GM1.4, measurement elevation z=0.140 m.

Figure 70: Horizontal velocity profiles for experiments GM1.4 (slope I=0.00200 and discharge Q=0.0588 m^3/s). Each time, the data collected the closest from the gravel bed (a,c) or the water surface (b,d) are shown. Flow direction and its intensity are given by the black quivers (scaled to plot axis, legend for reference), while the mounts area is coloured blue and labelled "Gravel mount".

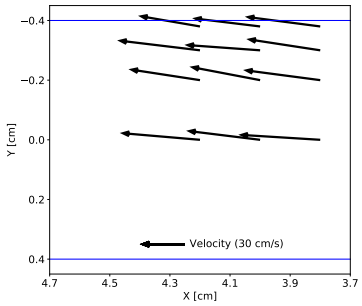

(a) GM2.1, measurement elevation z=0.0300 m.

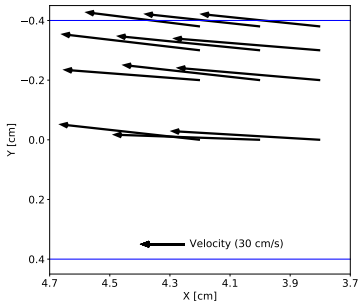

(b) GM2.1, measurement elevation z=0.0800 m.

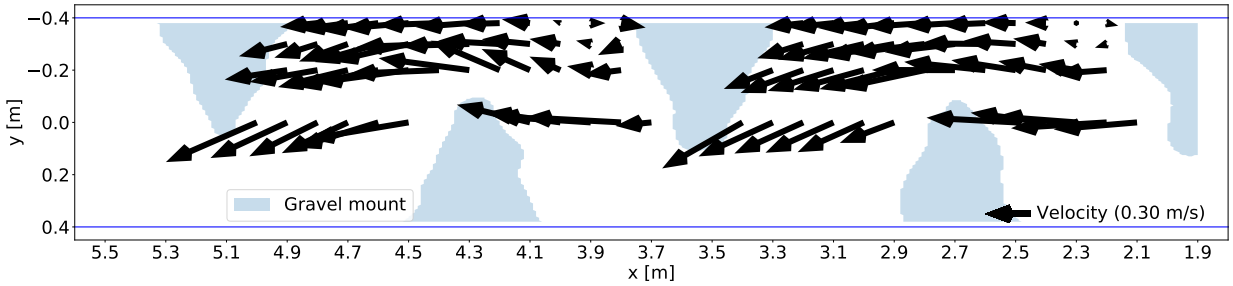

(c) GM2.3, measurement elevation z=0.0300 m.

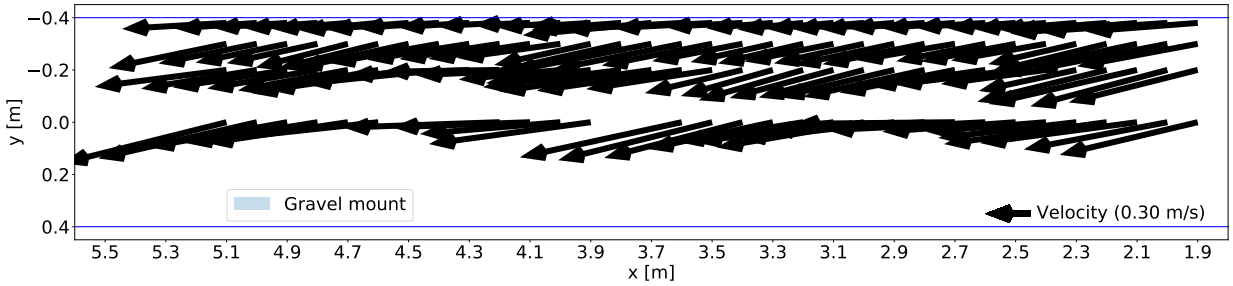

(d) GM2.3, measurement elevation z=0.0800 m.

Figure 71: Horizontal velocity profiles for experiments GM2.1 and GM2.3 (slope I=0.0100 and discharge Q=0.0588 m^3/s). Each time, the data collected the closest from the gravel bed (a,c) or the water surface (b,d) are shown. Flow direction and its intensity are given by the black quivers (scaled to plot axis, legend for reference), while the mounts area is coloured blue and labelled "Gravel mount".

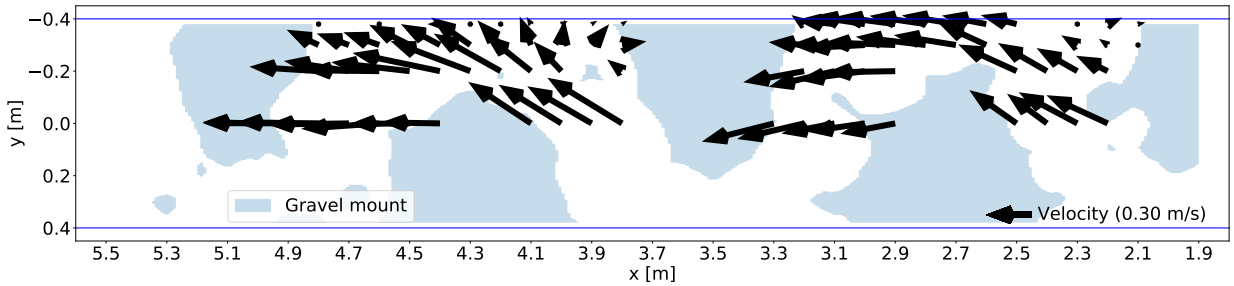

(a) GM2.4, measurement elevation z=0.0300 m.

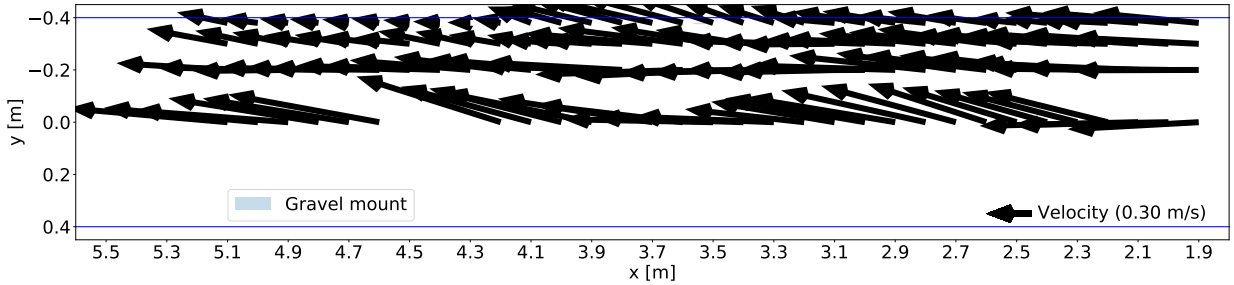

(b) GM2.4, measurement elevation z=0.0100 m.

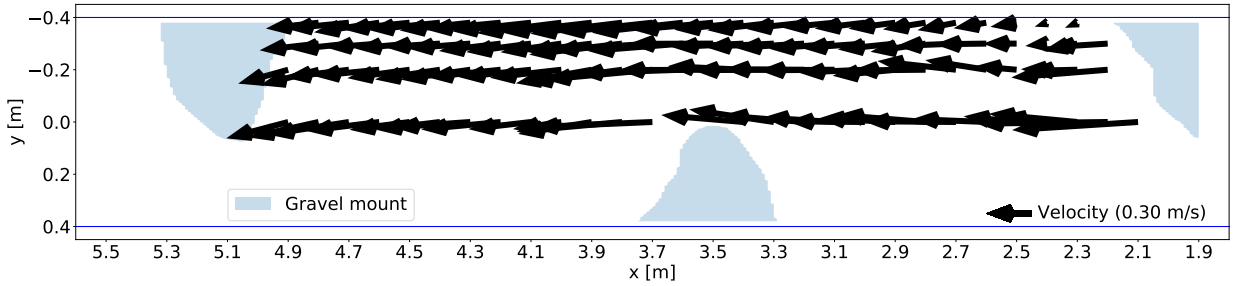

(c) GM2.5, measurement elevation z=0.0300 m.

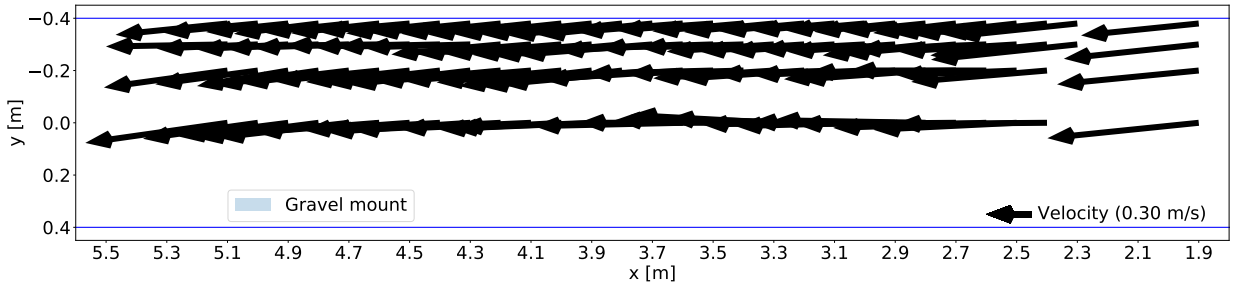

(d) GM2.5, measurement elevation z=0.0800 m.

Figure 72: Horizontal velocity profiles for experiments GM2.4 and GM2.5 (slope I=0.0100 and discharge Q=0.0588 m^3/s). Each time, the data collected the closest from the gravel bed (a,c) or the water surface (b,d) are shown. Flow direction and its intensity are given by the black quivers (scaled to plot axis, legend for reference), while the mounts area is coloured blue and labelled "Gravel mount".

B.3 Mounts area and refuge able area

The mounts area and refuge able area are presented in relationship with the y-coordinate (in absolute value). Since the triangular gravel mounts are constructed using only coarse gravel G1, the interstice area is considered 0.00 m^2. Experiments GM1.1 and GM2.1 have been conducted with flat gravel bed, the mounts area is therefore 0.00 m^3 everywhere. In the case of GM1.1, a small refuge able area is measured at $|y|$=0.380 m. In general, the largest refuge able areas are found along the sides of the channel, where the gravel mounts are the largest.

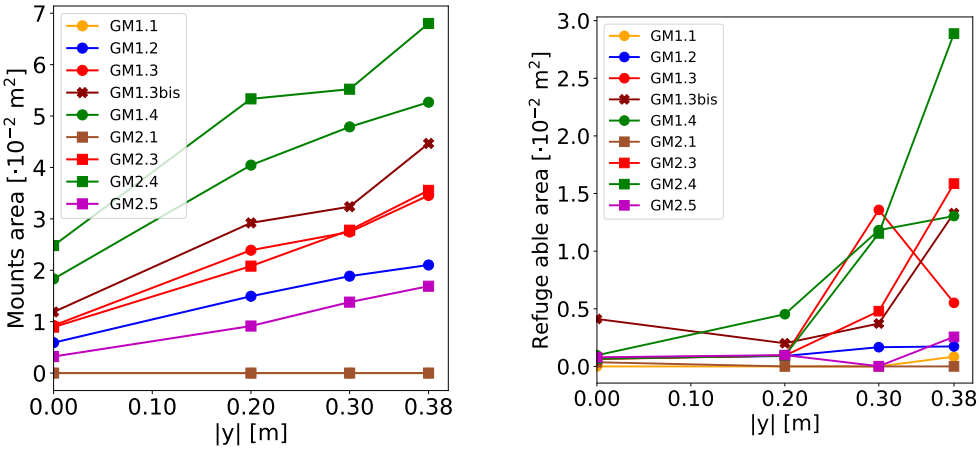

(a) Mounts area.

(b) Refuge able area.

Figure 73: Mounts area and refuge able area in relationship with the y-coordinate (in absolute value) for each experiment.

C Assembled boulders groynes

C.1 Average water depth and Froude number

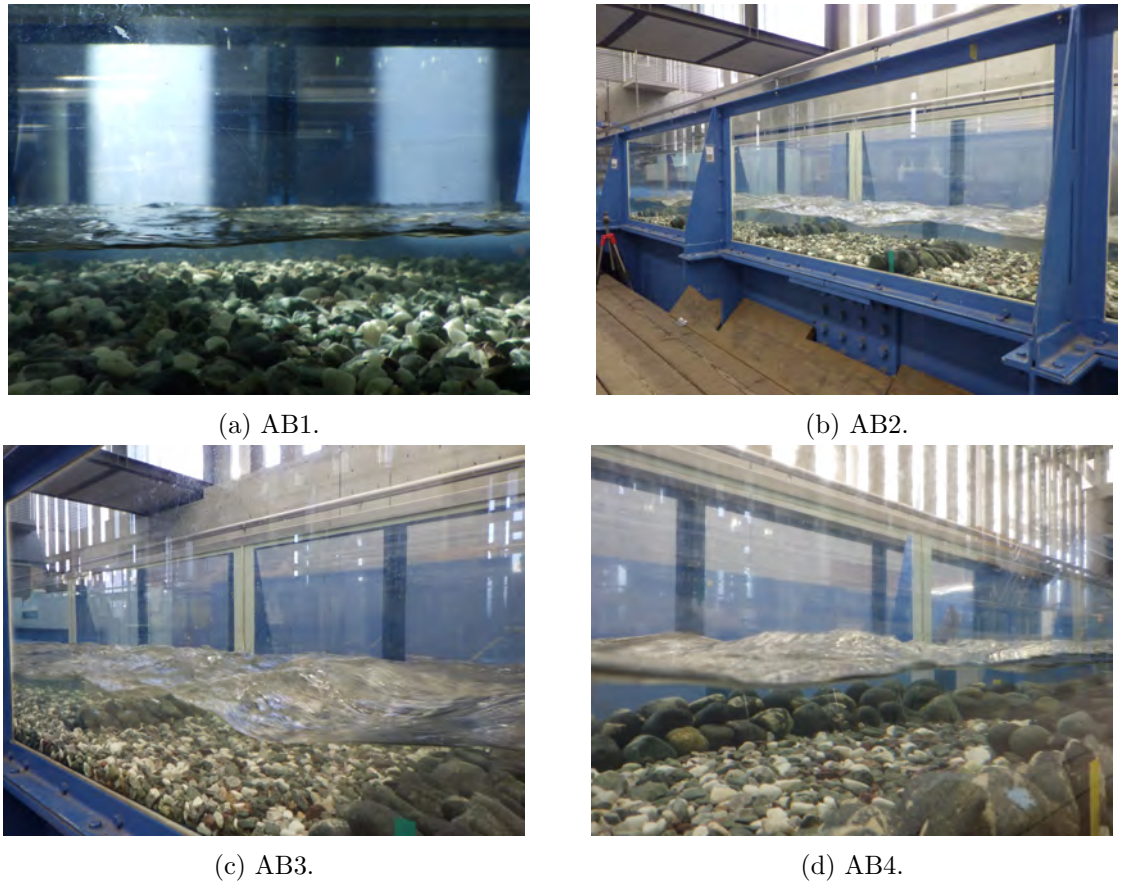

(a) AB1. (b) AB2.

(c) AB3. (d) AB4.

Figure 74: Water surface for the different experiments at discharge Q=0.0588 m^3/s and slope I=0.0100. The flow direction is always from right to left.

C.2 Horizontal velocity profiles

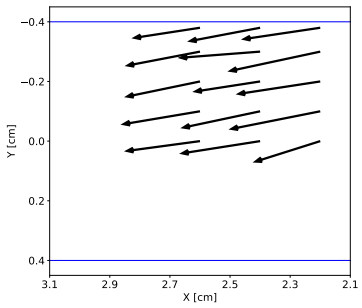

(a) AB1, measurement elevation z=0.0500 m.

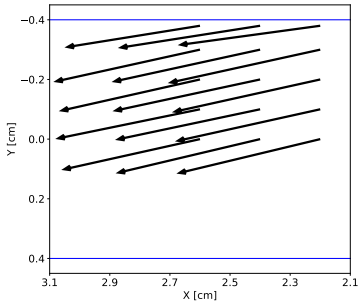

(b) AB1, measurement elevation z=0.0900 m.

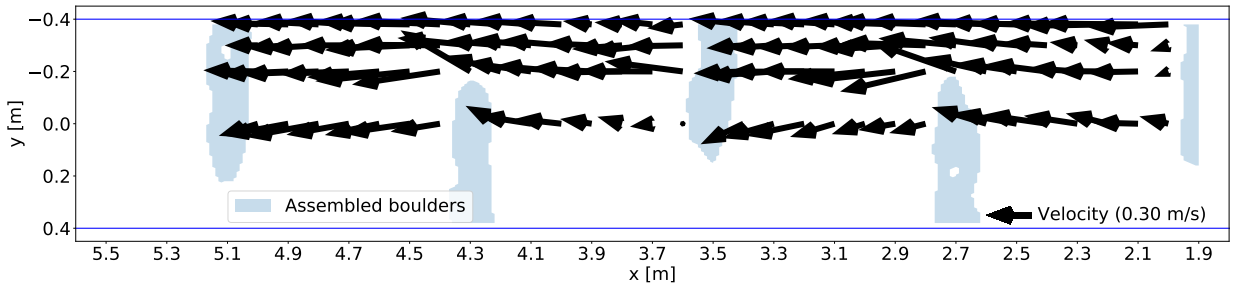

(c) AB2, measurement elevation z=0.0500 m.

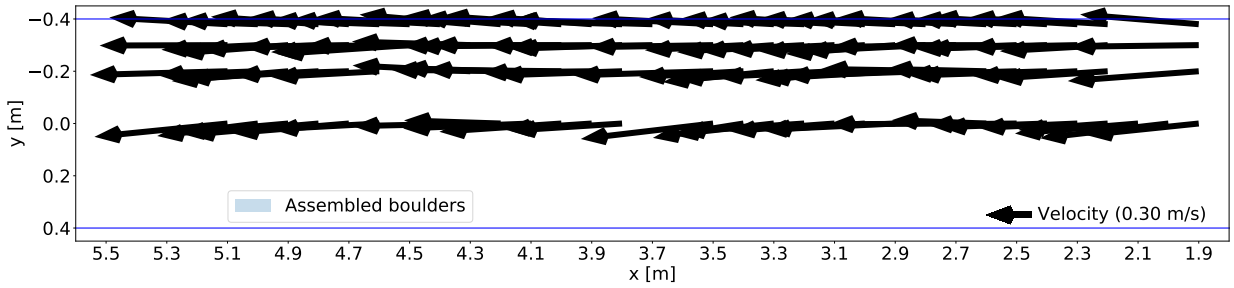

(d) AB2, measurement elevation z=0.100 m.

Figure 75: Horizontal velocity profiles for experiments AB1 and AB2 (slope I=0.0100 and discharge Q=0.0588 m^3/s). Each time, the data collected the closest from the gravel bed (a,c) or the water surface (b,d) are shown. Flow direction and its intensity are given by the black quivers (scaled to plot axis, legend for reference), while the mounts area is coloured blue and labelled "Assembled boulders".

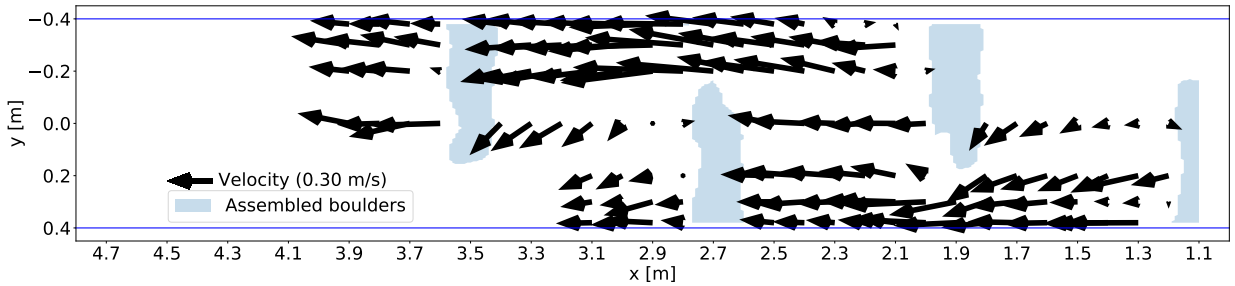

(a) AB3, measurement elevation z=0.0500 m.

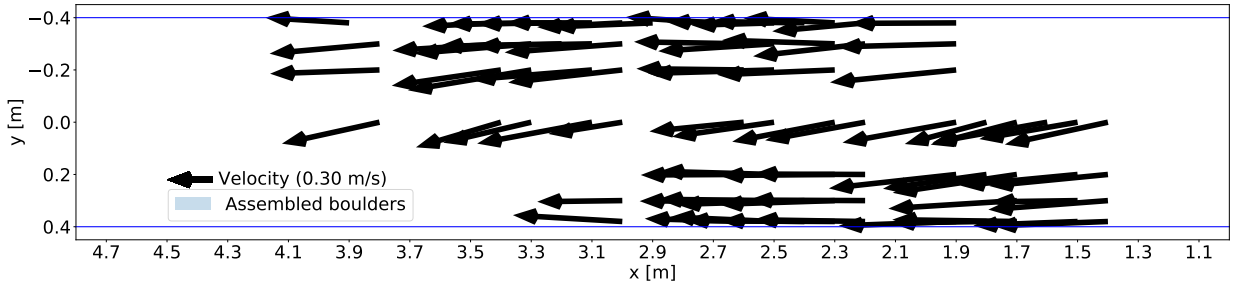

(b) AB3, measurement elevation z=0.140 m.

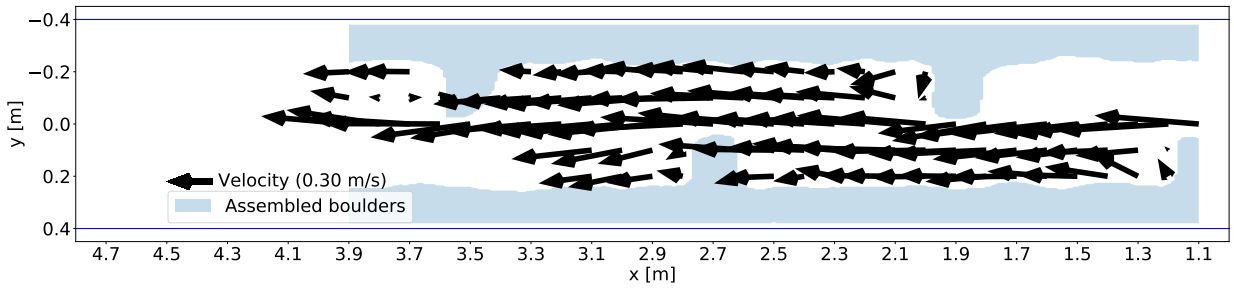

(c) AB4, measurement elevation z=0.0500 m.

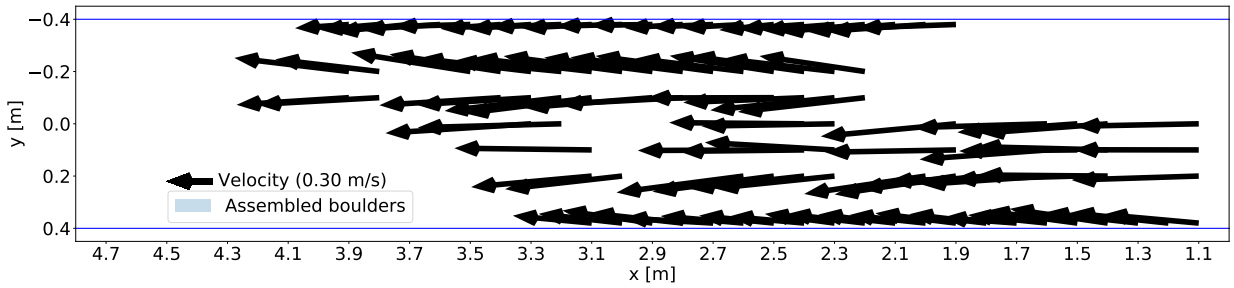

(d) AB4, measurement elevation z=0.140 m.

Figure 76: Horizontal velocity profiles for experiments AB3 and AB4 (slope I=0.0100 and discharge Q=0.0588 m^3/s). Each time, the data collected the closest from the gravel bed (a,c) or the water surface (b,d) are shown. Flow direction and its intensity are given by the black quivers (scaled to plot axis, legend for reference), while the mounts area is coloured blue and labelled "Assembled boulders".

C.3 Assembled boulders area, refuge able area and interstice area

The assembled boulders area, refuge able area and interstice area are presented in relationship with the y-coordinate (in absolute value). Since experiments AB3 and AB4 has been conducted on both sides of the channel, two lines are shown with the same colour. Experiment AB1 has been conducted with flat gravel bed, therefore the assembled boulders area and interstice area are both 0.00 m^2 everywhere. In the other experiments, the height is kept constant along each groyne's transverse length. For this reason, the assembled boulders area remains almost constant along the y-axis. For experiment AB4 at $|y|$=0.380 m the area is significant larger because of the extra assembled boulders constructed there. Since the definition of interstice area depends from the total construction area (30% of it to be precise), the plot lines in Sub-figures 77a and 77b have the same shape. The creation of refuge able areas does not seem to have a direct relationship with the y-coordinate. There are no significant variations between different measurement sides of the same experiment. For the successful formation of refuge able areas, the specific position of the assembled boulders is expected to be more important than their coordinate (i.e. how the boulders are placed is more important than where).

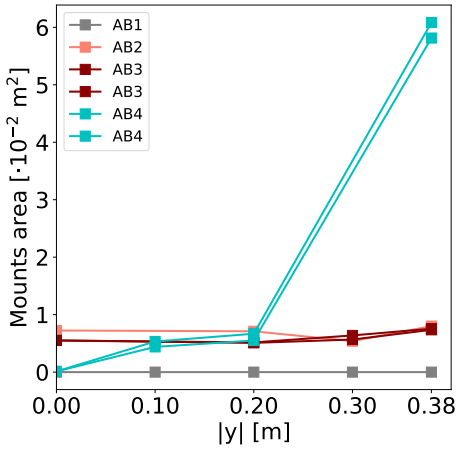

(a) Assembled boulders area.

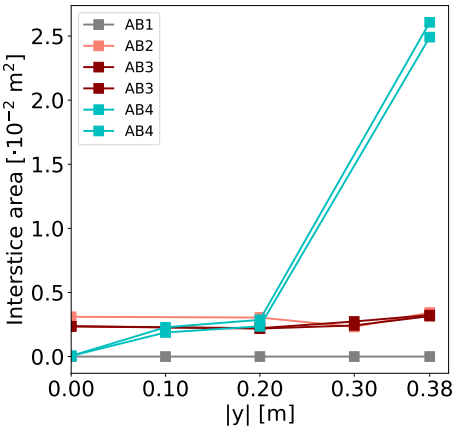

(b) Interstice area.

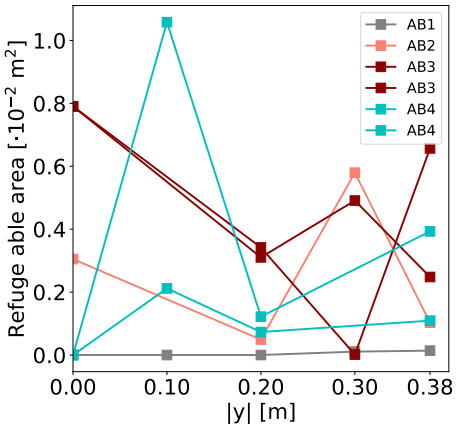

(c) Refuge able area.

Figure 77: Assembled boulders area, interstice area and refuge able area in relationship with the y-coordinate (in absolute value) for each experiment.

D Combination of boulders and gravel

D.1 Estimation of empty spaces inside the improved gravel mounts

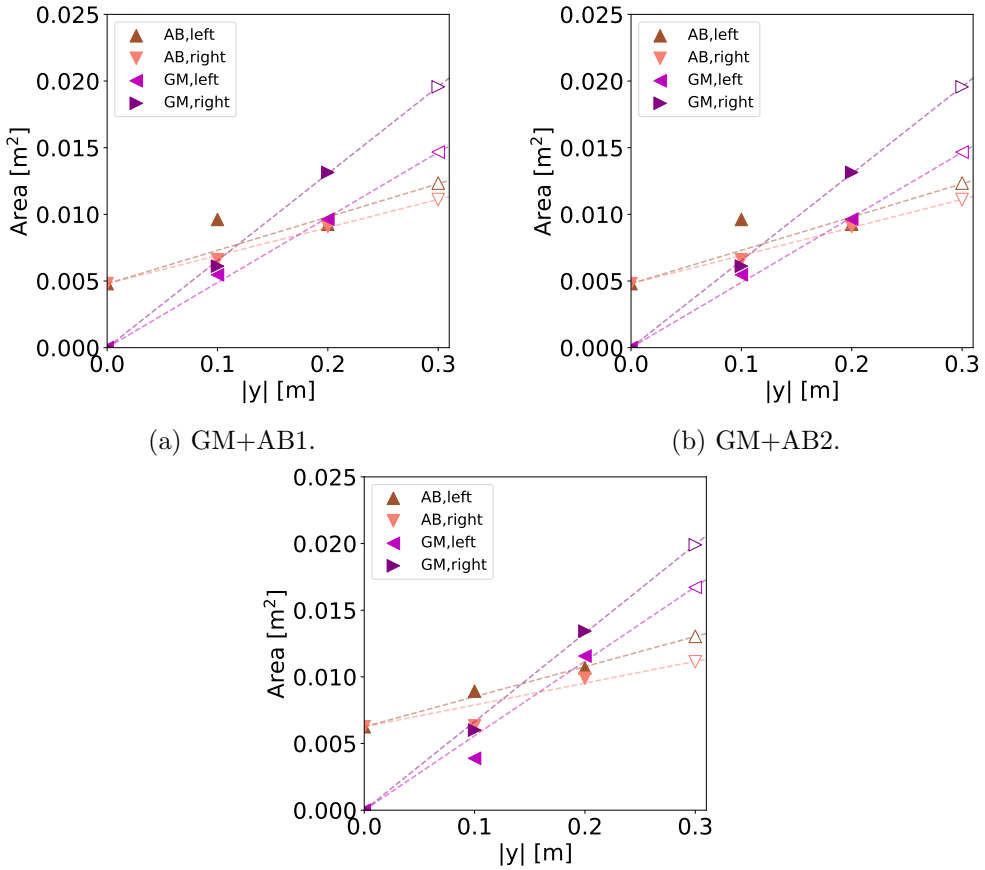

(a) GM+AB1.

(b) GM+AB2.

(c) GM+AB4.

Figure 78: Estimation of the gravel area (GM) and boulders area (AB) at coordinate y=±0.300 m for the other experiments besides GM+AB3 (presented in Figure 34).

D.2 Average water depth and Froude number

(a) GM+AB1, Q=0.00370 m^3/s.

(b) GM+AB2, Q=0.00550 m^3/s.

(c) GM+AB3, Q=0.0588 m^3/s.

(d) GM+AB4, Q=0.155 m^3/s.

(e) Q=0.155 m^3/s (failed experiment).

Figure 79: Water surface for the different experiments at slope I=0.0100. The flow direction is always from right to left.

D.3 Horizontal velocity profiles

Experiment GM+AB4 (Q=0.155 m^3/s) has been conducted twice since the first try has been classified as unsatisfactory and relegated to the Appendices here. A systematic error in the positioning of the electrical-magnetic current meter causes the horizontal velocity profiles to show the lateral velocity component erroneously shifted to the left (positive y-direction).

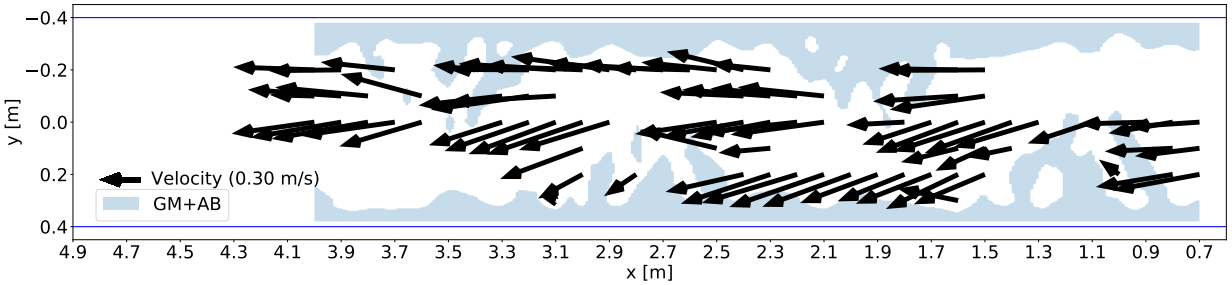

(a) Q=0.155 m^3/s (failed experiment), measurement elevation z=0.0500 m.

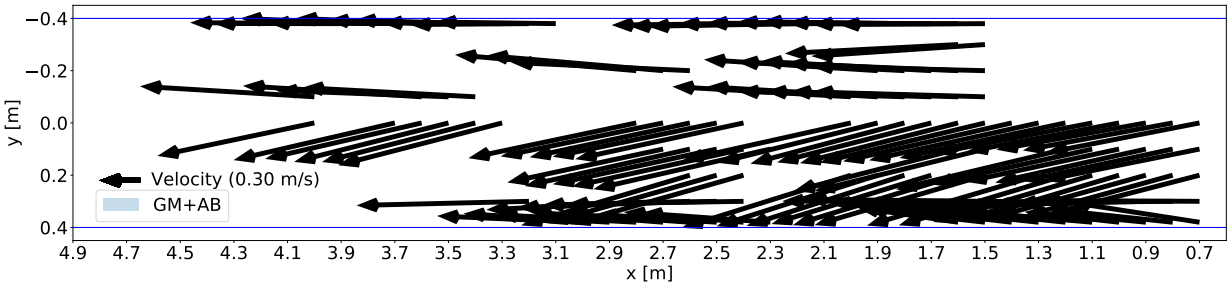

(b) Q=0.155 m^3/s (failed experiment), measurement elevation z=0.140 m.

Figure 80: Horizontal velocity profiles for the failed experiment (slope I=0.0100 and discharge Q=0.155 m^3/s). Each time, the data collected the closest from the gravel bed (a,c) or the water surface (b,d) are shown. Flow direction and its intensity are given by the black quivers (scaled to plot axis, legend for reference), while the mounts area is coloured blue and labelled "GM+AB".

D.4 Mounts area, refuge able area and interstice area

The mounts area, refuge able area and interstice area are presented in relationship with the y-coordinate (in absolute value). Each time two lines are shown with the same colour because data has been collected on both sides of the channel. When showing the mounts area and the interstice area at coordinate $|y|$=0.300 m, two values are given. The larger one is the results of the bed elevation measurement (assumed to be only build from assembled boulders), while the second one has been found by estimating the gravel and boulders areas (same method as explained in Sub-chapter 4.2.1). Since the same exact model is used for experiments GM+AB1 and GM+AB2, the mounts and interstice areas are almost identical. The only visible difference arrives at $|y|$=0.380 m, where only the area of the submerged boulders is considered and the average water surface for GM+AB2 is slightly higher. There is a significant difference between the plots for the mounts areas and the interstice areas. For the former, there is little separation between gravel mount area and side assembled boulders area, proving that the two have been homogeneously combined. In case of the interstice area, there is a clear separation at coordinate $|y|$=0.300 m since there are significant less boulders in the centre part of the channel compared with the sides. The creation of refuge able areas does not seems to be influenced by the y-coordinate. There are significant variations between different measurement sides of the same experiment. In this case again, the specific position of the assembled boulders is expected to be more important for the successful formation of refuge able areas than their coordinate.

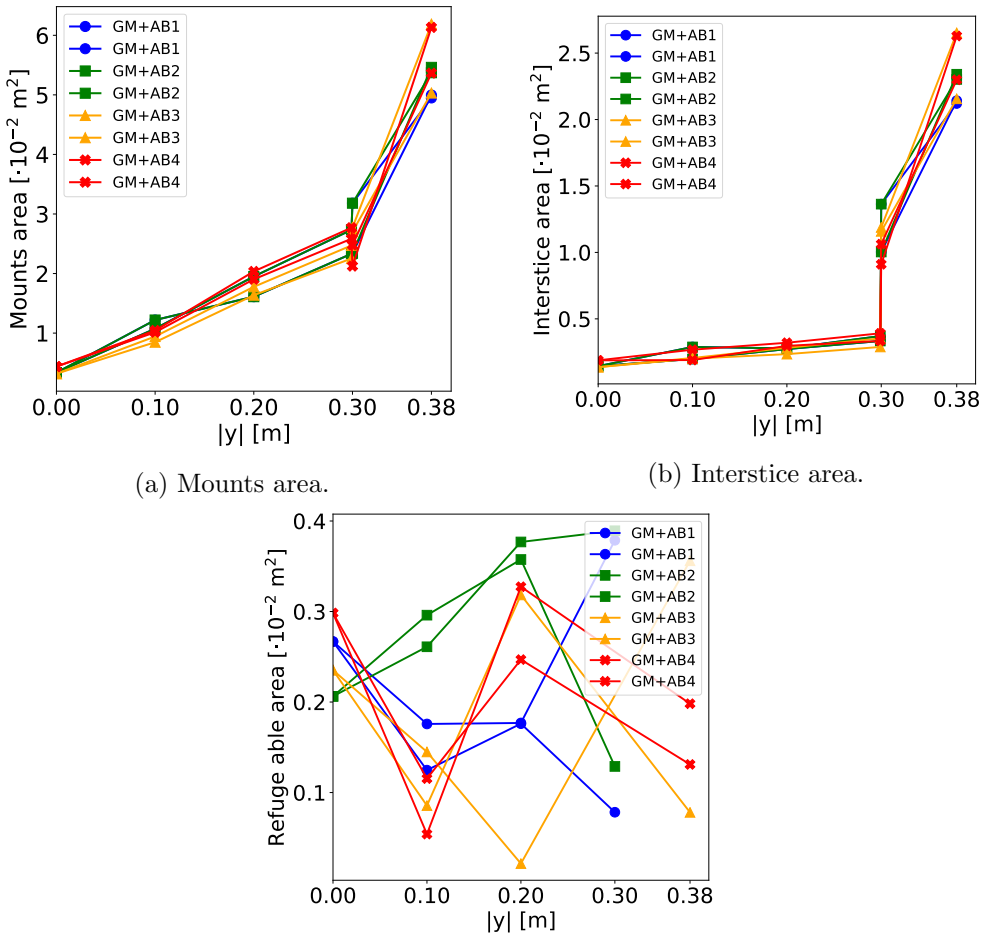

(a) Mounts area.

(b) Interstice area.

(c) Refuge able area.

Figure 81: Mounts area, interstice area and refuge able area in relationship with the y-coordinate (in absolute value) for each experiment.